FISH SKIN AS AN ALTERNATIVE BIOPOLYMER TOWARDS THE DEVELOPMENT OF ION CONDUCTING GREEN SOLID ELECTROLYTES IMPREGNATED WITH AMMONIUM NITRATE

NORLIN BINTI NADZRIN

INSTITUTE FOR ADVANCED STUDIES
UNIVERSITI MALAYA
KUALA LUMPUR

2023

FISH SKIN AS AN ALTERNATIVE BIOPOLYMER TOWARDS THE DEVELOPMENT OF ION CONDUCTING GREEN SOLID ELECTROLYTES IMPREGNATED WITH AMMONIUM NITRATE

NORLIN BINTI NADZRIN

DISSERTATION SUBMITTED IN FULFILMENT OF THE REQUIREMENTS FOR THE DEGREE OF MASTER OF PHILOSOPHY

INSTITUTE FOR ADVANCED STUDIES
UNIVERSITI MALAYA
KUALA LUMPUR

2023

UNIVERSITI MALAYA
ORIGINAL LITERARY WORK DECLARATION

Name of Candidate: **Norlin binti Nadzrin**
Matric No: **s2001934/1**
Name of Degree: **Master of Philosophy**
Title of Project Paper/Research Report/Dissertation/Thesis ("this Work"):
Fish Skin as an Alternative Biopolymer Towards the Development of Ion Conducting Green Solid Electrolytes Impregnated with Ammonium Nitrate
Field of Study: **Physical Science**

I do solemnly and sincerely declare that:

(1) I am the sole author/writer of this Work;
(2) This Work is original;
(3) Any use of any work in which copyright exists was done by way of fair dealing and for permitted purposes and any excerpt or extract from, or reference to or reproduction of any copyright work has been disclosed expressly and sufficiently and the title of the Work and its authorship have been acknowledged in this Work;
(4) I do not have any actual knowledge, nor do I ought reasonably to know that the making of this work constitutes an infringement of any copyright work;
(5) I hereby assign all and every rights in the copyright to this Work to the Universiti Malaya ("UM"), who henceforth shall be owner of the copyright in this Work and that any reproduction or use in any form or by any means whatsoever is prohibited without the written consent of UM having been first had and obtained;
(6) I am fully aware that if in the course of making this Work I have infringed any copyright whether intentionally or otherwise, I may be subject to legal action or any other action as may be determined by UM.

Candidate's Signature Date:

Subscribed and solemnly declared before,

Witness's Signature Date:

Name:
Designation:

ABSTRACT

In this study, new sequences of fish gelatin (FG) as polymer host for solid polymer electrolytes (SPE) impregnated with ammonium nitrate (NH_4NO_3) are prepared via solvent-casting method. Chitosan (CS) was blended with FG to provide extra pathways for protonic migration to boost up the conductivity. From FESEM micrographs, the blend of 60 wt. % FG and 40 wt. % CS, (CF4) are found to be miscible to one and another and from XRD analysis it is confirmed that the ratio is the most amorphous with the lowest degree of crystallinity ~ 15. 38 %. The most amorphous electrolyte in the salted single polymer system is found to be FG25 and that of the salted blended system, is CFs40. The interactions between the material have been determined from the band shifts and changes of the peak's wavenumber from FTIR spectroscopy analysis. The ionic conductivity of pure FG film has been identified to be 1.17×10^{-10} S cm^{-1} and optimised at 1.52×10^{-5} S cm^{-1} with the inclusion of 25 wt. % NH_4NO_3. The value has increased to 1.61×10^{-3} S cm^{-1} with the addition of 40 wt. % NH_4NO_3 in FG-CS polymer electrolytes system. The temperature dependence conductivity plot is Arrhenian. The variation in conductivity is accompanied by the changed in surface morphology as can be observed from FESEM analysis. Transport analysis showed that the trend in conductivity can be influenced by the mobility *(μ),* the diffusion coefficient (*D*) and number density (*n*) of ions. TGA and DSC are discussed to study the thermal properties of the electrolytes. The degradation temperature and glass transition temperature decreased as salt is added into the system due to the complexation of salt and the polymer. T_g decreased to 54.83 °C in FG25 and to 83.33 °C in CFs40. From TNM analysis, ions were found to be the dominant charge. t_{ions} values in the highest conducting electrolytes are 0.92 and 0.96 in FG25 and CFs40, respectively. LSV result confirms the suitability for the highest conducting electrolyte with ~2.6 V for both salted systems.

ABSTRAK

Dalam kajian ini, jujukan baru dari jelatin ikan (FG) sebagai perumah elektrolit polimer pepejal yang ditambah dengan NH_4NO_3 telah disediakan melalui kaedah penuangan larutan. Kitosan (CS) dicampur untuk memberikan laluan tambahan kepada pergerakan protonik bagi meningkatkan kekonduksian. Daripada mikrogam FESEM, campuran 60 wt. % FG dan 40 wt. % CS, (CF4) didapati serasi dan daripada analisis XRD, nisbah tersebut adalah yang paling amorfus dengan darjah kristaliniti terendah iaitu ~15.38 %. Elektrolit paling amorfus dalam sistem polimer tunggal bergaram ialah FG25 dan dalam sistem campuran bergaram, ialah CFs40. Interaksi antara bahan ditentukan dari pergerakan jalur dan perubahan bilangan gelombang puncak daripada analisis spektroskopi FTIR. Kekonduksian ionik bagi filem FG tulen 1.17×10^{-10} S cm^{-1} dan dioptimumkan kepada 1.52×10^{-5} S cm^{-1} dengan 25 wt. % NH_4NO_3. Nilai meningkat kepada 1.61×10^{-3} S cm^{-1} dengan 40 wt. % NH_4NO_3 dalam sistem elektrolit polimer FG-CS. Plot kebergantungan suhu terhadap kekonduksian adalah Arrhenian. Variasi kekonduksian disertai perubahan morfologi permukaan diperhatikan dari analisis FESEM. Parameter pengangkutan menunjukkan corak kekonduksian dipengaruhi oleh mobility, pekali difusi, dan kepadatan nombor ion. TGA dan DSC dianalisis untuk mengkaji sifat termal elektrolit. Suhu degradasi dan suhu peralihan kaca, T_g berkurang apabila garam ditambah ke dalam sistem disebabkan oleh kompleksasi garam dan polimer. T_g berkurang kepada 54.83 °C dalam FG25 dan kepada 83.33 °C dalam CFs40. Daripada analisis TNM, ion didapati menjadi cas dominan. Nilai ion dalam elektrolit paling tinggi pengkonduksian adalah 0.92 dan 0.96 dalam FG25 dan CFs40, masing-masing. Keputusan LSV mengesahkan kesesuaian untuk elektrolit paling tinggi pengkonduksian ~2.6 V untuk kedua-dua sistem yang mengandungi garam.

ACKNOWLEDGEMENT

First and foremost, I would like to thank God for the strength He has given throughout all the challenging moments of completing this dissertation. This journey has not been an easy journey, but it is worth it. Next, I would like to express my deepest gratitude to my supervisor, Associate Professor Dr. Mohd Fakhrul Zamani bin Abdul Kadir. Thank you for your endless constructive feedback and guidance regardless of place and time. Thank you for understanding all my situations and never failed to encourage me until I am able to finish this. I'd also like to thank Associate Professor Dr. Ninie Suhana binti Abdul Manan for the invaluable input and advice throughout the research process. All the feedbacks allowed me to deepen and refine my research, and the result presented in my thesis would be impossible without their supervision.

Furthermore, I am highly grateful to my husband, Mohd Rafy bin Abd Rajab and my mother, Sarifah Fauziah binti Syed Jaafar for endless support and infinite patience through my ups and downs. Without them, this dissertation would have taken even longer time to complete. Special gratitude to my late father who passed away during my study. He is the one who pushed me to step out from my comfort zone and step into a 'growth' zone. I always knew that you wanted the best for me.

This research would not have been possible without the scholarship awarded from Ministry of Education, Malaysia for providing me with generous financial support throughout my study and for the work funding, I would like to thank Ministry of Higher Education for FRGS/1/2019/STG07/UM/02/6 grant. I also would like to express my appreciation towards my lab mates for their willingness to share their time and insights, and to all the technicians that help me a lot in collecting good data. Thank you for all the contributions, which have made this dissertation possible.

TABLE OF CONTENTS

LIST OF TABLES

LIST OF FIGURES

LIST OF SYMBOLS

A	:	Pre-exponential factor
C	:	Capacitance of CPE
C_0	:	Vacuum capacitance
D	:	Diffusion coefficient
d	:	Thickness of electrolyte
d_B	:	Spacing between layers of atoms
e	:	Charge of electron
E_a	:	Activation energy
I_1	:	Initial current
I_2	:	Steady state current
k	:	Boltzman constant
l	:	Distance between two coordinating sites
m	:	Mass of ionic charge carrier
n	:	Number of mobile ions
n_B	:	The whole number of wavelengths
p	:	Deviation of plot
P_a	:	Areas of amorphous peaks
P_c	:	Areas of crystalline peaks
R_B	:	Bulk resistance
R^2	:	Regression value
T	:	Absolute temperature
t	:	thickness
T_g	:	Glass transition temperature
t_{ion}	:	Ionic transference number

t_e	:	Electron transference number
v	:	Velocity of ion propagation
X_c	:	Degree of crystallinity
Z_{CPE}	:	The impedance of CPE
Z_r	:	Real part of impedance
μ	:	Ionic mobility
θ	:	Angle
θ_B	:	Angle between the incident rays and the surface of the crystals
τ	:	Travelling time of ions
ω	:	Radial frequency
σ	:	Ionic conductivity
λ_B	:	Wavelength of the rays
ε_i	:	Dielectric loss
ε_r	:	Dielectric constant

LIST OF ABBREVIATIONS

AC	:	Alternating current
BSE	:	Bovine spongiform encephalopathy
CMC	:	Carboxymethyl cellulose
CMCS	:	Carboxymethyl chitosan
CEO	:	Cerium(IV) oxide
CF_3SO_3	:	Triflate
CH_3COOH	:	Acetic acid
COOH	:	Carboxyl
$CONH_2$	:	Amide group
CPE	:	Constant phase element
CS	:	Chitosan
DSC	:	Differential Scanning Calorimetry
DSSC	:	Dye-sensitized solar cell
Dex	:	Dextran
EIS	:	Electrochemical impedance spectroscopy
FESEM	:	Field emission scanning electron microscopy
FG	:	Fish gelatin
FTIR	:	Fourier transform infrared spectroscopy
H^+	:	Hydrogen ion
IL	:	Ionic liquid
LSV	:	Linear sweep voltammetry
$LiBF_4$	:	Lithium tetrafluoroborate
LiCL	:	Lithium Chloride
$LiCLO_4$	:	Lithium perchlorate

MC	:	Methylcellulose
$MgSO_4$	:	Magnesium sulfate
NH_4^+	:	Ammonium salt
NH_2	:	Amino group
NH_4Br	:	Ammonium bromide
NH_4Cl	:	Ammonium chloride
NH_4I	:	Ammonium iodide
NH_4NO_3	:	Ammonium nitrate
NH_4SCN	:	Ammonium thiocyanate
$NH_4CF_3SO_3$	:	Ammonium triflate
NO_3^-	:	Nitrate
OH	:	Hydroxyl
PE	:	Polymer electrolyte
PEG	:	Polyethylene glycol
PEO	:	Polyethylene oxide
PMMA	:	Polymethyl methacrylate
POZ	:	Poly(2-ethyl-2-oxazoline)
PPG	:	Polypropylene glycol
PS	:	Potato starch
PVA	:	Polyvinyl alcohol
PVdf	:	Polyvinylidene fluoride
PVdf-HFP	:	Poly(vinylidene fluoride-co-hexafluoropropylene)
PVP	:	Polyvinyl pyrrolidone
SPE	:	Solid polymer electrolyte
SS	:	Stainless steel

TGA	:	Thermogravimetric analysis
TNM	:	Transference number measurement
wt. %	:	Weight percentage
XRD	:	X-ray diffraction

CHAPTER 1: INTRODUCTION

1.1 Research Background

In this modern society, digital devices industry is growing rapidly. Battery is one of the primary and important components in this current growth. Consumers nowadays are more attracted to use electronic devices that are small, lightweight and portable with a longer lasting rechargeable battery (Dong et al., 2021). Several research have been done to produce a battery that can meet with the current demands. However, batteries that formerly employed liquid as electrolytes have some drawbacks. According to some research work, liquid electrolytes experience issues with leakage, electrode corrosion, a small operating temperature range, hermetic sealing, and internal battery short circuits (Aziz et al., 2020). Those issues could be due to the growth of metal dendrites during multiple charging and discharging process (Agrawal & Pandey, 2008; Dong et al., 2021; Yu et al., 2021). Thus, research and development on batteries nowadays are shifting from liquid based to solid based electrolytes. Studies have shown that solid electrolytes have higher temperature stability, low temperature operation, easy to construct and flexible in terms of their form factor (Azarian & Wootthikanokkhan, 2020; Dannoun et al., 2020).

Solid polymer electrolytes (SPE) were first reported in 1973 by Peter V. Wright. Wright found that a solid electrical conductor can be produced using polyethylene oxide (PEO) as a host and sodium salt as dopants. Charge carriers for ion conduction can be produced via the solvation of dopant salt in the polymer. In 1978, Michel Armand has brought out the potential of these material as a new class of solid electrolyte for energy storage application (Armand, 1994). He realized that the complex from lithium salt and PEO has turned out to be a good conductor that perfectly matches the electrodes

intercalation. Since then, similar polymers have been tested to produce solid electrolytes such as polypropylene glycol (PPG) (Saikia et al., 2011) and polyethylene glycol (PEG) (T. J. Singh & Bhat, 2003).

Synthetic polymer such as PEO that is originated from petroleum are non-biodegradable (Alves et al., 2016). Due to the current environmental issue, biopolymer is being used as an alternative to host ionic conduction in electrolytes. Natural polymers are the types of polymers produced from raw materials found in nature. Natural polymers can be modified to produce a better electrolyte system with improved properties (Sudhakar, Selvakumar & Bhat, 2018). Natural polymers exhibit extra uniqueness such as thermally stable, easy handling, non-corrosive, abundance in nature and inexpensive (Aziz et al., 2019). Furthermore, biopolymers are non-toxic, biodegradable, and biocompatible (Aziz et al., 2020; Selvalakshmi et al., 2017).

Biopolymers such as starch, gelatin, agar, cellulose, pectin, gum, natural rubber, chitosan, carrageenan and agarose has been widely investigated as polymer electrolytes (Azli et al., 2020; Kadir & Hamsan, 2018; L. S. Kumar & Selvasekarapandian, 2021). In this work, biopolymer-based electrolyte made of fish skin gelatin (FG) will be investigated. To the best knowledge up to date, the usage of fish gelatin as solid biopolymer electrolytes is still new. Considering these research tendencies, the aim of this study is to produce a novel SPE based on fish gelatin that will be doped with ammonium salt. It has been reported that the loosely bound hydrogen ion (H^+) in ammonium salts (NH_4^+) are good proton donors that responsible for ionic conduction (Shenbagavalli et al., 2022).

Polymer blending has been extensively studied since it claimed to be an easy method used to improve the ionic conductivity of electrolyte system (Aziz et al., 2020). Through the formation of new bonds, polymer blend can enhance the physical characteristics of pure components of a single polymer (Qiao et al., 2017). In this work, chitosan (CS) is blended with fish skin gelatin (FG) and several tests are conducted to study the effect on blending CS with FG. Previous study have shown that CS is compatible with FG (Fakhreddin et al., 2013; Qiao et al., 2017).

Massive potential for the fabrication of SPEs with excellent electrochemical properties has been successfully established. SPEs offer a superior alternative for substituting liquid electrolytes in the production of electrochemical devices. Problems such as leakage, corrosion and explosion can be avoided by using SPEs. On the other hand, it is also important to consider alternatives to conventional polymers. Gelatin and other natural polymers make an excellent alternative. They function well as SPEs and are abundant in nature, non-toxic, cheap, and biodegradable (Jothi et al., 2022). Most studies on gelatin usually refer to mammalian gelatin which comes from cows or pigs. Nonetheless, the increased need for gelatin alternatives to bovine and porcine sources, driven by concerns over bovine spongiform encephalopathy (BSE) and religious considerations, has generated significant interest in fish gelatin (Ahmad & Benjakul, 2011; Fox & Hanawa , 2004).

A study has been carried out to investigate the usage of collagenous fish waste in food and cosmetic packaging. To date, there are few research that has been done on fish gelatin as ion conducting SPE. The goal of this research is to synthesise and characterise biopolymer electrolytes using fish skin gelatin doped with ammonium salt. The used of

biopolymer electrolytes is expected to give a promising result towards the development of green technology electrochemical devices.

1.2 Objectives of the Study

The objectives of the study are as follows:

- To develop solid biopolymer electrolytes employing fish skin gelatin impregnated with ammonium nitrate.
- To evaluate the physical and electrical properties in solid biopolymer electrolytes system.
- To study the effect of polymer blending in solid biopolymer electrolytes system.

1.3 Dissertation Organization

This present work is aiming to achieve the objectives that have been listed in subtopic 1.2. Fish skin gelatin and chitosan are employed as a polymer host to develop solid biopolymer electrolytes via solution casting techniques. This dissertation contains eight chapters. Chapter 1 will introduce the background study on solid polymer electrolytes. Chapter 2 provides the literature review and the previous works related to solid biopolymer electrolytes. The reason on why fish skin gelatin, chitosan and ammonium nitrate were chosen in this research will be elaborated in Chapter 2 as well. Chapter 3 provides the details on the preparation of the polymer electrolytes with the characterization techniques involved such as X-ray diffraction analysis (XRD), Fourier transform infrared spectroscopy (FTIR) and Field Emission Scanning Electron Microscope (FESEM).

In this research work, 3 systems will be developed and analysed according to the experimental set up and the results will be discussed in Chapter 4, 5 and 6. The results on the development of electrolytes system from fish skin gelatin doped with different amounts of NH_4NO_3 salt (FG-NH_4NO_3) will be presented in Chapter 4. XRD will be used to investigate the amorphousness of the film as salt is added to the system. The interactions between the host polymer and the salt will be studied and discussed based on FTIR and the structural changes of the films will be analysed via FESEM micrographs. Other properties such as electrical impedance and transport parameters of the electrolytes system will also being studied and discussed using several different formulations and techniques.

The conductivity and other properties of the electrolytes can be improved using polymer blend techniques. Different ratio of chitosan will be blended with fish gelatin to develop a blended polymer host (FG-CS). The compatibility and miscibility between these two polymers will be investigated from both surface and cross-section micrograph of the blended polymer via FESEM. The interactions between chitosan and fish skin gelatin will be distinguished via FTIR spectrometer. The degree of crystallinity of the blended system will be determined from XRD analysis. All results pertaining to the blended system will be analysed and discussed in Chapter 5. Salted blended polymer electrolytes system comprises of fish gelatin, chitosan, and NH_4NO_3 (FG-CS-NH_4NO_3) will be analysed in Chapter 6. In this part, the effect of salt to the blended system on the physical and electrical performance of solid biopolymer electrolyte will be evaluated. Comparison on the results will be made with the previous single polymer salted system. The relation between all systems will be discussed in Chapter 7 and concluded in Chapter 8. The novelty of this work and the further works will be suggested in this last chapter.

CHAPTER 2: LITERATURE REVIEW

2.1 Introduction

Population growth increases the amount of energy required to meet their needs, and as portable technologies evolved, energy storage is becoming more significant nowadays (Garidepalli et al., 2022). Battery is one of the well-known forms of chemical energy storage among the current energy storage technologies. A battery is an electrochemical energy storage mechanism that converts chemical energy into electrical energy by facilitating the flow of ions from anode to cathode that is separated by a conductive electrolyte (Sohaimy et al., 2022). The design of high-performance electrochemical devices has underwent substantial research to provide secure and affordable energy storage solutions (Dannoun et al., 2022).

A polymer is a molecule made up of smaller molecules that are repeated and connected in 2- or 3-dimensional networks to build long or massive molecular chains (Ibnu et al., 2022). Due to that variable structure, polymeric materials can have a broad variety of physical, chemical, and mechanical properties (Aziz et al., 2020). Polymer electrolytes (PEs) are crucial for electrochemical devices due to their numerous unique benefits over commercial liquid electrolytes including their ability to form thin films, leakage-free, lightweight, flexible, easy to handle, transparent and good conductivity value (Aziz et al., 2020; Hamsan et al., 2020; Xun et al., 2019).

Researchers have extensively studied various methods to enhance the properties of PEs with the primary focus on improving their conductivity since it is a crucial aspect. Blending two or more polymers as PEs could be one of the alternatives with good

advantage to significantly increase their ionic conductivity. As a result, polymer blends have drawn the interest of past research due to their ability to develop novel materials through polymer combinations. These blends possess unique qualities that set them apart from single polymer and elevate their performance (Abdullah et al., 2022).

2.2 Natural Polymer

Development of a new generation of biobased polymers, for example polymers that derived from renewable resources and biodegradable through the action of living organism, is progressing rapidly. This is especially true in various energy generation and storage applications, where plastics are frequently integrated into manufacturing processes, despite their lack of eco-friendliness (Hamed et al., 2022). Unfortunately, the extensive utilization of these products has led to the generation of harmful pollutants (Xu et al., 2022a). The commercial batteries and electronic devices that are commonplace today incorporate electrolytes known for their high conductivity yet exposed to unwanted risks due to their hazardous and non-biodegradable nature, leading to a significant threat to the environment and biodiversity (Zhao et al., 2022).

Researchers all over the world have started to replace synthetic polymers with biopolymers because of their biodegradability and biocompatibility (Jothi et al., 2022; Leo et al., 2021). These benefits have led towards the establishment of biobased polymers as key contributors to the progress of environmentally friendly technology. Biopolymers can be categorized into four groups as tabulated in Table 2.1 based on their synthesis method, source, and the chemical composition of their backbone (Deshmukh et al., 2017).

Table 2.1: Classification of biodegradable polymers.

Categories	Example	References
Biomass products from agro	Polysaccharides Example: Starch, chitosan, gum Protein, lipids Example: Collagen, Gelatin, Gluten	(Abdulwahid et al., 2022; Deshmukh et al., 2017; Koc et al., 2020)
Microorganism extraction	Polyhydroxy-alkenoates Example: Poly(hydroxybutyrate)	
Biotechnology synthesis	Polylactides Example: Polylactic acid	
Petrochemical products	Polycaprolactones Polyester amides Aliphatic co-polyesters Aromatic co-polyesters	

2.3 Polymer Electrolyte (PE)

A polymer electrolyte (PE) is produced by dissolving salt into polymer matrix with a high molecular weight (P. Singh et al., 2022). According to Xu et al (2022) the ability of biopolymers to interact with the salt cations and conduct ions is attributed to the presence of hydrophilic -OH, -COOH, $-NH_2$, and $-CONH_2$ groups along with other functional moieties in the polymers. Examples of synthetic polymers that have been studied as polymer electrolytes are poly(vinyl pyrrolidone), poly(acrylonitrile), poly(methyl methacrylate), and poly(vinyl chloride) (Aziz et al., 2019; Garidepalli et al., 2022; Selvalakshmi et al., 2017). PEs have been used to produce electrochromic window, solar cells, solid state batteries, electrochromic display devices, electric vehicles because of the PEs properties such as transparent, light weight, safe, high ionic conductivity and versatile (Chattopadhyay et al., 2023; P. Singh et al., 2022).

There are three categories of PEs; liquid PEs, gel PEs and solid PEs. Solid PEs are preferred over liquid and gel for various reason that will be discussed in subtopic 2.4. The performance of PEs can be improved with physical treatment such as blending or cross-linking two different polymers. Beside physical treatment, PEs can also be improvised using chemical addition such as by adding plasticizer, filler, salts and ionic liquids (P. Singh et al., 2022). The concentration of the ions, viscosity of the electrolytes and the diffusivity are the factors that determined the ionic conductivity of liquids electrolytes (Ehrlich et al., 2023). Ghazali and Samsudin (2022) reported two criteria for a polymer to be served as an effective polymer electrolyte host: (1) the segmental motion of the polymer must be easily accomplished and (2) the material should have a low glass transition temperature in order to have a low cohesive energy.

2.4 Solid Polymer Electrolyte (SPE)

Solid polymer electrolyte (SPE) can be categorized as a polymer that has the ability in conducting ions. They are also referred as solid solvents, possessing ion transport characteristics akin to those found in traditional liquid ionic electrolyte solutions used in batteries and supercapacitors (Ong et al., 2020). SPEs have garnered significant attention owing to their built-in safety features and extensive operational temperature span, attributed to the absence of combustible liquid constituents. Moreover, they hold a very promising potential advantages concerning both gravimetric and volumetric energy density. (Abdulkareem, 2021; Yu et al., 2019). One of the SPEs setup was created through the disintegration of alkali metal salts within a polar polymer matrix. Upon the breakdown of the polymer matrix structure, electron-donor groups within the polymer will form a dative bond with cations from the inorganic salts. Under the influence of electric field,

these ions will be detached and starts their movement from one segment of the chain to another. (Aziz et al., 2020; Ong et al., 2020).

Chattopadhyay and co-workers (2023) reported that SPEs are considered to serve as electric vehicles (EVs) batteries. This is due to the improved in safety, a longer cycle life and a higher energy density (Chattopadhyay et al., 2023). SPEs also have been used in lithium-ion batteries, sodium-ion batteries, dye-sensitive solar cells, fuel cells, capacitors and many more (Ge et al., 2021; Teo & Buraidah, 2021).

2.5 Gelatin as polymer host in SPE

Gelatin is a proline and hydroxyproline protein that can be obtained by hydrolysing collagen (Siburian et al., 2020). Figure 2.1 shows the structure of gelatin according to its amino acid composition (Ramos et al., 2016). Animal skins and bones are the source of gelatin. Gelatin has historically been utilised extensively as an emulsifier, foaming agents, biodegradable packaging materials, and colloid (Oliveira et al., 2019; Rayung et al., 2020). Gelatin is frequently used in the food packaging industry because it can create a flexible and nearly colourless film (Lu et al., 2022; Ramos et al., 2016). Since it was discovered that gelatin can conduct electrical current, it has already been investigated for several electrochemical studies (Alam et al., 2021; Bommalapura et al., 2021).

Gelatin is one of the many different types of biopolymers currently in the market. Due to its high transparency, adhesiveness and plasticity, gelatin has gained interest in producing flexible energy devices such as supercapacitor, batteries and DSSC (Azarian & Wootthikanokkhan, 2020). Based on the reviews, solid polymer electrolyte that used

gelatin as host polymer have given a promising result in producing ion conducting film. The presence of lone pair electrons as shown in Figure 2.1 able to facilitate ion transport, offering gelatin as a good candidate for ionic conduction (Aziz et al., 2022). Table 2.2 shows the previous work on gelatin-based polymer electrolyte.

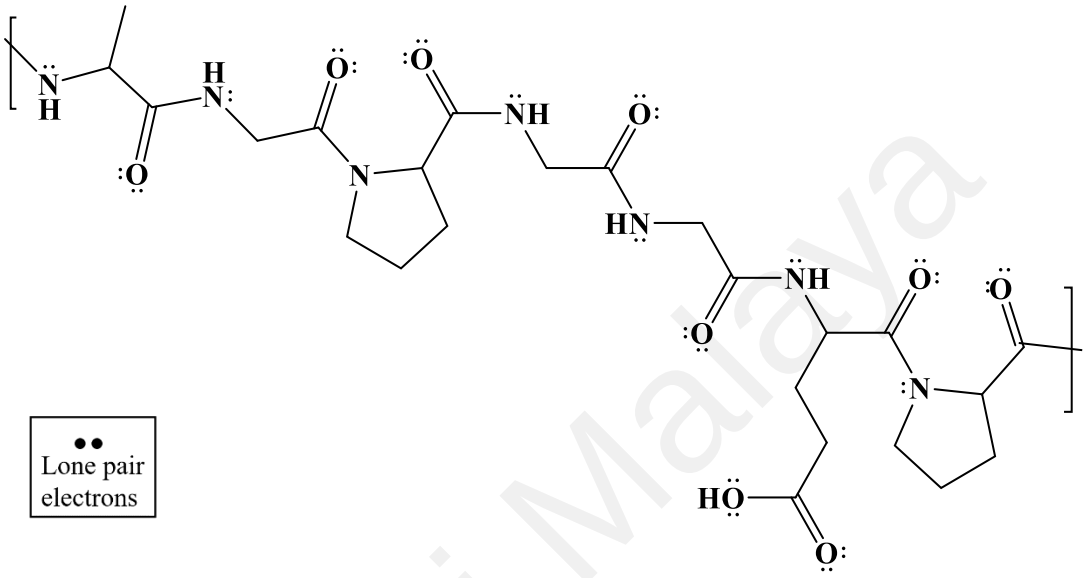

Figure 2.1: Structure of gelatin.

Table 2.2: Review of earlier works on gelatin-based polymer electrolytes.

Electrolyte	Highest conductivity at room temperature	References
Gelatin-$LiCLO_4$	3.58×10^{-6} S cm^{-1}	(Kadir, 2021)
Gelatin-CF_3SO_3-IL	1.18×10^{-4} S cm^{-1}	(Leones et al., 2012)
Formaldehyde gelatin-$LiClO_4$-glycerol	1.04×10^{-4} S cm^{-1}	(Ramadan et al., 2014)
Formaldehyde gelatin-LiCl-glycerol	2.02×10^{-4} S cm^{-1}	(Ramadan et al., 2014)
Gelatin-NH_4NO_3-glycerol	1.67×10^{-4} S cm^{-1}	(Aziz, et al., 2022)

Collagen has traditionally been extracted from the skin and bones of terrestrial mammals like cows and pigs (Liu et al., 2015). However, due to the bovine spongiform encephalopathy (BSE) and religious restrictions, its use has been limited (Liao et al.,

2018). Due to this concern, researchers are looking for a substitution to mammalian gelatin. Gelatin from fish skin has attracted much attention due to its diversity of aquatic species. The advantages of using aquatic animals include low disease risk, no dietary limitations, and high collagen yield (Jafari et al., 2020; Wang, 2021).

Processed by-products have also been thought of as potential substitute sources of collagen (Ahmad & Benjakul, 2010). Due to their capacity to create an extensible, almost colourless film, by-products from the fishing industry, such as heads, skin, bones, and scale, have recently come under consideration (Ramos et al., 2016) . As it produces between 70 and 85 percent of the entire catch weight in by products, the fish processing business has promising future (Salvatore et al., 2020). In order to reduce the amount of disposable trash, research has been conducted to examine the usage of collagenous fish waste in pharmaceuticals, cosmetic and food packaging items (Liu et al., 2021; Ramos et al., 2016).

However, studies on fish gelatin based solid polymer electrolytes are still very limited and not fully optimized. Kadir (2021) reported that fish gelatin doped with 25 wt. % of $LiClO_4$ has obtained a conductivity value up to 3.58×10^{-6} S cm^{-1}. Considering these research tendencies, the current work is intended to develop a new SPE based on fish gelatin that will be doped with ammonium salt to increase the ionic conductivity value.

2.6 Chitosan as host polymer in SPE

Chitosan is a natural linear polysaccharide with the average molecular weight of 100 – 500 kDa, which is derived from deacetylation of chitin in the presence of alkali

(Deshmukh et al., 2017). Chitosan is one of the natural abundant resources that is biodegradable, nontoxic, simple to use and possesses an excellent film forming ability as well as good mechanical properties (Hadi et al., 2021; Martins et al., 2012). Chitosan is mostly derived from shrimp waste and widely employed as a natural polymer in various applications, for examples, in biomedical material, drug delivery, waste water treatment and tissue engineering (Aziz et al., 2019; Koc et al., 2020;Wang et al., 2015). Figure 2.2, shows the chemical structure of chitosan (Martins et al., 2012).

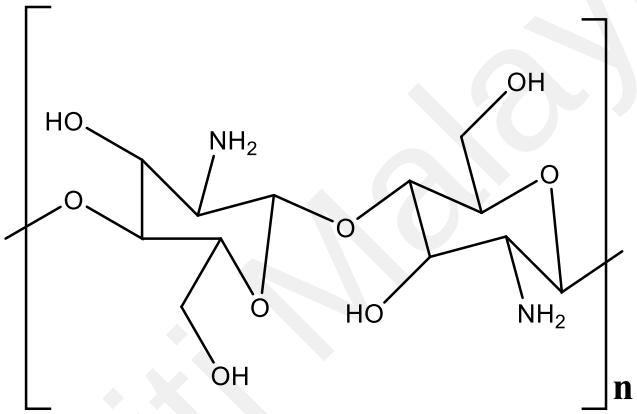

Figure 2.2: Structure of chitosan.

Chitosan contains free amino groups in its structure which make it able to dissolve in dilute aqueous acidic solvents (Deshmukh et al., 2017). The amine and hydroxyl groups on the backbones of chitosan promote a good complexation, chemical modification and salt dissociation which makes chitosan a good candidate as a polymer host for ionic conduction (Abdulwahid et al., 2022; Leo et al., 2021). Table 2.3 shows examples on the highest conductivity achieved in room temperature for chitosan-based polymer electrolytes from the previous studies. A key aspect of chitosan is its capacity to be moulded into a wide range of morphologies, including hydrogels, porous scaffolds, and films (Dannoun et al., 2021).

Table 2.3: Review of earlier works on chitosan-based polymer electrolytes.

Electrolyte	Highest conductivity at room temperature	References
CS-$MgCl_2$-glyerol	1.03×10^{-3} S cm^{-1}	(Hamsan et al., 2020)
CS-$LiCLO_4$-glycerol	1.20×10^{-3} S cm^{-1}	(Aziz et al., 2021)
CS-NaI	1.11×10^{-4} S cm^{-1}	(Rahman et al., 2021)
CS-$LiCO_2CH_3$-glycerol	5.19×10^{-4} S cm^{-1}	(Asnawi et al., 2020)

2.7 Polymer Blending

Developing a brand-new polymer can be a time consuming and expensive process, thus incorporating desirable properties from individual materials into polymer blends would be advantageous. It is well known that polymer blending can create new interactions that enhances the physical qualities of pure components (Qiao et al., 2017). Figure 2.3 depicts a cartoon illustration for the increment of amorphous region in polymer electrolyte after blending which in turns, increase the mobility of ion diffusions.

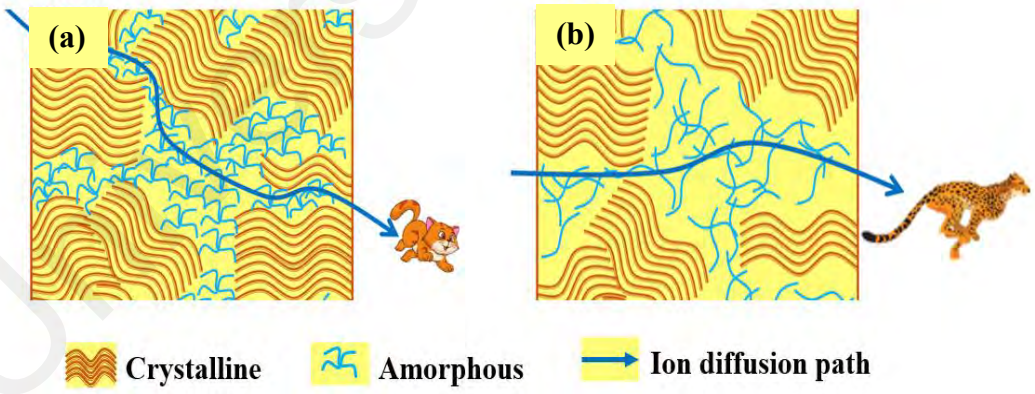

Figure 2.3: Cartoon illustration of polymer electrolyte (a) before and (b) after blending.

Depending on how much of each polymer is present in the mixture, the physical properties differ from those of the parent polymers and the compatibility of polymers in blend systems determines how effectively a property is modified (Toh et al., 2021). Galindo and co-workers (2019) have reported that polymer blending has effected the film

morphology, structure and as well as the electronic properties. Mazuki (2020) has reported that a single polymer based PVdf-HFP that has a conductivity value of PVdf blended with PMMA has increased from ~10^{-10} S cm^{-1} to ~10^{-7} S cm^{-1}. The conductivity value of chitosan as a single host as listed in Table 2.3 have improved as another polymer is blended with it. The improvement of the conductivity value due to blending chitosan with other polymers can be clearly observed in Table 2.4.

Table 2.4: Review of earlier works on blended chitosan-based polymer electrolytes.

Electrolyte	Highest conductivity at room temperature	References
CS-CMC-NH_4Br	2.12×10^{-5} S cm^{-1}	(Muhamaruesa & Mohd Isa, 2017)
CS-Dex-NH_4SCN	1.28×10^{-4} S cm^{-1}	(Kadir & Hamsan, 2018)
CS-PEO-$LiClO_4$	7.34×10^{-4} S cm^{-1}	(Aziz et al., 2019)
CS-Agar-$LiCLO_4$-PEG	4.56×10^{-4} S cm^{-1}	(Leo et al., 2021)
CS-PEO-$LiCLO_4$-glycerol	4.16×10^{-4} S cm^{-1}	(Dannoun et al., 2021)

2.8 Fish gelatin-chitosan as host polymer in SPE

There are few drawbacks reported pertaining to the usage of fish gelatin. Fish gelatin are basically has low mechanical strength, poor stability against moisture and poor water barrier properties (Hosseini et al., 2022). To produce solid polymer electrolyte, the film must have a good mechanical strength as well as good stability against moisture. It is well known that polymer blending can create new interactions that enhance the physical qualities of pure components (Qiao et al., 2017). Blending polymers instead of developing new polymer are more effective to achieve physical and chemical properties that are impossible to be achieved when using single polymers (Yahya et al., 2017).

The blending of polymers has the capability to reduce the crystalline nature of polymer electrolytes and can enhance the mobility of segments within the host polymer. This improvement is facilitated through interactions within the blend system, which encompass hydrogen bonding, ionic interactions, and dipole interactions (Polu et al., 2015). Blend system are effortless to prepare and the physical properties are easy to control through compositional change (Li et al., 2018). However, it is important that the blend system to be miscible to one and another in order to produce a solid polymer electrolytes system with better properties (Polu et al., 2015). Abdul Wahid and co-workers (2022) mentioned that by blending polymers, there will be more interaction sites for the ions to hop and exchange. Thus, with addition of salt into the blend system, the conductivity will increase compared to single polymer electrolytes system.

Fish gelatin has low resistance against water vapor permeation which can be resolved by blending with other polymers (Mousavi et al., 2021). Chitosan is a linear copolymer of glucosamine and N-acetyl-glucosamine in a β-(1-4) linkage that usually is obtained from chitin throughout deacetylation process (Leones et al., 2017). Chitosan has high mechanical strength, biodegradable, non-toxic, low production cost, good film forming abilities and able to dissolve ionic salts for SPEs applications (Leones et al., 2017; Wang et al., 2015; Yahya et al., 2017). Previous studies have shown that the blend of gelatin with chitosan able to improve the biological performances and physical properties (Wang et al., 2015). This combination have been widely studied in biomedical applications such as drug carriers and drug release, and tissue engineering scaffolds (Jătariu et al., 2011). Hence, combining gelatin with chitosan to create biocomposites with unique characteristics appeared to be a promising method (Wang et al., 2015). Compared to pure gelatin films, the mechanical and physical properties of the composite

films made from gelatin and chitosan are observed to be improved (Fakhreddin et al., 2013; Jridi et al., 2014; Nagahama et al., 2009).

Roy and Rhim (2021) combine chitosan and gelatin with addition of CEO and rutin shows that the film has a strong antibacterial and antioxidant activity which used in active packaging applications. Previous studies have shown that the blend of chitosan and gelatin are able to be applied as biodegradable food packaging with good physical properties (Liu et al., 2020; Yeddes et al., 2020). This blend has also penetrated wound dressing market. Because of their good film forming property, non-toxic, biodegradable and biocompatible, these combinations have proven could improve the healing effect of wound fabricated from them (Kenawy et al., 2019).

It has been demonstrated that gelatin and chitosan could produce hydrogen bonds as well as electrostatic interactions (Taravel & Domard, 1995). Moreover, numerous complexes of the two biopolymer molecules are formed as a result of these promising interactions (Yin et al., 2005). Gelatin and chitosan are compatible and the miscibility between gelatin and chitosan to produce a wide range of solutions and films are reported to be promising (Qiao et al., 2017). Voron and co-workers (2016) confirmed the occurrence of electrostatic interaction between positively charged amino-groups in chitosan and negatively charged amino acid Glu and Asp residues in gelatin and hydrogen bonds for the blend polymer. Certain chitosan disadvantages such as lack of elasticity has come to attention and due to that problem chitosan is altered by blending with other polymers (Mousavi et al., 2021). However, the study on fish gelatin blend with chitosan still relatively new thus this research aims to investigate the effects of blending fish gelatin with chitosan in polymer electrolyte system.

2.9 Ammonium salt-ammonium nitrate as proton donor

Various salts such as lithium, sodium, silver and ammonium salt have been utilised as ionic dopants (Ge et al., 2021; Mohd Asnawi et al., 2020). The most common ionic dopants is lithium salt which are relatively expensive, reactive to water, and can cause harmful effects at high temperatures (Osman et al., 2012). Solvents that can dissolve inorganic salts such as sodium and potassium iodide are very limited. Therefore, the usage of ammonium salt is an excellent alternative for a cheaper and uncomplicated to handle (Hamsan et al., 2019). Kumar and co-workers (2012) also reported that ammonium salts has the ability to produce a flexible film that is desired for a good conductor.

It has been reported that the loosely bound H^+ ion from ammonium cations (NH_4^+) are good proton donors that responsible for ionic conductivity (Shenbagavalli et al., 2022). Some ammonium salt is chosen due to its low lattice energy, its low in price (Dennis et al., 2022), and relatively high conductivity. Examples of ammonium salts that have been previously doped in SPE are ammonium iodide (NH_4I) (Aziz et al., 2021), ammonium bromide (NH_4Br) (Hamsan et al., 2020), ammonium thiocyanate (NH_4SCN) (Kadir & Hamsan, 2018) and ammonium nitrate (NH_4NO_3) (Saeed & Abdullah, 2020). Beside enhancement of ionic conductivity, it is also crucial to preserve the flexibility of the SPE by controlling the amount of salt into the polymer (Hassan et al., 2018). Low lattice energy type of ammonium salts with less than 600 kJ mol^{-1}, are considered not suitable for the fabrication of polymer electrolyte membranes due to ion association between anions and cations (Mohamad et al., 2020).

Motivated by these findings, solid biopolymer electrolyte in the present work will be impregnated with NH_4NO_3 to serve as ion dopant. NH_4NO_3 embodied lower lattice energy of 648.9 kJ mol^{-1} which is still lower than other ammonium salts such as NH_4Cl and NH_4Br, which have lattice energies of 698 kJ mol^{-1} and 655 kJ mol^{-1}, respectively, (Mohamad et al., 2020). It has been demonstrated that NH_4NO_3 has the ability to boost up the conductivity of a polymer host, such as methylcellulose (Abdullah et al., 2020) from $\sim 10^{-11}$ S cm^{-1} to $\sim 10^{-5}$ S cm^{-1} and polyvinyl alcohol (Saeed & Abdullah, 2020) from $\sim 10^{-9}$ S cm^{-1} to $\sim 10^{-5}$ S cm^{-1}.

CHAPTER 3: METHODOLOGY

3.1 Introduction

In this work, three systems of fish gelatin-salt (FG-NH_4NO_3), fish gelatin-chitosan (FG-CS) and fish gelatin-chitosan-salt (FG-CS-NH_4NO_3) were prepared. Ammonium nitrate (NH_4NO_3) was used as dopant to provide the charge carriers (H^+). All solid biopolymer electrolytes were prepared using solvent-casting method. The fish FG-CS films were developed to determine the most suitable ratio to be chosen as the polymer host based on the degree of crystallinity. The blend with lowest degree of crystallinity was further doped with NH_4NO_3. Then, the properties of biopolymer electrolytes were characterized using several techniques such as electrochemical impedance spectroscopy (EIS), Fourier transform infrared (FTIR), X-Ray diffraction (XRD), thermogravimetric analysis (TGA), differential scanning calorimetry (DSC) and field emission scanning electron microscopy (FESEM).

3.2 Materials

The substances employed in this investigation comprises of gelatin extracted from cold-water fish skin (solid, bioreagent: G7041), chitosan with degree of deacetylation >75% acquired from Sigma-Aldrich, and ammonium nitrate with a molecular weight of 80.04 g mol^{-1} obtained from Systerm. Distilled water served as the solvent for the initial system, while 1 % acetic acid (Sigma Aldrich) was introduced for the second and third systems. All materials were utilized without any supplementary processing.

3.3 Sample Preparation

3.3.1 Fish gelatin-NH_4NO_3 System

The electrolytes were prepared by the solvent-casting method. The host polymer, FG with mass of 2g was dissolved in 100 mL of deionize water. The solution was then stirred using magnetic hot plate bar stirrers up to 60 °C for a complete dissolution. Then, different amount of NH_4NO_3 ranging from 5 wt. % to 40 wt. % were added into the solution. The mixtures were then stirred using magnetic bar stirrers until homogenous solutions were obtained. The solutions were then casted in different plastic Petri dishes and left to dry at room temperature in a drying cabinet. Figure 3.1 shows a solid transparent membrane after the solutions has dried. Then, all samples were peeled out and kept in a desiccator filled with silica gel desiccants for further drying process. Table 3.1 summarizes the compositions of the polymer.

Table 3.1: The composition of FG-NH_4NO_3 solid polymer electrolytes.

Sample designation	FG (g)	NH_4NO_3 (wt. %)	NH_4NO_3 (g)
FG0	2	0	0.000
FG5	2	5	0.105
FG10	2	10	0.222
FG15	2	15	0.353
FG20	2	20	0.500
FG25	2	25	0.667
FG30	2	30	0.857
FG35	2	35	1.077
FG40	2	40	1.333

3.3.2 Fish gelatin-chitosan System

Chitosan and fish gelatin with different percentages were dissolved in two different glass beakers, each containing 50 mL of 1 % acetic acid. Both beakers were

stirred using magnetic bar stirrer for 2 hours. Then, the solutions were mixed and continuously stirred until homogenous solutions were obtained. The solutions were then casted in different plastic Petri dishes and left to dry at room temperature in a drying cabinet. Solid transparent membranes were obtained after the solutions has dried. Then, all samples were peeled out and kept in a desiccator filled with silica gel desiccants for further drying. Figure 3.1 presents the sample on the petri dish for (a) FG0, (b) C10 and (c) CF4. Table 3.2 summarizes the compositions of the FG-CS polymer blend system.

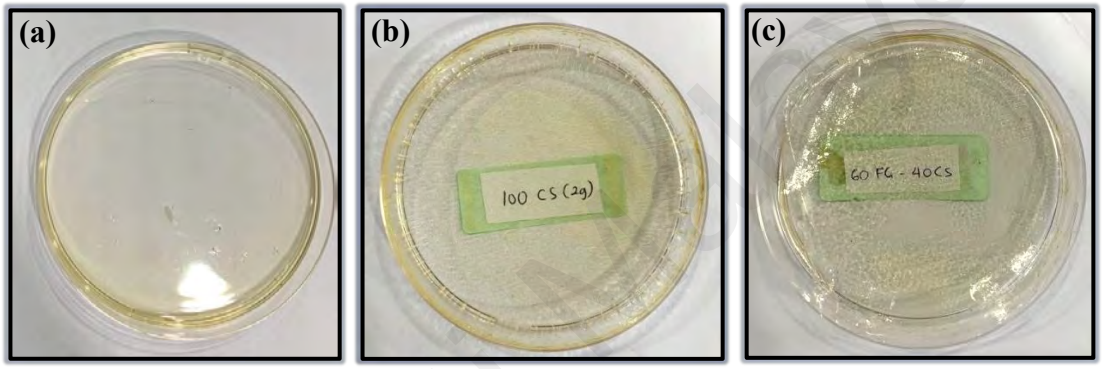

Figure 3.1: Film of selected samples (a) FG0, (b) C10, and (c) CF4.

Table 3.2: The composition of FG-CS solid polymer electrolytes.

Designations	Fish gelatin: Chitosan (%)	Polymer Blend	
		Fish Gelatin (g)	Chitosan (g)
FG0	100:0	2	0.0
CF1	90:10	1.8	0.2
CF2	80:20	1.6	0.4
CF3	70:30	1.4	0.6
CF4	60:40	1.2	0.8
CF5	50:50	1.0	1.0
CF6	40:60	0.8	1.2
CF7	30:70	0.6	1.4
CF8	20:80	0.4	1.6
CF9	10:90	0.2	1.8
C10	0:100	0.0	2.0

3.3.3 Fish gelatin-chitosan-NH_4NO_3 System

The blend with the lowest degree of crystallinity in FG-CS system was chosen as the polymer host. Different amounts of NH_4NO_3 ranging from 5 wt. % to 60 wt. % were added into the FG-CS solution and stirred until the solutions become homogenous. All solutions were casted onto Petri dishes and left to dry to form films. All the films were kept in desiccator filled with silica gel desiccants to eliminate extra moisture. Based on XRD analysis, the film with the lowest degree of crystallinity was found to be CF4 with 60 wt. % of fish gelatin and 40 wt. % of chitosan. Table 3.3 shows the compositions and designations for FG-CS-NH_4NO_3.

Table 3.3: The composition of FG-CS-NH_4NO_3 solid polymer electrolytes.

Sample designation	FG (g)	NH_4NO_3 (wt. %)	NH_4NO_3 (g)
CF4	2	0	0.000
CFs10	2	10	0.222
CFs20	2	20	0.500
CFs30	2	30	0.857
CFs40	2	40	1.333
CFs50	2	50	2.000
CFs60	2	60	3.000

3.4 Electrolytes Characterization

3.4.1 X-Ray Diffraction (XRD)

XRD is a rapid analytical technique which is commonly used to determine the atomic arrangements of crystal or amorphous structures of a material. X-ray diffraction is basically occurred based on constructive interference of monochromatic X-rays and a crystalline sample. The interaction of the incident rays with the sample produces

constructive interference (and a diffracted ray) when conditions satisfy Bragg's Law as shown below:

$$n_B\lambda_B=2d_B \sin \theta_B \quad \text{(Equation 3.1)}$$

where n_B is the whole number of wavelengths, λ_B is the wavelength of the rays, d_B stands for the spacing between layers of atoms and θ_B stands for the angle between the incident rays and the surface of the crystal. This law relates the wavelength of electromagnetic radiation to the diffraction angle and the lattice spacing in a crystalline sample.

Siemens D5000 X-ray diffractometer was employed with 2θ from 5° to 80° at 0.1° resolution. These diffracted X-rays are then detected, processed, and counted. All the data were then deconvoluted using OriginPro8 software to separate the crystalline and amorphous peaks. The R-square value for the fitting must be >0.96. Degree of crystallinity for selected electrolytes were determined from the results obtained.

3.4.2 Fourier Transform Infrared Spectroscopy (FTIR)

FTIR was used to identify the chemical bonds in a molecule by producing an infrared absorption spectrum where the interactions among the materials were studied. Infrared radiation was passed through a sample. Some radiation was absorbed, and some was transmitted. FTIR provided information based on chemical composition and physical state of the whole sample as it is sensitive to the changes in molecular structure. The FTIR studies were performed using Spotlight 400 Perkin-Elmer spectrometer in the wavenumber ranged from 500 cm^{-1} to 4000 cm^{-1} at a resolution of 1 cm^{-1}. FTIR was done at room temperature. In this work, FTIR studies were analysed to confirm the interactions between the fish gelatin-NH_4NO_3, fish gelatin-chitosan and fish gelatin-chitosan-NH_4NO_3.

3.4.3 Field Emission Scanning Electron Microscope (FESEM)

FESEM is a type of electron microscope that produces images of a sample by scanning the surface with a focused beam of electrons. The electrons were interacted with atoms in the sample, producing various signals that contain information about the surface topography and composition of the sample. In this work, Hitachi SU8220 was used to conduct the analysis at ×1.5 k and ×2.0 k magnification for both cross-sections and surfaces of the polymer electrolytes, respectively. FESEM provided high resolution of images that are useful for evaluating the surface of the materials. FESEM micrographs helped to shed some light to explain the trend in conductivity.

3.4.4 Electrochemical Impedance Spectroscopy (EIS)

Electrochemical Impedance is a measurement of current that pass through a cell after applying an AC potential to an electrochemical cell. The polymer electrolyte films were cut into small pieces and sandwiched between a stainless-steel electrode with area of 2.01 cm^2 as in Figure 3.2.

Figure 3.2: Stainless steel holder for EIS testing.

The impedance of the films was measured using HIOKI 3532-50 LCR Hi-Tester. The frequency was selected between 50 Hz to 5 MHz from 298 K to 373 K. Then, the

data was plotted and value of the bulk resistance, R_B was obtained from Nyquist Plot. R_B value was used to find the conductivity σ, of the electrolyte via the equation:

$$\sigma = \frac{t}{R_B A} \qquad \text{(Equation 3.2)}$$

where t is the thickness of sample and A is the area of electrode-electrolyte contact. The thickness of the film will be measured using a digital micrometre. From the impedance data obtained, other properties can also be determined for example dielectric properties and transport properties.

3.4.5 Thermogravimetric Analysis (TGA)

Thermogravimetric analysis (TGA) is one of the methods used to study thermal properties. Different materials have different decomposition temperatures. The decomposition temperature was altered when salt was impregnated into the polymer electrolyte. The thermal stability of polymer electrolytes and the films' moisture content was determined from the thermogram curve. The thermal degradation temperature and the amount of weight loss were detected from the curve. TGA were performed using simultaneous thermal analyser (STA-6000) from Perkin Elmer. The sample weight around 5 mg was heated from room temperature up to 700 °C at a heating rate of 10 °C/min in a nitrogen gas flow.

3.4.6 Differential Scanning Calorimetry (DSC)

DSC is a thermal analysis to measure the change in physical properties as a function of temperature and time. Segmental motion is one of the crucial components in ionic conduction. Ionic conduction is more efficient in electrolytes that have a better segmental motion. Segmental motion was analysed using glass transition temperature

(T_g). In DSC analysis, T_g was determined from the graph of temperature against heat flow. TA Instruments Q200 was used with the operating temperature ranging from -40 °C to 150 °C, 150 °C to 0 °C and 0°C to 150 °C at 10 °C min^{-1} respectively in 50 ml min^{-1} nitrogen gas of heating / cooling / heating rate. The samples were sealed in aluminium pan with range of 5 mg to 8 mg with reference pan sit together on a heater. The first heating process is to remove traces of water.

3.4.7 Transference Number Analysis

The conducting species in electrical conductor can be identified using transference number analysis (TNM). V&A Instrument DP3003 was employed in order to determine whether the major contribution in this electrolyte comes from ion or electron. A constant 0.80 V was applied to polarize the cell. The highest conducting electrolyte was sandwiched between stainless steel (SS) with the configuration of SS|electrolyte|SS at room temperature.

3.4.8 Linear Sweep Voltammetry (LSV)

Electrochemical potential stability evaluation is one of the requirements for polymer electrolytes to be used in energy storage devices. The conducting electrolyte's decomposition potential was calculated from the LSV response. Digi-IVY DY2300 potentiostat was used to study the limiting voltage of the electrolyte. Both working and counter electrodes used were stainless steel where the arrangement of the cell for LSV analysis was SS|electrolyte|SS. The scan rate of 1 mV s^{-1} from 0 to 2.20 V was used at room temperature.

CHAPTER 4: FISH GELATIN-SALT SYSTEM

4.1 Introduction

This chapter will discuss the results of employing fish gelatin as a host for polymer electrolytes, doped with ammonium nitrate, NH_4NO_3. Several techniques have been used to study the physical and electrical properties of the polymer electrolyte system.

4.2 X-Ray Diffraction (XRD)

Studies have shown that electrolytes with high amorphous region exhibited a better conductivity values (Naachiyar et al., 2021; Shukur & Kadir, 2015). Therefore, XRD analysis will be very handy to determine the electrolytes amorphous region in order to strengthen and to confirm the evaluation of conductivity studies. Figure 4.1 represents the XRD pattern of bare fish gelatin film, FG0, which is used as the reference.

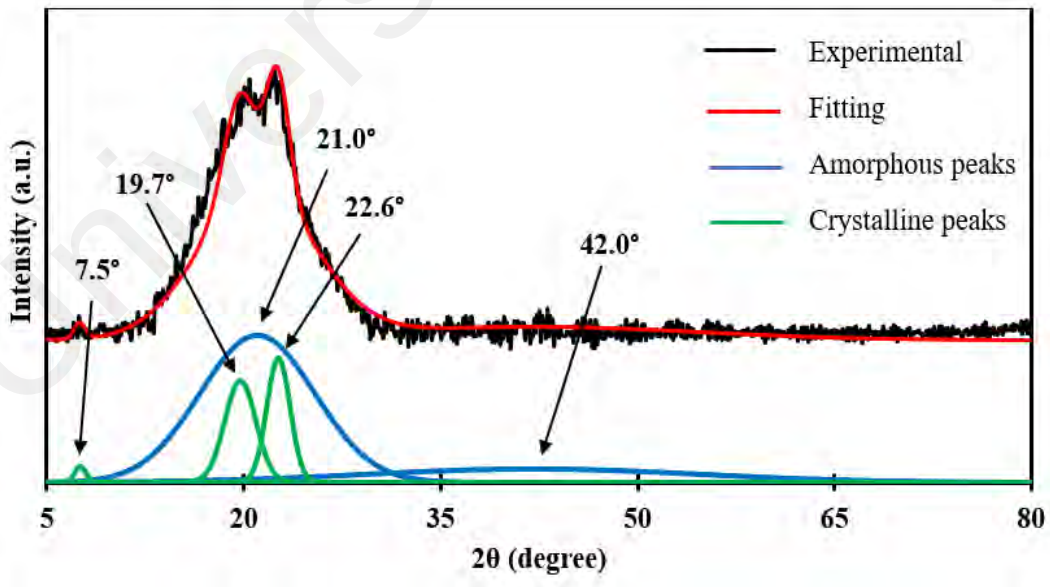

Figure 4.1: Deconvoluted XRD patterns of FG0.

To distinguish the crystalline sharp peaks from the amorphous broad peaks, the original graph was fitted using Gaussian distribution via OriginPro8 software, resulting

in the green and blue lines, respectively. This analysis known as deconvoluted XRD, provides a detailed characterization of the film's structure. The deconvoluted XRD pattern of FG0 exhibits prominent crystalline peaks at 2θ = 7.5°, 19.7° and 22.6° which aligned with the previous studies that have identified similar peaks of fish gelatin (Kadir, 2021).

Figure 4.2 represents the XRD pattern for FG15. It can be observed that the amorphous peak at 21.0° for FG0 previously has shifted to 21.5° when 15 wt. % NH_4NO_3 is added. Meanwhile, the crystalline peaks at 19.7° and 22.6° have down shifted to 19.9° and 22.4°, respectively which suggests that there are formation of complexation occurred between polymer and salt (Aziz et al., 2020). The crystalline region decreased as salt concentration increased from 0 wt. % to 25 wt. %.

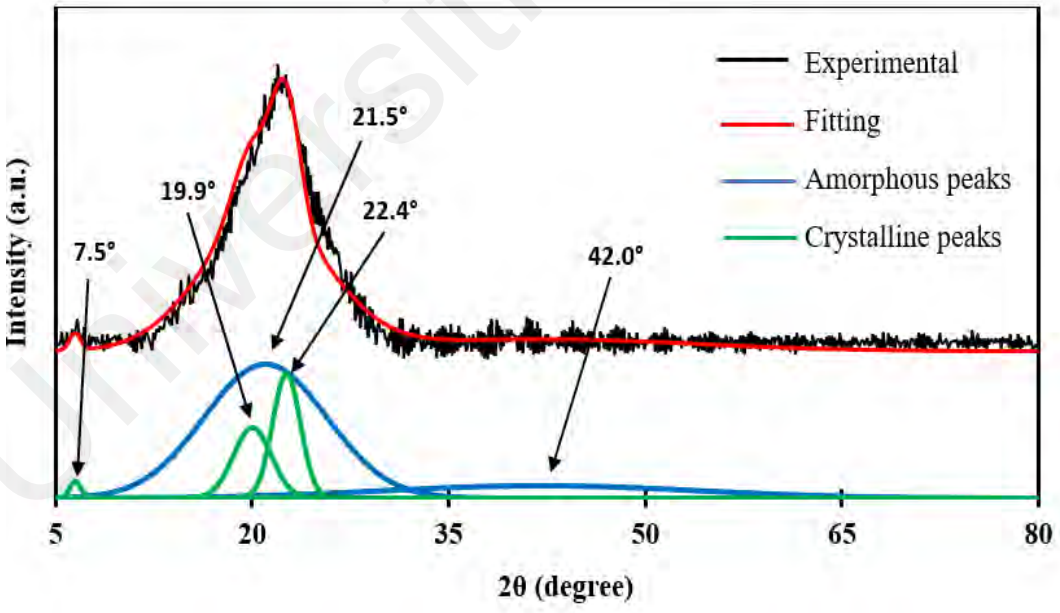

Figure 4.2: Deconvoluted XRD patterns of FG15.

Figure 4.3 displays deconvoluted XRD pattern for FG25 that shows similar trend as FG15 where shifting in peaks positions occurred and the crystalline region also decreased indicating that the salt has fully dissolved in the electrolytes (Ge et al., 2021). As the concentration of NH_4NO_3 increases from 0 wt. % to 25 wt. %, dissociation of ions become greater, thus led to an increase in amorphous region of the electrolyte film.

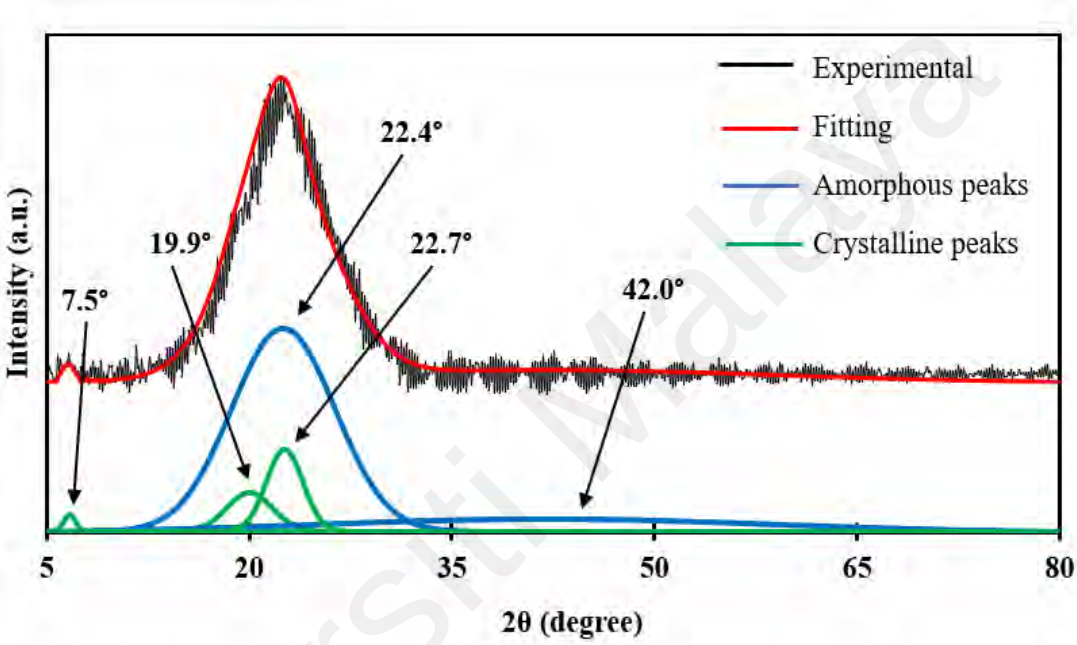

Figure 4.3: Deconvoluted XRD patterns of FG25.

This finding highlight that more ions have formed complexes with the functional groups of the polymer host. Such behaviour is highly desirable as it contributes to an increase in conductivity (Moniha et al., 2018). Ghazali and his co-workers (2022) reported that the addition of NH_4NO_3 to the electrolyte could be the cause of distortion in XRD spectra which proved that the presence of salt on the electrolyte would change the patterns. According to the authors, the distortion was a result of a negatively charged electron pairs of -COO- and the detachment of NH_4^+ ion that has been detached from NH_4NO_3. These bonds disruption contributed to the amorphous characteristic of the system (Ghazali et al., 2022).

Figure 4.4 depicts the XRD pattern of the fish gelatin system with the additional of 30 wt. % of NH_4NO_3. It can be detected that the XRD spectrum displays sharp peaks. Additional crystalline peaks are observed at 2θ = 22.5°, 28.8°, 32.8° and 39.8°, which corresponds to the crystalline NH_4NO_3 peaks. The presence of these peaks indicates the existence of undissociated salts in the samples which is consistent with the previous findings by Moniha and co-workers (2018).

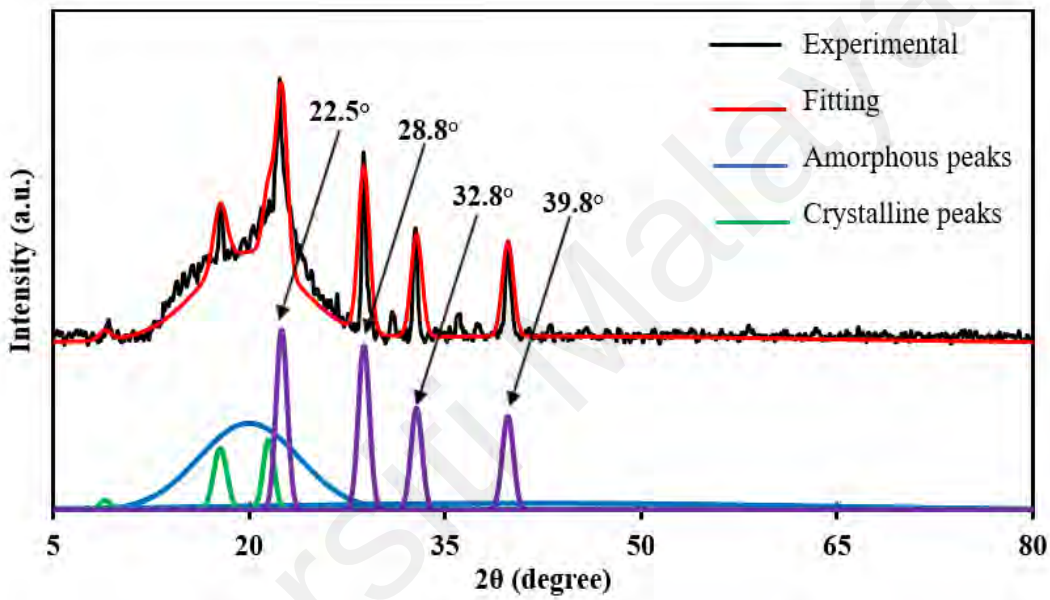

Figure 4.4: Deconvoluted XRD patterns of FG30.

According to the same authors, the cations (NH_4^+) and anions (NO_3^-) reassociated back to form ammonium salt that is protruded out of the sample surface. Saeed and Abdullah (2020) also noticed a similar NH_4NO_3 salt peaks in the XRD pattern, which can be attributed to the recrystallization phenomenon with increasing salt concentration. However, it is important to note that an increase in crystallinity will not benefit electrolytes system as it contributes to a decrease in conductivity value (Saeed & Abdullah, 2020).

The XRD spectra demonstrate a correlation with the physical appearance of the polymer electrolyte films that have been formed. Figure 4.5 (a) illustrates the physical appearance of FG0, where the absence of salt results in a transparent film. In the case of FG15 and FG25 as presented in Figure 4.5 (b) and (c), respectively, the addition of 15 wt. % and 25 wt. % of NH_4NO_3 to the system yields transparent films, indicating good compatibility between the polymer and salt within this range. This observation is comparable with previous studies on gelatin-based samples (Ramadan et al., 2014). However, Figure 4.5 (d) shows that the addition of 30 wt. % of NH_4NO_3 had dramatically transform the physical appearance of FG30 revealing an opaque film. The presence of 30 wt. % of NH_4NO_3 have made the electrolyte film more crystalline inferring that undissolved salt particles remain within the mixture.

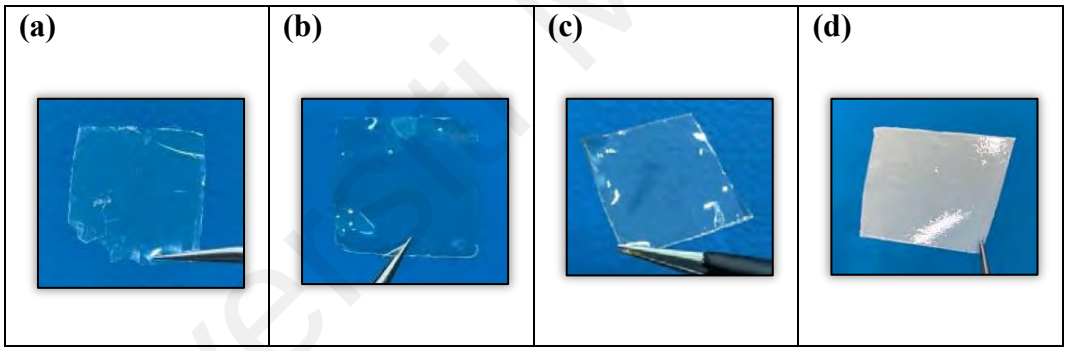

Figure 4.5: The physical appearance of electrolyte film (a) FG0, (b) FG15, (c) FG25 and (d) FG30.

To determine the most amorphous film, the degree of crystallinity (X_c) crystallite is determined using the following Equations 4.1. The data are tabulated in Table 4.1:

$$X_c = \frac{P_c}{P_c + P_a} \times 100\% \qquad \text{(Equation 4.1)}$$

where P_c is the areas of crystalline peaks and P_a is the areas of amorphous peaks.

Table 4.1: Parameters obtained from the deconvolution analysis of XRD patterns.

Electrolyte	X_c (%)
FG0	26.18
FG15	19.94
FG20	17.23
FG25	15.77
FG30	37.98
FG35	39.96

It is apparent from the Table 4.1 that the % of X_c have dropped from 26.18 % to 15.77 % for FG0 and FG25 respectively. This could be due to the presence of salt disrupting the crystalline structure of the fish skin gelatin resulted in higher amorphous region in the polymer electrolyte (Moniha et al., 2018). In this work, the lowest X_c which demonstrate the smallest crystallite size was also found in FG25. As the amount of salt increases, the cohesive force between the polymer host and salt is disrupted initiated in the decrement of X_c (Hafiza & Isa, 2020). With the addition of more than 25 wt. % of NH_4NO_3, the X_c increases which confirmed by the XRD spectra that shows additional crystalline peaks emerged due to the recrystallization of salt on the surface of the films. From XRD studies, in this FG-NH_4NO_3 system, FG25 is found to be the most amorphous region with the least degree of crystallinity.

4.3 Fourier Transform Infrared (FTIR)

Interactions between ions in an electrolyte solution are generally known to be a factor that will modify the vibrational modes of molecules. In order to study the interactions in polymer electrolyte, many researchers has agreed that FTIR analysis could be one of the useful tool that can be used to investigate the interactions that are defined

by the shifting of peaks or changes in peak intensity (Basu & Tarafdar, 2016; Kadir, 2021; Nuvoli et al., 2021). Figure 4.6 depicts the FTIR spectra of fish skin powder and pure fish gelatin film (FG0). It can be observed that IR absorption bands such as amide A, B, and I-VII are presence that could be induced by the proteins and polypeptides in gelatin (Hidayati et al., 2021). As fish skin dissolved in distilled water, amide A peak becomes more intense. This could be due to the interaction of water with hydroxyl band in fish skin powder. The intensity of other peaks such as amide I and amide II also show a notable increase. The peaks found in Figure 4.6 agrees relatively well with several previous studies as listed in Table 4.2.

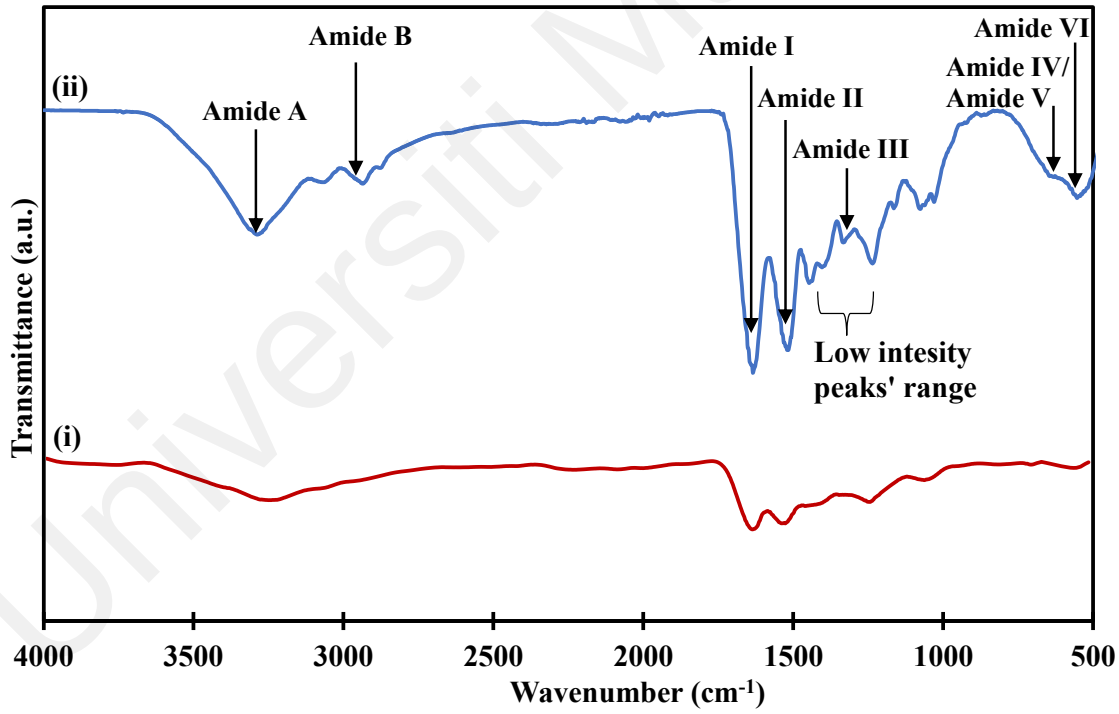

Figure 4.6: FTIR spectra of (i) fish skin powder and (ii) FG0.

Table 4.2 shows the nature of bond that are corresponded to their respected frequency. The peaks observed in Figure 4.6 revealed that amide A and amide B groups are found in the gelatin polymer with broad peak observed in the frequency range of 3100

cm^{-1} to 3500 cm^{-1} and 2894 cm^{-1} to 3000 cm^{-1}, respectively. It can be detected that high intensity peaks of 1630 cm^{-1} and 1530 cm^{-1}, are found in the amide I and amide II groups, respectively. However, low intensity peaks can be observed in the absorption band situated in between 1250 cm^{-1} and 1500 cm^{-1} as observed in Figure 4.6. Similar peaks for gelatin were identified by Abisharani and co-workers (2021) between 1250 cm^{-1} and 1500 cm^{-1}. The authors also stated that this range is attributable by aliphatic C-H bending vibration.

Table 4.2: Characteristics of IR bands

Frequency (cm^{-1})	Nature of Bond	Type	References
3100-3500	N–H stretching with hydrogen bonding	Amide A	(Abisharani et al., 2021; Basu & Tarafdar, 2016; Kadir, 2021; Nuvoli et al., 2021)
2800-3000	CH_2 symmetric and antisymmetric stretching	Amide B	
1600-1690	C=O stretching	Amide I	
1480-1575	Bending vibration of N–H groups and stretching vibrations of C–N groups	Amide II	
1200-1340	C–N stretching vibrations coupled to N–H in-bending vibrations	Amide III	
626-767	OCN bending	Amide IV	
640-800	NH bending	Amide V	
537-606	C=O bending	Amide VI	
200	Skeletal movement	Amide VII	

Figure 4.7 depicts a selected FTIR spectra obtained for various NH_4NO_3 contents, ranging from 0 wt. % to 30 wt. %. Figure 4.7 (a) focuses on FTIR spectra region from 1100 cm^{-1} to 1500 cm^{-1} whilst Figure 4.7 (b) represents the FTIR spectra region from 600 cm^{-1} to 1000 cm^{-1}. From Figure 4.7 (a), the peak of amide III has shifted to a

lower wavenumber, from 1336 cm^{-1} to 1306 cm^{-1}, as salt content increases from 0 wt. % to 25 wt. %, respectively. Conversely, the peak at 1306 cm^{-1} for FG25 has shifted to a higher wavenumber, to 1308 cm^{-1} for FG30. Amide III that corresponds to C-N stretching vibrations connected to N-H bending vibrations is listed in Table 4.2 (Ahmad & Benjakul, 2011).

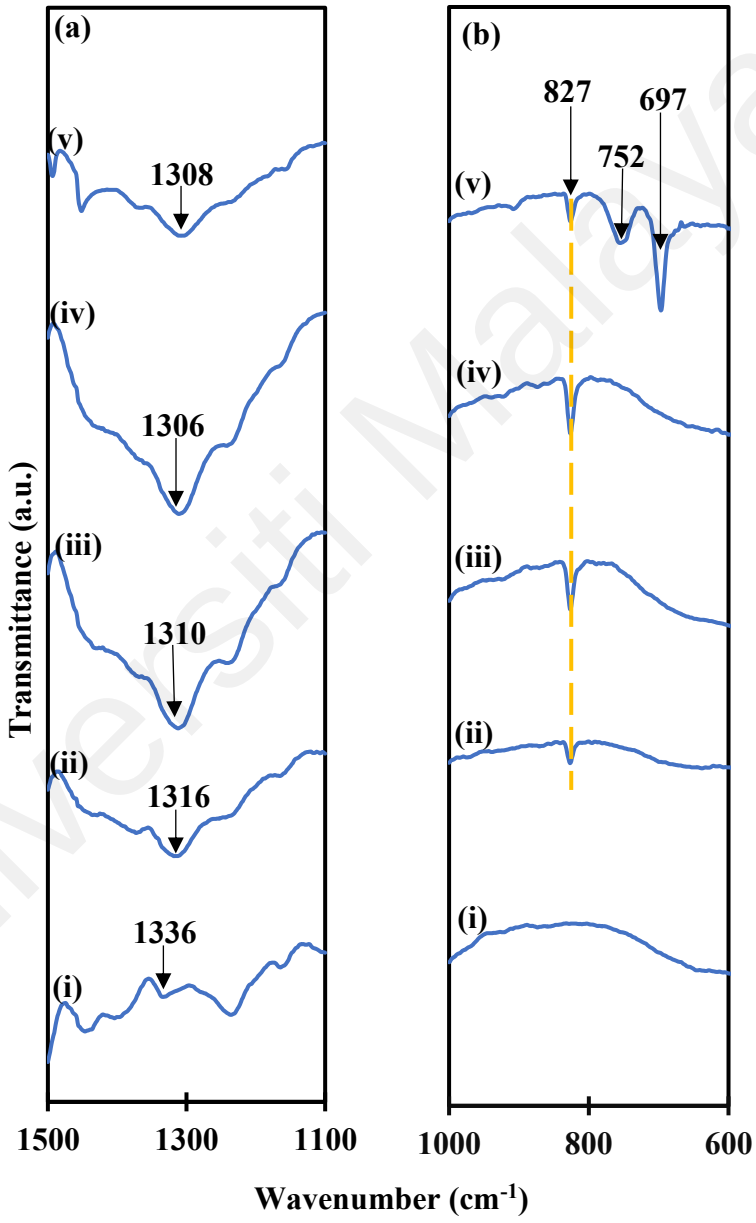

Figure 4.7: FTIR spectra with various salt amount of FG-NH_4NO_3 in (a) 1100 – 1500 cm^{-1} spectra region, (b) in 600 – 1000 cm^{-1} spectra region for (i) FG0, (ii) FG15, (iii) FG20, (iv) FG25 and (v) FG30

The shift indicates occurrence of complexation between atoms in the amide III functional group and H^+ from the salt. More cations are available to interact with the atoms as more salt is added into the system. The interactions causing wavenumber shifts that infers conductivity increment as more interactions occurred in the polymer electrolyte. The research study by Hamsan and co-workers (2017), also found that as the wavenumber of the complexes shifted to a lower value, the conductivity values increases as the salt concentration rises.

Figure 4.7 (b) exhibits a new peak that is attributed by the introduction of NH_4NO_3, which appears at 827 cm^{-1}. Notably, in the case of FG0, spotless peak is observed in this region as the peak observed in this region is attributed to the symmetric bending mode of NO_3^- from the NO group that comes from the salt (Kadir et al., 2011; Moniha, 2018; Shuhaimi et al., 2012). As NH_4NO_3 is added to the system, the peak's intensity rises but does not significantly shift to a higher or lower wavenumber. The findings suggest that the polymer host and NO_3^- anions did not interact, as indicated by a steady wavenumber (Kadir et al., 2011). With 30 wt. % of salt added into the system, additional significant peaks at 752 cm^{-1} and 697 cm^{-1}, which related to NO_3^- ion peaks emerged as obtained in FG30 spectrum (Hamsan et al., 2017). This observation consistent with the XRD findings for FG30 presented in Figure 4.4, which confirm the occurrence of salt recrystallization. The possible interactions between FG-NH_4NO_3 are illustrated in Figure 4.8.

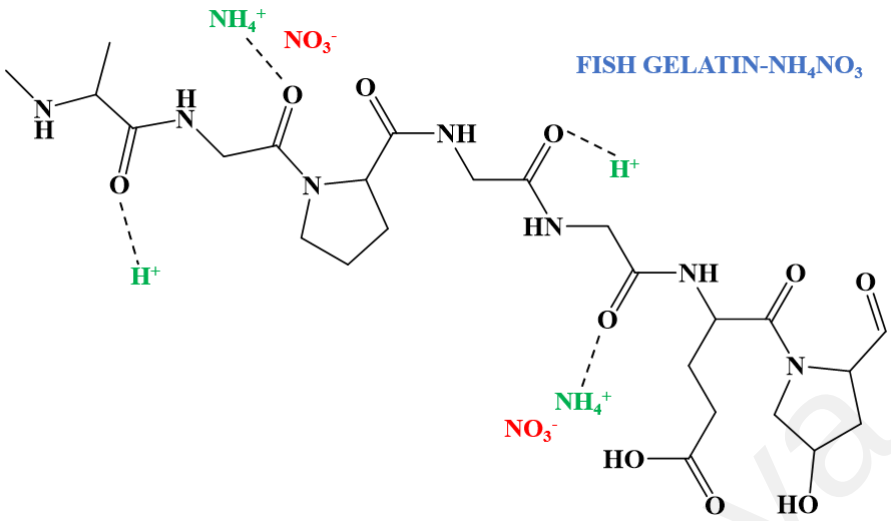

Figure 4.8: Illustration for possible interactions between FG-NH_4NO_3.

4.4 Field Emission Scanning Electron Microscopy (FESEM)

FESEM is used to analyse the change in surface morphology when various amounts of NH_4NO_3 is impregnated into the fish gelatin polymer electrolyte. In this research, a smooth and homogenous surface is observed for FG0 as shown in Figure 4.9. The studies from previous research showed that the surface of gelatin depends on the method of extraction.

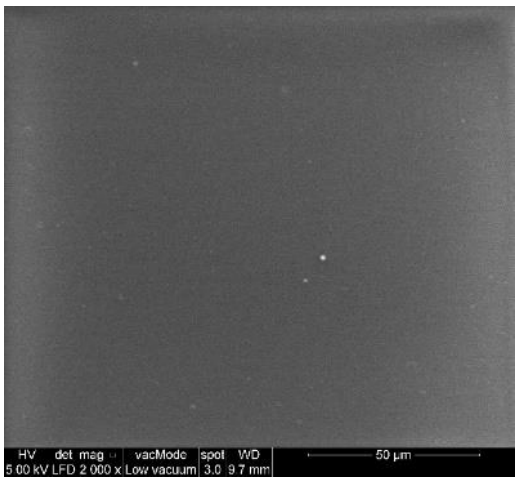

Figure 4.9: Surface morphology for FG0.

Sghayyar and co-worker (2020) reported that the gelatin surface from tilapia fish that extracted via ultra-sonication and lyophilization have a lamellar structure with wrinkled morphologies. However, a smooth, homogeneous and compact surfaces were discovered by other authors employing hot water extraction from fish scales (Wu et al., 2018) and casting method of gelatin powder obtained from Sigma-Aldrich.

Figure 4.10 (a) and Figure 4.10 (b) illustrates the surface morphology for FG15 and FG20, respectively. As salt is added into the system, the surface exhibited a small grain structure that can be considered as ion traps in the polymeric network (Kadir et al., 2010). Arof and co-worker also claimed that the grain dispersed on their electrolyte surface to be the ion trap has assists the electrolyte conductivity (Arof et al., 2011). This texture also indicates that there is a higher number density of ions with the addition of salts and a good compatibility between the polymer host and the salt (Kadir, 2021; Qiang et al., 2018).

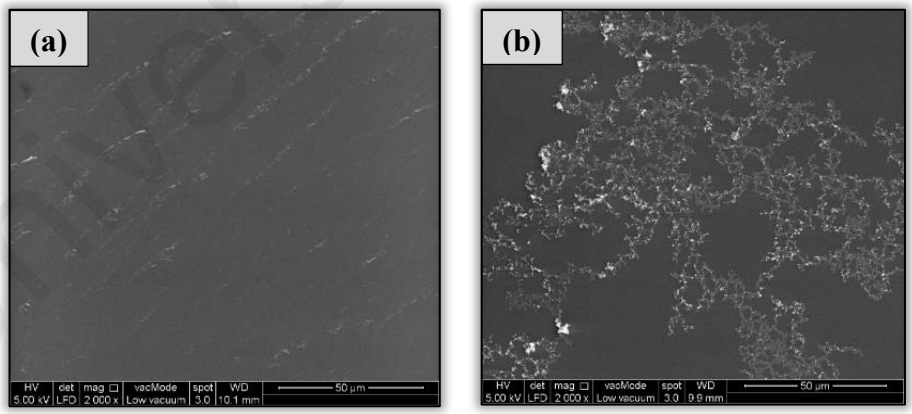

Figure 4.10: Surface morphology for (a) FG15 and (b) FG20.

Therefore, it can be assumed that NH_4NO_3 is able to successfully be embedded into fish gelatin polymer host. The electrolytes become more amorphous as the surface has changed to a denser structure and improved the segmental properties of the polymer which assists the increment of conductivity value (Kadir & Hamsan, 2018).

Based on XRD result, FG25 possesses the lowest degree of crystallinity and no obvious crystalline peaks that is contributed by NH_4NO_3. However, the size of the grain has become larger on the surface of FG25 as shown in Figure 4.11 (a) that in return increase the number of ion traps which will boost up the conductivity value. With addition of 30 wt. % of salt is added into the system, the agglomeration of salt can be evidenced clearly. The FESEM result of FG30 as depicted in Figure 4.11 (b) is consistent with the findings from XRD and FTIR where it is confirmed that the ion association rate is higher than the ion dissociation rate. As too much salt is added into the system, the salt is not able to be fully solvated by the polymer hence recrystallized after drying (Arof et al., 2011). This phenomena will led to the loss of large amount of charge carries due to the recombination of cations and anions to become salt that obviously will reduce the conductivity value of the polymer electrolytes (Abdulkadir et al., 2021; Kadir & Hamsan, 2018).

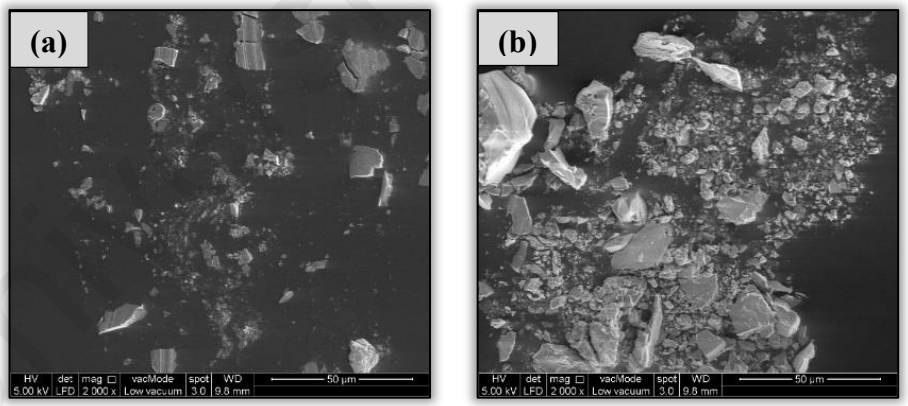

Figure 4.11: Surface morphology for (a) FG25 and (b) FG30.

4.5 Impedance Study

The Nyquist plot for selected electrolytes at room temperature are shown in Figure 4.12. Incomplete semicircle and semicircle plots are observed for FG0 and FG15 as depicted in Figure 4.12 (a) and (b), respectively. The bulk resistance, R_B can be detected

from the interception of the semicircle and the horizontal axis. The incomplete semicircle arc for low salt concentration indicates that there aren't enough ions for conduction (Azli et al., 2020).

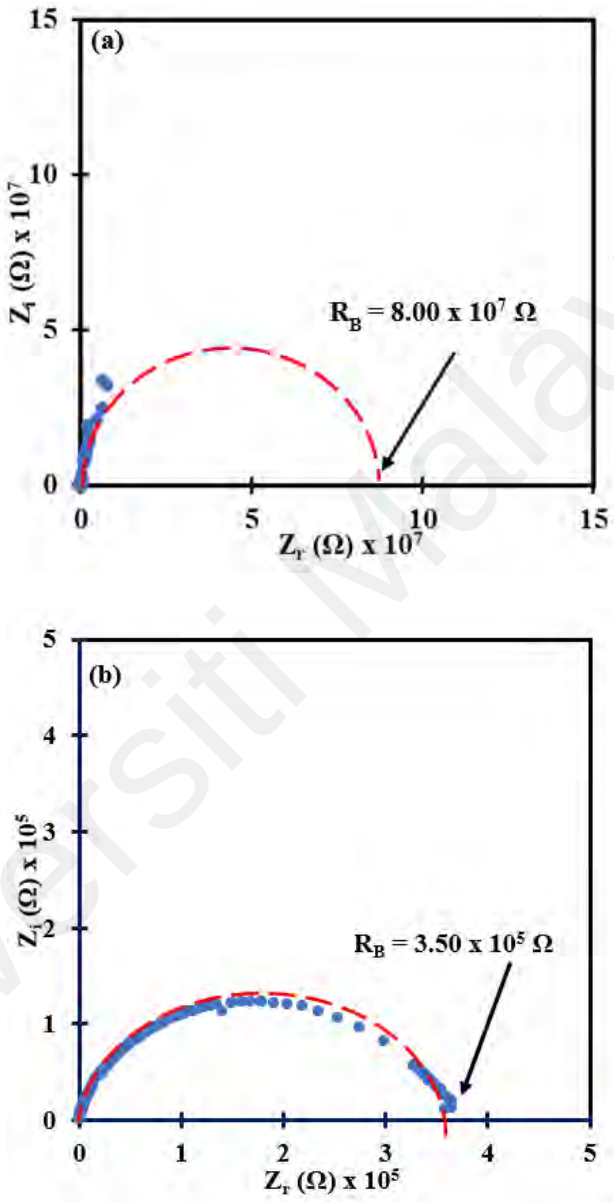

Figure 4.12: Nyquist plot for (a) FG0 and (b) FG15.

It can be seen that the samples with more than 15 wt. % of salt addition, the plot comprises of a combination of semicircle and inclined spike where R_B value can be detected from the interception of semicircle and spike as represented in Figure 4.13 (a) and (b). The semicircle plot at high frequency is due to the migrations of ions in the

electrolyte, while at low frequency, the spike portrays the polarization effect in the electrolyte (Aziz et al., 2020; Brza et al., 2020).

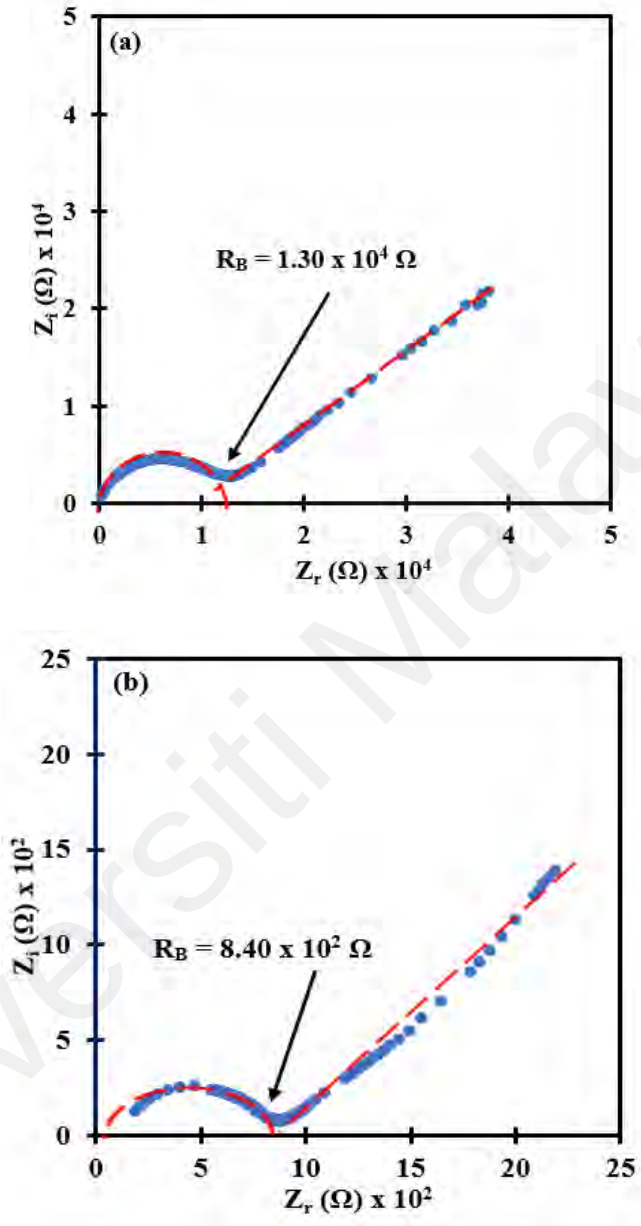

Figure 4.13: Nyquist plot for (a) FG20 and (b) FG25.

The R_B values decreased as more salt added up to 25 wt. % as illustrates in Figure 4.12 (a) and (b) and Figure 4.13 (a) and (b). The shortage of the R_B value indicates that there are more ions available due to the increment of NH_4NO_3 content which enhanced the ionic migration from one electrode to another (Aziz et al., 2019). However, in Figure 4.14, the R_B value for FG30 is higher than FG25. When there are too much salt in the

system, the ions will become too close to one another that led to the recrystallization of salt which in turn will downgraded the ion migration.

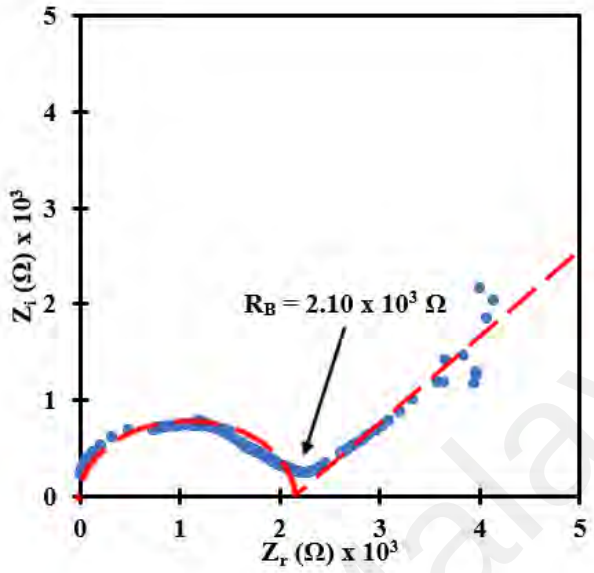

Figure 4.14: Nyquist plot for FG30.

4.6 Conductivity study of Salted System

In this work the conductivity value is calculated using Equation 3.2. The conductivity value at different amount of NH_4NO_3 concentration is shown in Figure 4.15. The conductivity for fish gelatin film, FG0 in this investigation is equivalent to (1.17 ± 0.15) x 10^{-10} S cm^{-1}, which is comparable to the value previously reported by Kadir (2021). With 15 wt. % of NH_4NO_3 salt was introduced to the polymer host, the conductivity raised to (3.12 ± 0.58) x 10^{-8} S cm^{-1}. The conductivity is further spiking up to a maximum value of (1.52 ± 0.30) x 10^{-5} S cm^{-1} when 25 wt. % of NH_4NO_3 is added into the system. The conductivity increases as more salt is added into the system which in return supplying more free charge carriers to be transported by the polymer host (Neto et al., 2014; Premalatha et al., 2016; Ramadan et al., 2014). The conductivity studies in this work are in good agreement with the XRD trend that has been discussed in subtopic 4.1. FG25 possesses the lowest X_c. It has been reported that amorphous region is

favourable for ionic mobility (Abdullah et al., 2018) which is comparable with the result in this work.

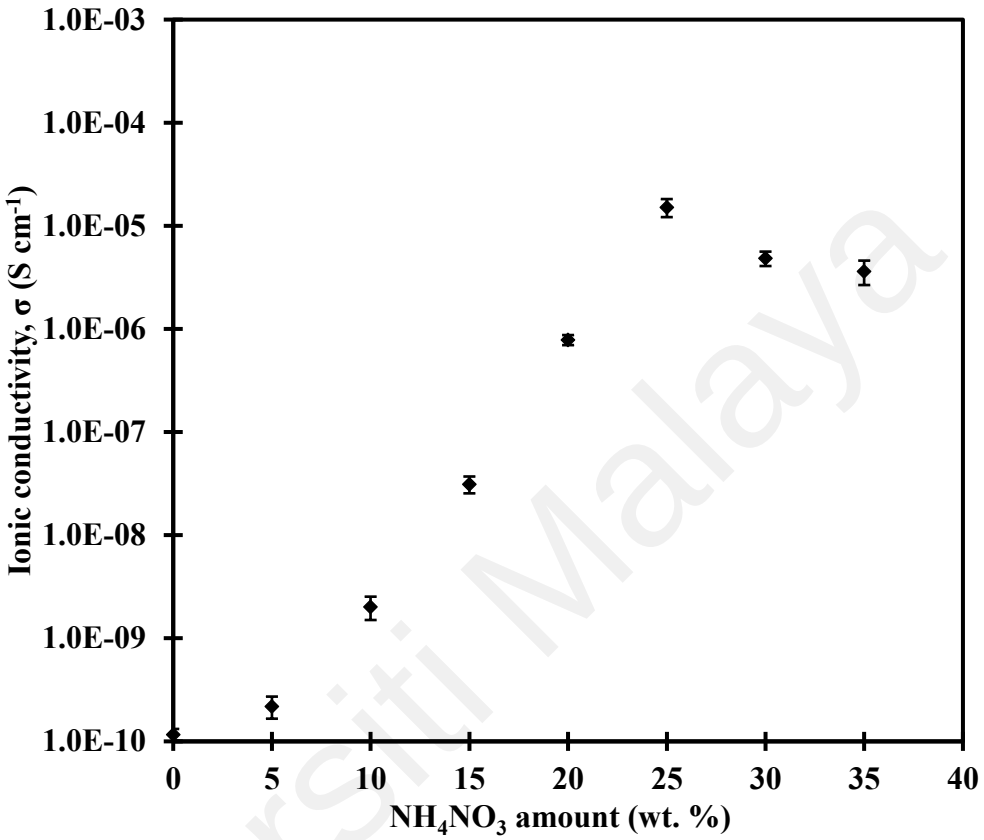

Figure 4.15: Room temperature conductivity of FG-NH_4NO_3.

The conductivity decreases when more than 25 wt. % of salt added into the system. The dissociated ions tend to recombine due to the close distance between them which explained why the conductivity values have decreased to $(4.85 \pm 0.77) \times 10^{-6}$ S cm^{-1} and $(3.63 \pm 0.96) \times 10^{-6}$ S cm^{-1} for FG30 and FG35, respectively. The ions recombined to form salt again which effected the amount of mobile ions causing the conductivity to be badly reduced (Hadi et al., 2021). This result is supported by the XRD data as depicted in Figure 4.4 where distinctive peaks attributed by NH_4NO_3 can be clearly seen. FTIR spectra for FG30 in Figure 4.7 also showed clear peaks related to NH_4NO_3

salt. Conductivity at elevated temperatures of FG-NH_4NO_3 electrolytes is analysed via temperature-dependent Arrhenius relationship equation:

$$\sigma = Ae^{\frac{-E_a}{kT}} \qquad \text{(Equation 4.2)}$$

where A is a pre-exponential factor, E_a (eV) is activation energy, k is a Boltzmann constant and T (K) is the absolute temperature. Figure 4.16 shows a linear conductivity-temperature plot for all electrolytes where the regression value is close to unity suggesting that the system obeys Arrhenius rule.

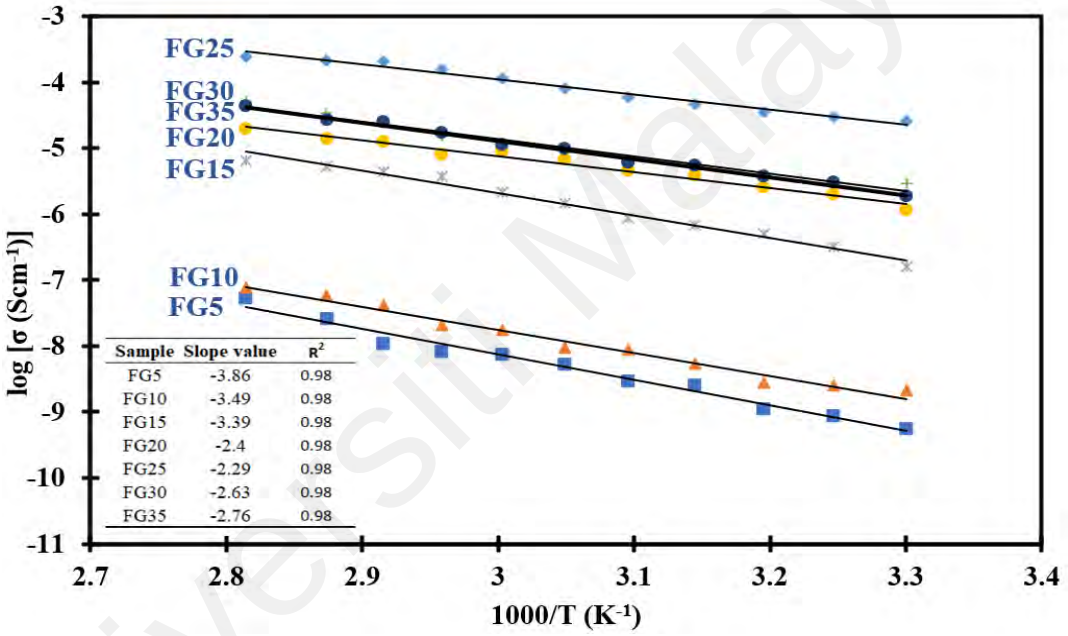

Figure 4.16: The conductivity of salted electrolyte at various temperatures.

According to Lim and co-workers (2017), the polymer segment's vibration mode rises at higher temperatures, allowing a quicker ionic hoping mechanism, thus increases the conductivity value. Previous reports that used NH_4NO_3 as dopant employing polymer such as PVA (Saeed & Abdullah, 2020), MC-PVA (Abdullah et al., 2018) and starch-MC (Hamsan et al., 2017) also have discovered the same behaviour that follows Arrhenius rule. This rule demonstrates that the electrical conduction occurs as the charge carriers move from one unoccupied site to another site.

Minimum energy that is required for the charge to move or best known as activation energy is analysed and presented in Figure 4.17. Generally, it is known that electrolytes with lower activation energy indicates higher conductivity as the charge is easier to move. Thus, the value of activation energy (E_a) for electrolytes at different salt concentrations were determined from the slope of the linear fit and plotted in Figure 4.15. In this study, the highest conducting electrolyte is FG25 that demonstrates the lowest value of activation energy of 0.454 eV. The activation energy increased to 0.522 eV with 30 wt. % of salt, and the results show similar trend as more salt added.

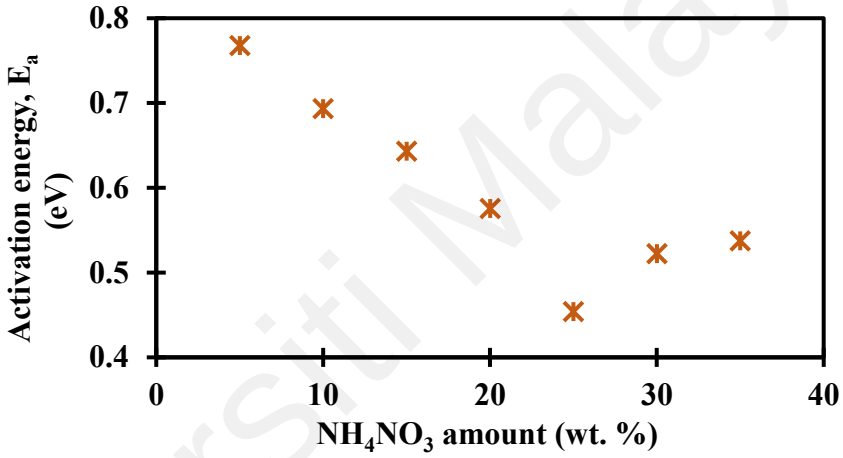

Figure 4.17: The activation energy of salted electrolytes at various temperatures.

This aligns well with prior research indicating that as the concentration of salt increases, the quantity of ions within the polymer electrolyte also increases, leading to a reduction in activation energy. This decrease in activation energy is attributed to the diminishing energy barrier for proton transport. (Boopathi et al., 2016; Hamsan et al., 2017). The value of the activation energy is similar to research by Boopathi and co-workers (2016), as the authors observed that the highest conductivity is 1.67×10^{-5} S cm^{-1} with 0.44 eV E_a as 20 wt. % of NH_4NO_3 was doped to an agar-based electrolyte. In a different study by Majid and Arof (2005), the highest conductivity values and E_a for chitosan doped with NH_4NO_3 were discovered to be 2.53×10^{-5} S cm^{-1} and 0.45 eV, respectively.

4.7 Ionic Transport Analysis

The ionic conductor has an energy gap that allows the mass of the conducting species' ions to be thermally excited from localised ionic states to free-ion-like states, where an ion spreads throughout the solid (Ahmed & Abdullah, 2020; Chai & Isa, 2013). Rice and Roth model is employed in order to obtain the travelling time (τ), the number of mobile ions (n), mobility (μ) and diffusion coefficient (D) that can be calculated using Equation 4.3, 4.4, 4.5, and 4., respectively.

$$\tau = \frac{l}{v} \qquad \text{where} \qquad v = \sqrt{\frac{2E_a}{l}} \qquad \text{(Equation 4.3)}$$

$$n = \frac{3\sigma kTm}{2Ze^2E_a\tau \exp\left(-\frac{E_a}{kT}\right)} \qquad \text{(Equation 4.4)}$$

$$\mu = \frac{\sigma}{nq} \qquad \text{(Equation 4.5)}$$

$$D = \left(\frac{kT\sigma}{ne^2}\right) \qquad \text{(Equation 4.6)}$$

where v is velocity of ion propagation, E_a is the activation energy, m is the mass of ionic charge carrier, k is the Boltzman constant, T is the temperature and e is the charge of the electron. The average free path between two coordinating sites (l) which the ions may hop is 10 Å (Ahmed & Abdullah, 2020; Chai & Isa, 2013). In this work, the conducting species from NH_4NO_3 is the proton source, H^+ (Hamsan et al., 2020; Saadiah, 2020). Table 4.3 displays the transport parameters of the salted electrolytes.

According to previous studies, the ionic diffusion can be a useful measure to assist conductivity investigations and has a significant impact on the conductivity of the electrolyte (Cyriac et al., 2022; Dannoun et al., 2021). As ion diffusion increases, the conductivity increases. Addition of salt into the system, has made τ increases from 0.84 $\times 10^{-13}$ s to 1.04 $\times 10^{-13}$ s and n increases from 0.28 $\times 10^{22}$ cm^{-3} to 1.19 $\times 10^{22}$ cm^{-3} for FG5 and FG25, respectively.

Table 4.3: Transport parameters of FG-NH_4NO_3 system at room temperature.

Sample	σ (S cm^{-1})	τ (s)	η (cm^{-3})	μ (cm^2 V^{-1} s^{-1})	D (cm^2 s^{-1})
FG5	2.19×10^{-10}	0.84×10^{-13}	0.28×10^{22}	4.83×10^{-13}	1.24×10^{-14}
FG10	2.02×10^{-9}	0.87×10^{-13}	0.39×10^{22}	3.27×10^{-12}	8.39×10^{-14}
FG15	3.12×10^{-8}	0.90×10^{-13}	0.89×10^{22}	2.20×10^{-11}	5.65×10^{-13}
FG20	7.84×10^{-7}	0.97×10^{-13}	1.06×10^{22}	4.63×10^{-10}	1.19×10^{-11}
FG25	1.52×10^{-5}	1.04×10^{-13}	1.19×10^{22}	7.97×10^{-9}	2.05×10^{-10}
FG30	4.85×10^{-6}	1.00×10^{-13}	1.43×10^{22}	2.11×10^{-9}	5.43×10^{-11}
FG35	4.00×10^{-6}	0.98×10^{-13}	2.52×10^{22}	9.89×10^{-10}	2.54×10^{-11}

The highest conducting sample (FG25) exhibits the highest μ and D values of 7.97×10^{-9} cm^2 V^{-1} s^{-1} and 2.05×10^{-10} cm^2 s^{-1}, respectively. However, as more than 25 wt. % of salt is added to the system, the conductivity has abruptly decreased. This phenomenon has been triggered by the ions aggregation that in return will contribute to the formation ion clusters. The dipole interaction between the medium's protons increases and reduces ionic mobility and diffusion (Ahmed & Abdullah, 2020).

At high NH_4NO_3 concentrations, H^+ ions became congested in the electrolytes that contributes toward a large number of trapped ions. Extra energy is needed for all the trapped ions to mobile in the polymer matrix, which led to the decreased in ionic mobility and diffusion of ions, respectively. There is a space restriction in the polymer host, which prevents it from sustaining the large amount of H^+ ions attributed by the salt above 25 wt. % (Mazuki et al., 2022). Nevertheless, the number of mobile ions (n) keep on spiking up even after the systems have more than 25 wt. % of salt. Presumably the large concentration of NH_4NO_3 composition in the polymer electrolytes generated an overcrowding n, which had no effect on ionic conductivity (Muhamaruesa & Mohd Isa, 2017).

Previous study on CS-POZ complexed with NH_4NO_3 salt by Tahir and co-workers (2022) found that for highest conducting electrolyte with conductivity 3.87×10^{-6} S cm^{-1}, the n, μ and D are $\times 10^{22}$ cm^{-3}, $\times 10^{-9}$ cm^2 V^{-1} s^{-1} and $\times 10^{-11}$ cm^2 s^{-1}, respectively. The values reported were comparable to this study. The values for n, μ and D calculated are $\times 10^{22}$ cm^{-3}, $\times 10^{-9}$ cm^2 V^{-1} s^{-1} and $\times 10^{-10}$ cm^2 s^{-1}, respectively.

4.8 Dielectric study

Dielectric analysis allows in providing a more extensive explanation on the conductivity pattern. The dielectric properties can be determined from the complex permittivity where Equation 4.7 and Equation 4.8 can be used to calculate the charge stored in an electrolyte (ε_r) and energy dissipates to migrate ions (ε_i) through instant electric reversal, respectively.

i) Dielectric constant, $\varepsilon_r = \frac{Z_i}{\omega C_0((Z_r)^2+(Z_i)^2)}$ (Equation 4.7)

ii) Dielectric loss, $\varepsilon_i = \frac{Z_r}{\omega C_0((Z_r)^2+(Z_i)^2)}$ (Equation 4.8)

where Z_r is the real part of impedance, Z_i is the imaginary part of impedance, ω is the radial frequency and C_0 stands for the vacuum capacitance. The frequency dependence at room temperature for the real and imaginary parts of the complex permittivity for electrolyte films with different salt amount is illustrated in Figure 4.18 (a) and (b), respectively.

The graph demonstrates that at low frequency, the dielectric permittivity value is large and as frequency increases, the permittivity value decreases. At low frequencies, the charge builds up at the electrode-electrolyte interface as the dipoles in the chain

polymer have enough time to orient themselves in the direction of the electric field (Abdullah et al., 2018). However, the polarisation reduces at higher frequencies due to the significant periodic reversal of the electric field that causes very low values of ε_r and ε_i (Sreekanth et al., 2021). This finding is similar to a research established by Rasali and Samsudin (2018). The authors found that the dielectric permittivity decreases as frequency increases. The result shows that this FG-NH_4NO_3 electrolyte system is a non-Debye type as there is no relaxation peaks detected in Figure 4.16, thus the increase in conductivity is mainly contributed by the number density of mobile ions rises as salt was added to 25 wt. %.

The ε_r and ε_i values at all frequencies increased along with the salt content. The amount of salt used has resulted in an increment of ion dissociation, which produces more mobile ions and improves ionic conductivity. The ε_r and ε_i values dropped as 30 wt. % NH_4NO_3 is added to the system due to ion recombination (Hamsan et al., 2017). Besides amount of salt, the effect on temperature to the dielectric properties have also been examined in this research. Figure 4.19 (a) and (b) display the changes in ε_r and ε_i values for the highest conducting electrolyte at high temperatures, respectively. As the temperature increases, the ion dissociation increases resulted in improvement of ion mobility (Muthuvinayagam & Gopinathan, 2015). This is consistent with the conductivity study in this work where it can be observed that as the temperature increases, the conductivity increases.

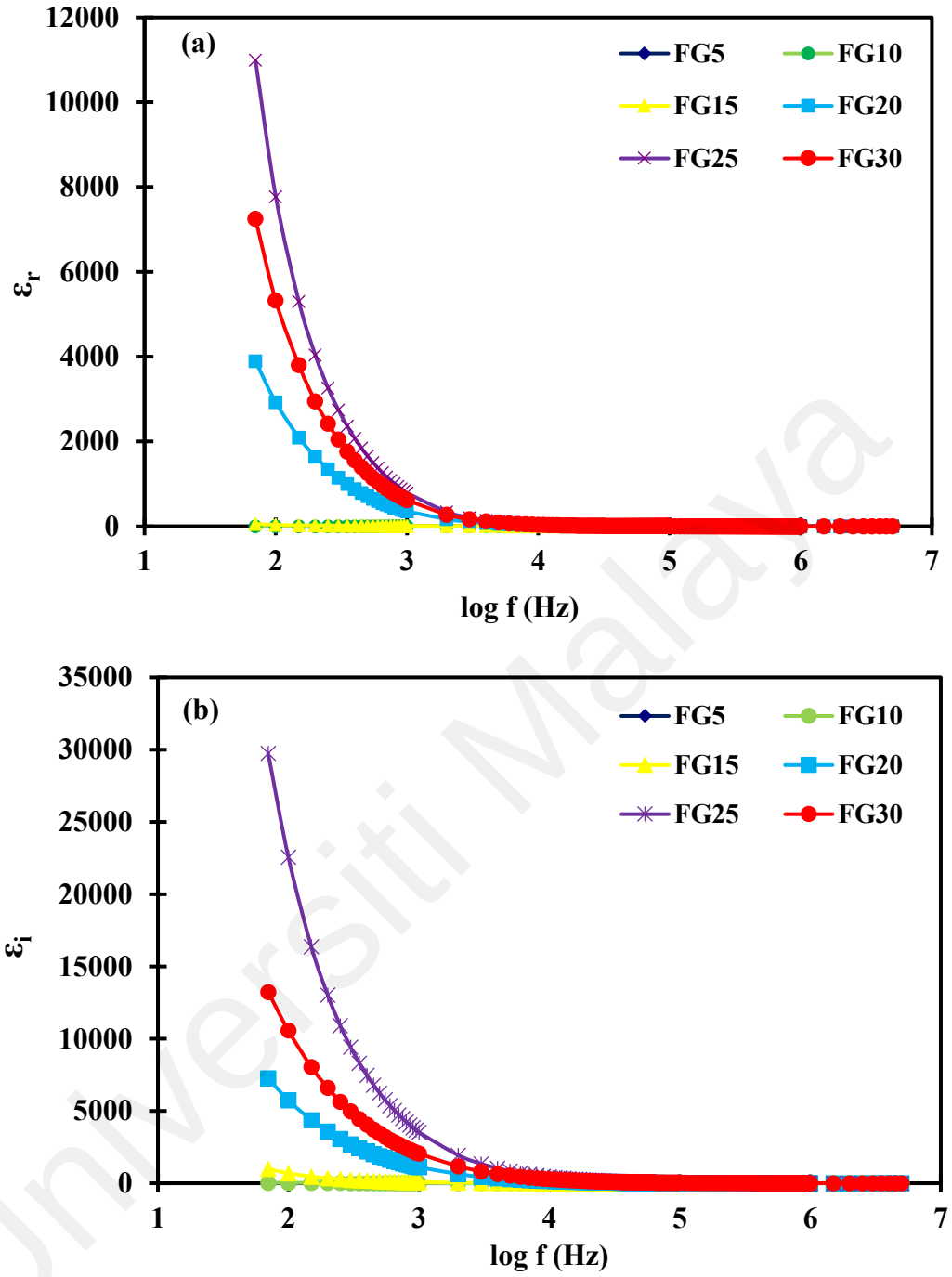

Figure 4.18: (a) The dielectric constant and (b) dielectric loss at room temperature.

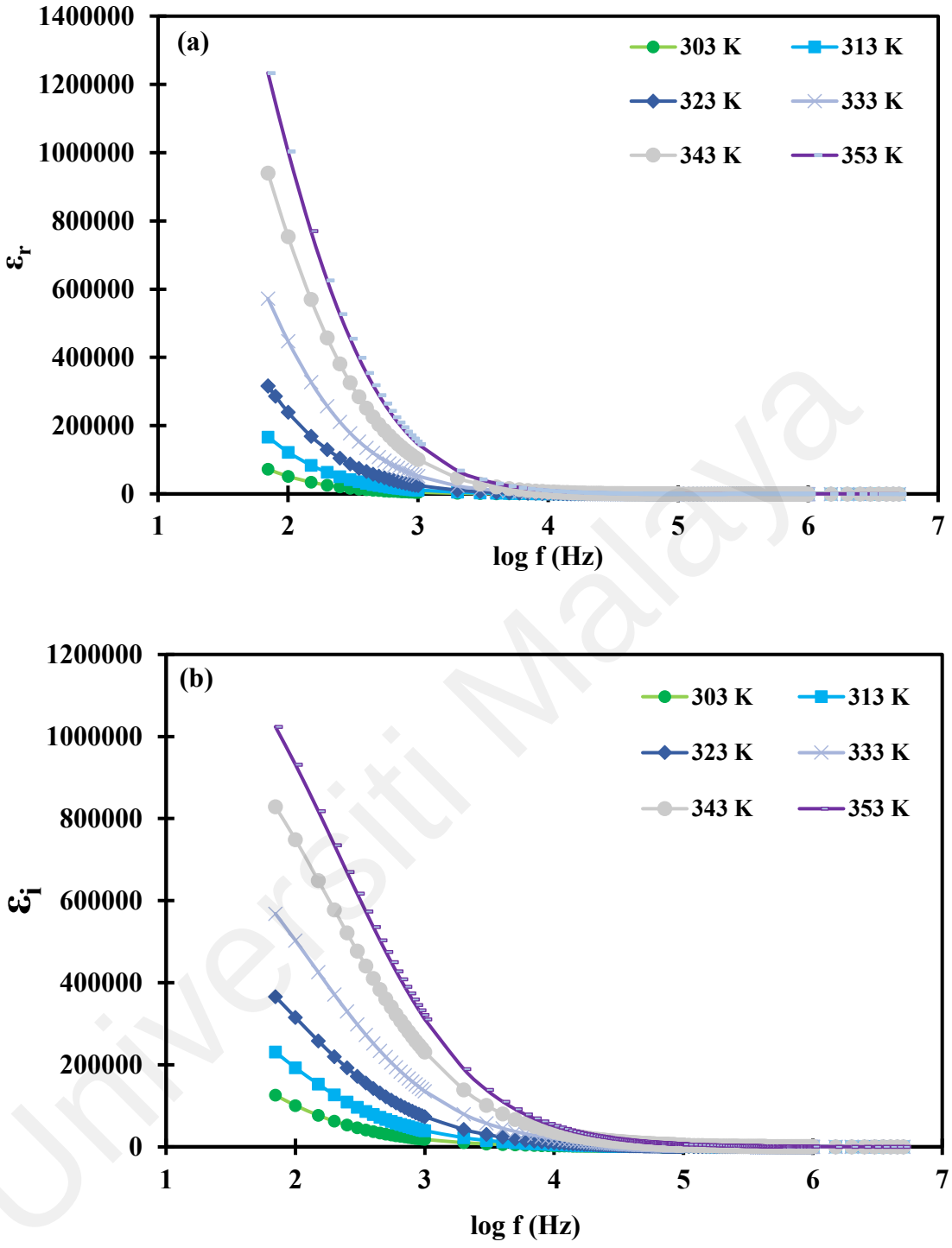

Figure 4.19: (a) The dielectric constant and (b) The dielectric loss at different temperatures.

4.9 Thermogravimetric Analysis (TGA)

Thermodynamic characteristics of polymer complexes provide important information about the stability and stiffness of the film. TGA has been used to investigate thermal stability, the temperature at which polymers decompose, and weight loss that results from heating the samples in a controlled environment. Gelatin is primarily composed of proteins and has a high moisture content hence the thermal decomposition of fish gelatin is likely to produce varied amounts of nitrogen-bearing components as the volatiles (Thomas et al., 2021). It is known that polymer electrolyte's chains are unable to maintain their original shape while being heated therefore the deterioration was more distinct with the addition of salt. This is also in good agreement with FTIR and XRD characteristics that suggest the phenomena could be due to the interaction of the salt with the polymer backbone.

Figure 4.20 shows the TGA curve for the selected salted electrolytes from 100°C to 600°C. The curves of the salted films possess three stages of degradation. The first degradation at ~130°C to ~180°C is due to unbound water weight loss (Azmi et al., 2020). The second degradation occurs between ~220°C to ~250°C corresponds to the degradation of NH_4NO_3. Previous studies found that NH_4NO_3 is degraded at ~160 °C to 230 °C into NH_3, HNO_3, H_2O, and N_2O when heated (Chaturvedi & Dave, 2013; Izato & Miyake, 2015; Skarlis et al., 2014). The degradation temperature for the selected electrolytes is presented in Figure 4.21. From figure 4.21, it can be observed that adding salt causes the decomposition temperature to gradually shift to a lower temperature, indicating a minor reduction in thermal stability. Cyriac and co-workers (2022) reported a similar observation that the degradation temperature decreased as amount of dopant increased which might be due to the complexation of salt and the polymer. However, the

electrolytes can still acquire most of the energy storage devices as the thermal stability criteria is found to be around 100 °C (Cyriac et al., 2022).

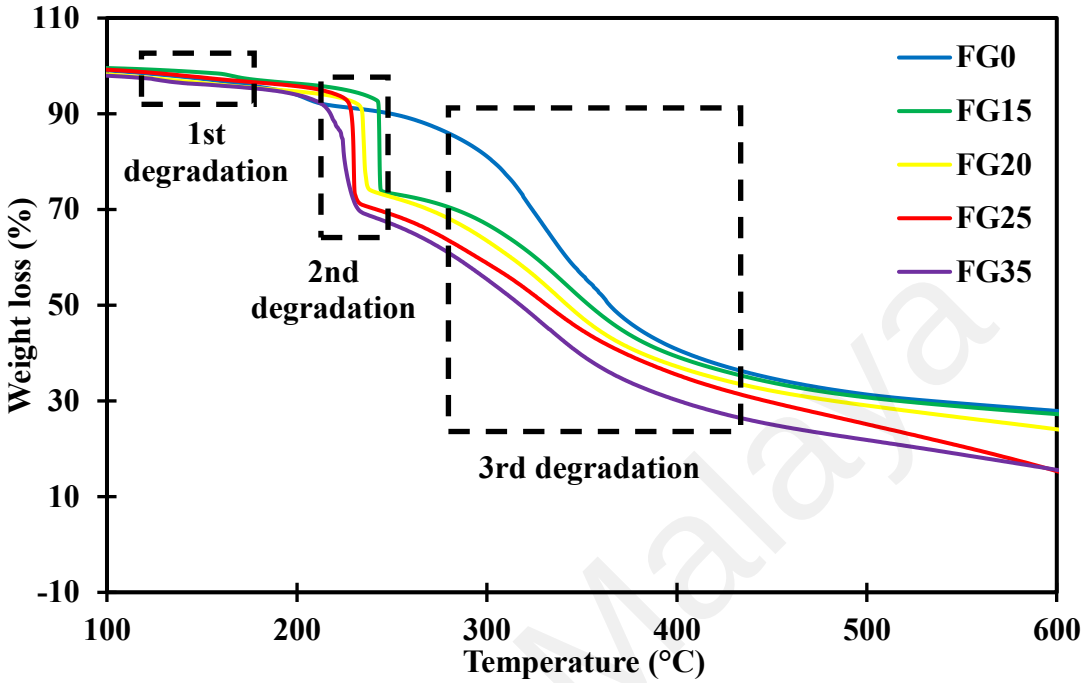

Figure 4.20: TGA thermograms of selected electrolytes.

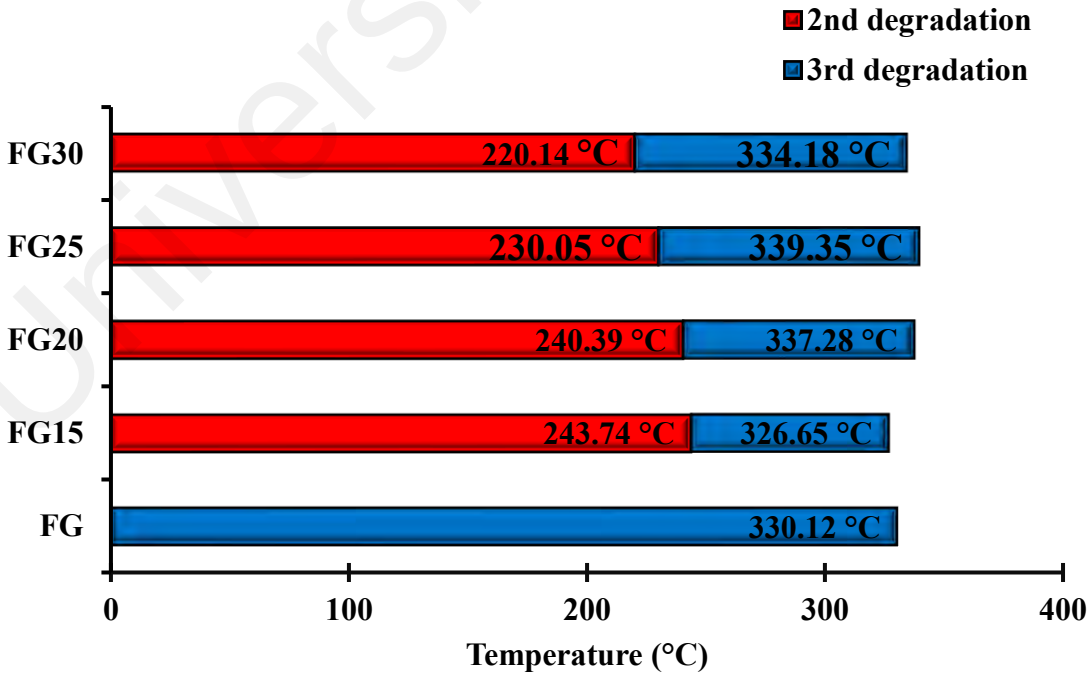

Figure 4.21: Degradation temperature for selected salted electrolytes.

Figure 4.22 shows the weight loss for selected electrolytes at different amount of NH_4NO_3. As more salt is added into the system, the more weight loss can be observed. This is due to the disruption of hydrogen bond between polymer chains by the presence of salt (Kadir, 2021). Third degradation is due to the bigger size of protein in fish gelatin that started to degrade around 330°C which is comparable with previous work elsewhere (Azmi et al., 2020; Thomas et al., 2021).

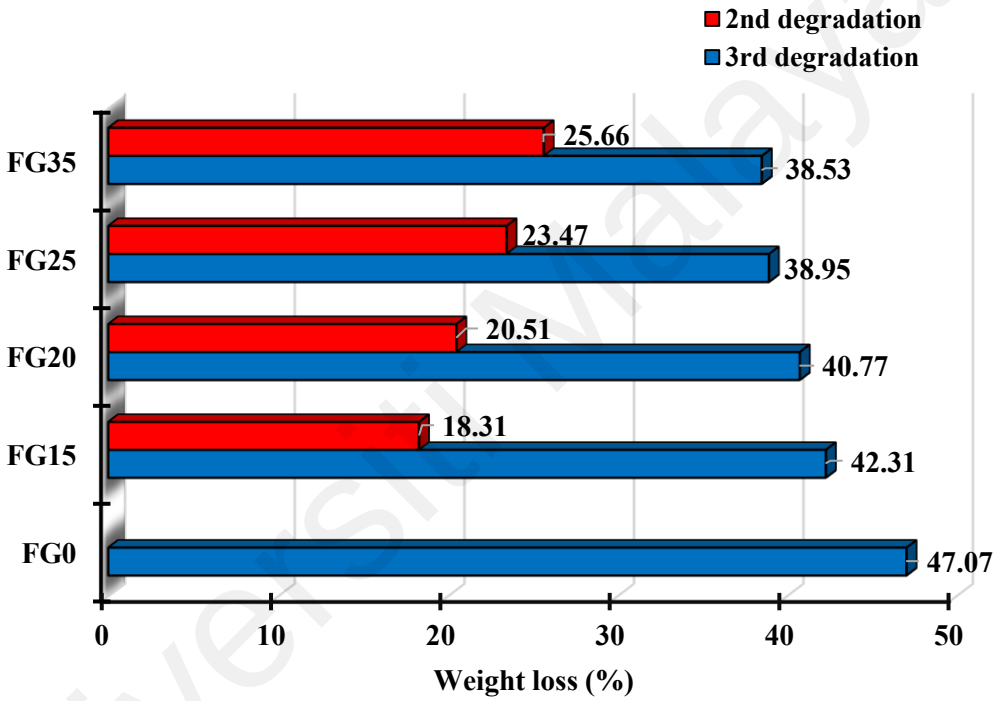

Figure 4.22: Weight loss for selected salted electrolytes.

4.10 Differential Scanning Calorimetry (DSC)

One of the methods to study the miscibility of a polymer and salt is by investigating the thermal properties of the films. The glass transition temperature (T_g) is determined from DSC analysis. The values of glass transition temperature are the taken as the midpoint of the change in heat capacity from a glassy state to rubbery state. T_g can be associated with the crystallinity of the film samples (Martins et al., 2012). The T_g values varies as the values depends on the preparation method and the films condition at

certain relative humidity (RH). For example, Hosseini and co-workers (2013) reported the T_g value of a plasticized fish skin gelatin is ~29.8 °C at ~50% RH. The addition of plasticizer into the film will build a hydrophilic hydroxyl groups as active site which attract water molecules and reduce the T_g value. On the contrary, Kchao and co-workers (2019) reported a higher T_g value for unplasticized fish gelatin. Another previous research by Qiao and co-workers (2017) that the T_g value for dehydrated gelatin film is ~190 °C. The value found in this study for FG0 that was kept in desiccator after the film had been formed is comparable with the study from Staroszczyk and co-workers (2012). The T_g value discovered in their study is ~99 °C for unplasticized cod fish skin with 35 – 45 % RH. The T_g values obtained for FG0 is found to be 98.27°C as can be seen in Figure 4.23.

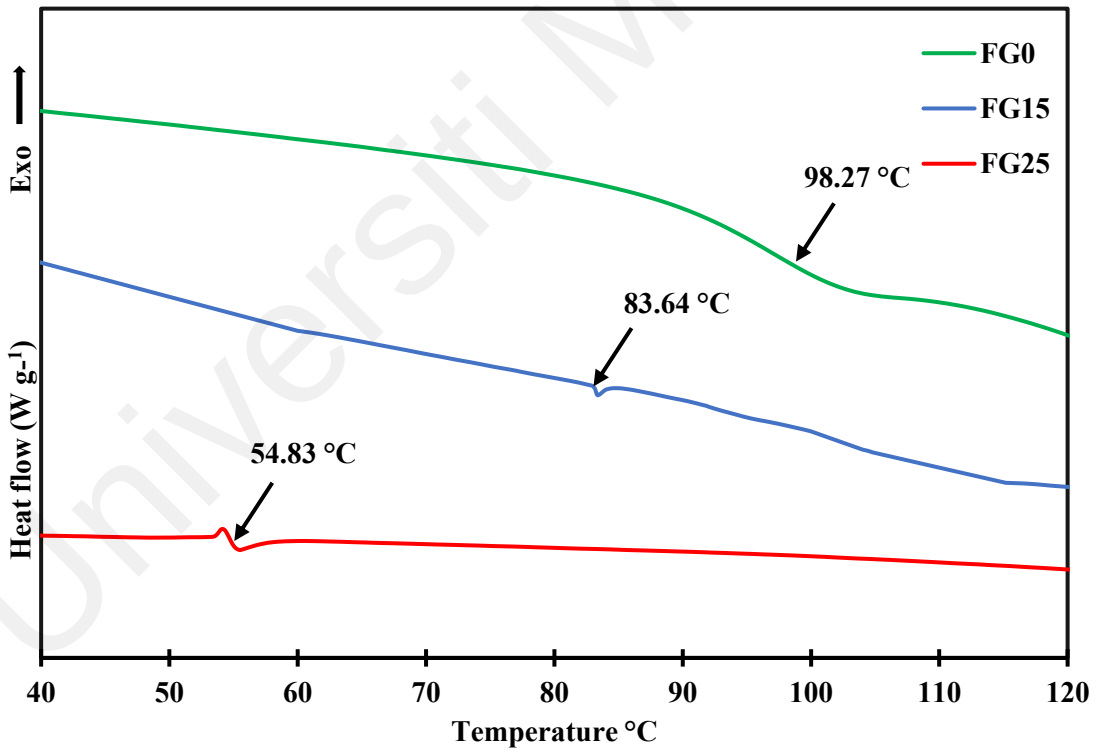

Figure 4.23: DSC for selected salted electrolytes.

In this work, the T_g value decreased from 98.27 °C to 54.83 °C for FG0 and FG25, respectively. The abrupt dropped in T_g value is possible since the presence of salt increases the dissociation of H^+ from NH_4NO_3 for migration process (Rasali et al., 2018). The addition of salt also resulted in the weakening of the dipole-dipole interactions between the polymer chains that causes higher segmental motion (Chitra et al., 2020). XRD analysis seem to be in good agreement, where it is found that as 25 wt. % salt is added into the system, the polymer backbone becomes more flexible that leads to the decrement of the degree of crystallinity. The decreases of T_g in this work is comparable with other studies such as work by Hamsan and co-workers (2017) reported the value of T_g decreases as NH_4NO_3 salt increases in methyl cellulose-starch blend due to the enhancement of the flexibility of the polymer matrix. This trend also similar to the study of electrolyte based on alginate, doped with NH_4NO_3 where T_g decreases from 66.44° to 64.09° for pure alginate and with addition of 25 wt. % of salt, respectively (Rasali et al., 2018).

4.11 Transference Number Analysis (TNM)

Transference number analysis can be used to identify the conducting species. The electrolyte with highest conductivity is sandwiched between two conducting stainless steel (SS) electrodes. By polarising the blocking electrode of cell configuration SS|FG25|SS and observing the potentiostatic current as a function of time, the overall contribution of the total ionic conductivity of the polymer electrolyte is identified. The use of stainless steel as an electrolyte allows the flow of electrons while preventing the flow of ions in the circuit. The transference numbers to determine the number of ion (t_{ion}) and electrons (t_e) in the electrolyte are calculated using Equation 4.9 and 4.10, respectively;

$$t_{ion} = \frac{I_1 - I_2}{I_1} \quad \text{(Equation 4.9)}$$

$$t_e = 1 - t_{ion} \quad \text{(Equation 4.10)}$$

where I_1 is the initial current and I_2 is the steady state current. Figure 4.24 shows the polarization current plot against time for FG25. The current flow shows a rapid drop from 1.3 µA to a saturated current of 0.1 µA.

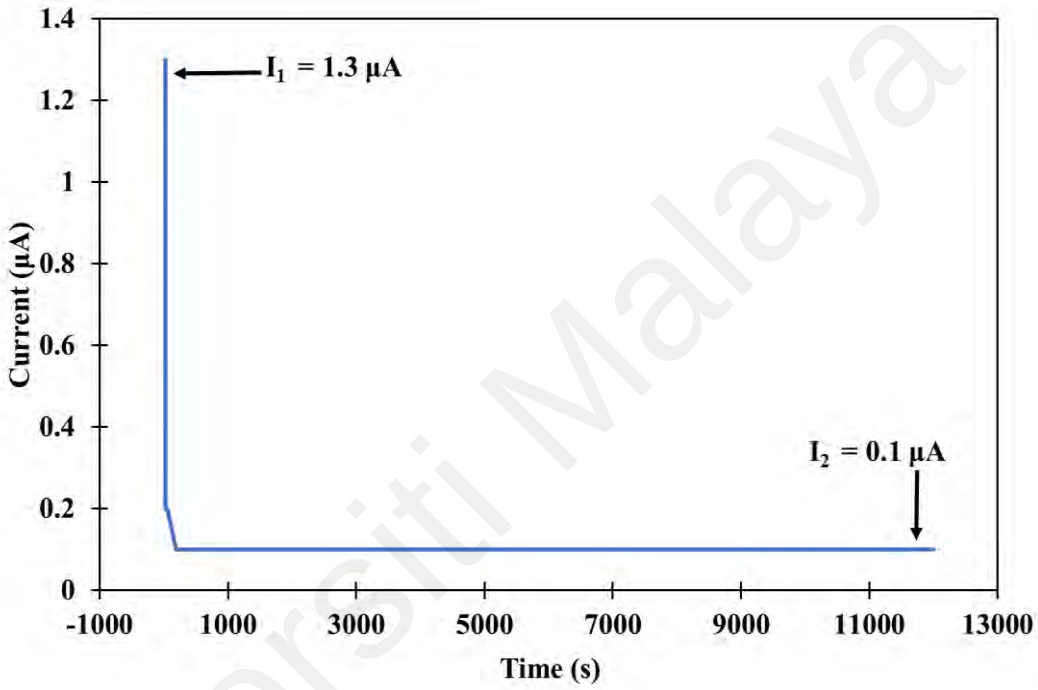

Figure 4.24: Plot of ionic transference number for FG25.

The rapid drop indicates that the electrolyte used is an ionic conductor and the steady state current is reached when the diffusion process balances the movement of the ions (Aziz et al., 2020). Based on the calculations, the t_{ion} and t_e are determined to be 0.92 and 0.08, respectively. The results show that the number of ions is a lot higher than the number of electrons, thus the main charge carriers are ions which comes from cations and anions. The results in this section is comparable with previous findings where Kadir (2021) discovered that the t_{ion} for the highest conducting electrolyte of FG-$LiClO_4$ is 0.97 whilst Aziz and co-workers (2020) found that the t_{ion} for the highest conducting electrolyte of CS-NH_4NO_3 is 0.92.

4.12 Linear Sweep Voltammetry (LSV)

The electrochemical stability and the maximum working voltage for the highest conducting electrolytes, FG25 is verified using LSV technique. It is known that some electrochemical devices, like capacitors and batteries, have a certain working voltage requirements (Dannoun et al., 2021). As shown in Figure 4.25, the current is steady at early stage and at about 2.5 V, the current has increased drastically.

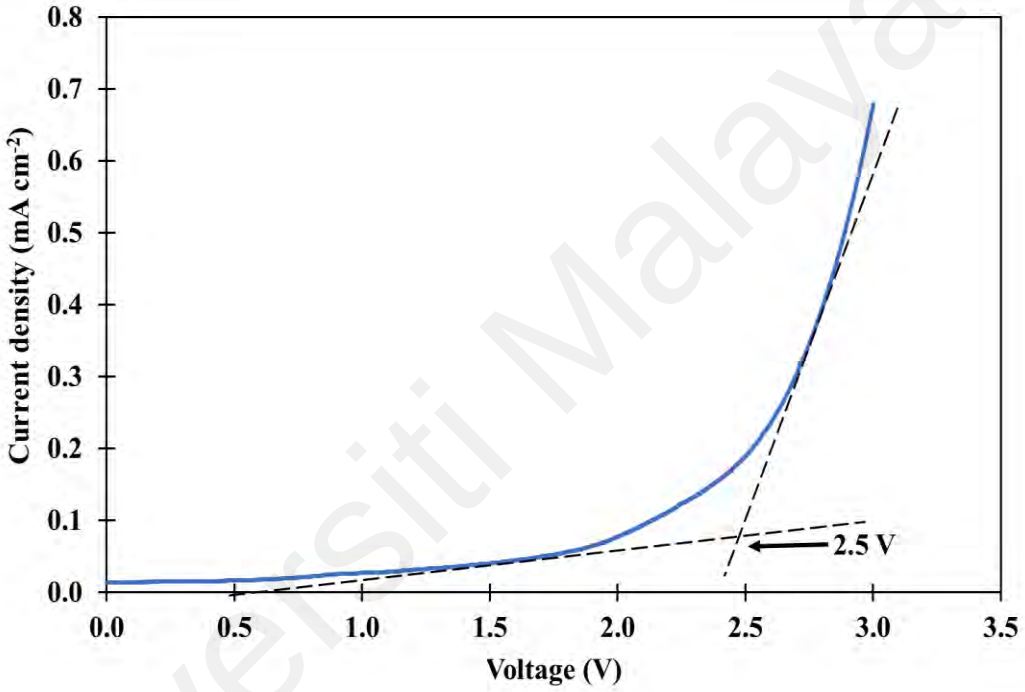

Figure 4.25: LSV plot for FG25.

The drastic change in current indicates that the electrolyte is breaking down (Hemalatha et al., 2019). This infers that the electrolyte will no longer be working at a higher voltage than 2.5 V which should be good enough for energy storage devices (Aziz et al., 2022). This value is similar with previous studies by Kadir (2021) and Aziz et al. (2020) as the authors discovered the breakdown voltage for the reported electrolytes are 1.88 V and 2.32 V, respectively.

CHAPTER 5: CHARATERIZATIONS OF POLYMER BLENDS, FG-CS

5.1 Introduction

To improve the electrochemical properties, polymer blending is one of the method to be developed for the application in a electrochemical devices (Sundaramahalingam et al., 2019). The objective of this chapter is to understand the miscibility, amorphousness and compatibility of the fish gelatin-chitosan (FG-CS) blend. The techniques used are FTIR, XRD, TGA, DSC, and FESEM.

5.2 X-Ray Diffraction (XRD)

The FG-CS ratio with the lowest degree of crystallinity will serve as the polymer host for blending system. The choice of a suitable ratio for polymer blend is crucial to serve as polymer host in electrolytes. To determine the best ratio to serve as polymer host, XRD analysis has been carried out for all the blended FG-CS films. The peaks obtained from XRD analysis are compared with pure fish gelatin film (FG0) that have been discussed in Chapter 4 and pure chitosan (C10) that is analysed in this chapter. Figure 5.1 illustrates the XRD pattern for the blended FG-CS system at different chitosan ratio. The XRD pattern reveals that when fish gelatin and chitosan polymers are blended, changes in the intensity of the peaks are observed. From Figure 5.1, it is observed that XRD spectrum for CF4 exhibits the broadest peak. This strengthens the fact that the addition of chitosan able to improve the amorphousness of the polymer electrolyte. The data is further examined by employing deconvolution method via OriginPro 8 software.

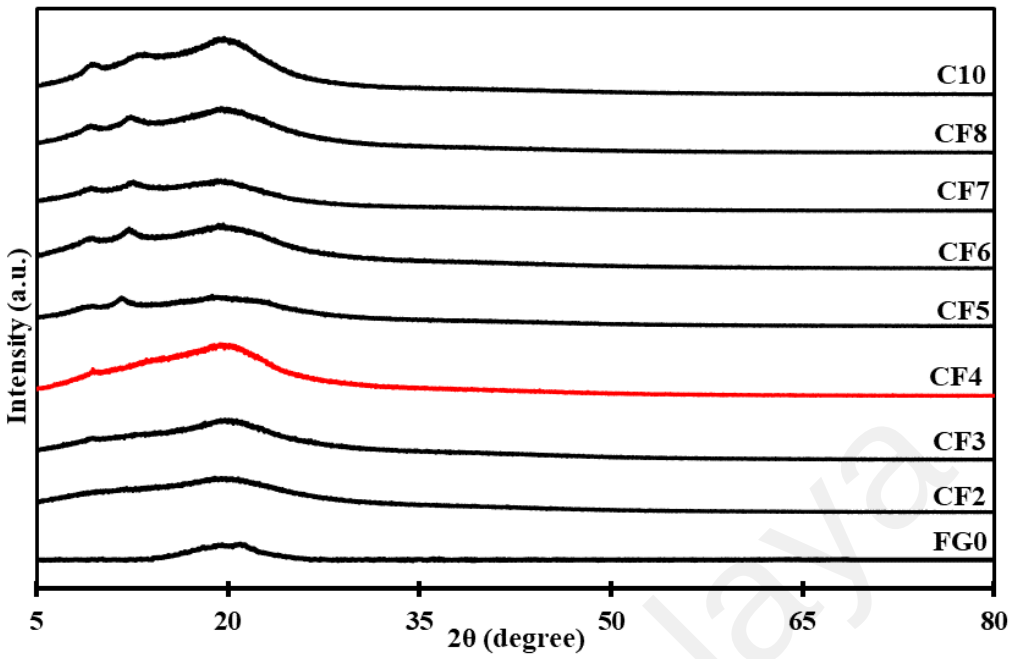

Figure 5.1: XRD pattern of FG-CS at different ratios.

Figure 5.2 displays the deconvoluted XRD pattern of bare chitosan film, C10, which is used as the reference. The crystalline sharp peaks can be distinguished from the amorphous broad peaks by fitting Gaussian distribution in OriginPro8 software, resulting in the green and blue lines, respectively.

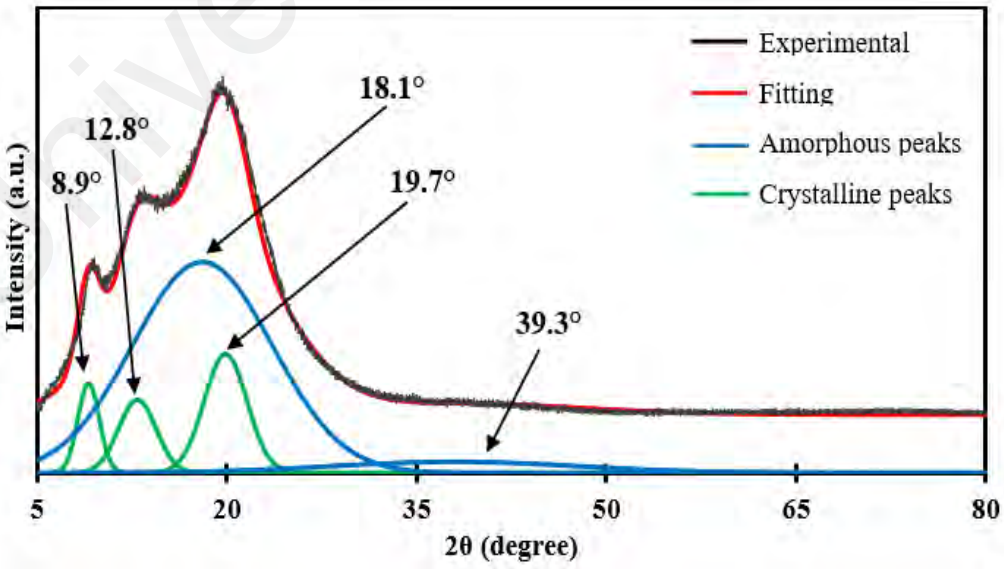

Figure 5.2: Deconvoluted XRD pattern of C10.

The deconvoluted XRD pattern of C10 exhibits prominent crystalline peaks at 2θ = 8.9°, 12.8° and 19.7° with two broad amorphous peaks at 2θ = 18.1° and 39.3°. The crystalline peaks are related to the characteristic of hydrate "tendon" of chitosan (Aguirre-pranzoni et al., 2023) and the inter- and intra-hydrogen bonds formed by the functional groups of different monomers and the chains (Tahir et al., 2022). The peaks are similar with previous reported value (Abdulwahid et al., 2022; Tahir et al., 2022).

The crystalline peaks from fish gelatin are observed to be suppressed when chitosan is introduced into the blend which in turn have made the amorphous peaks become broader. This implies that there is a molecular miscibility in the blend polymers (Abdulkareem, 2021; Abdulwahid et al., 2022). Figure 5.3 illustrates XRD pattern for 80 wt. % FG:20 wt. % CS ratio. It can be observed that the crystalline peaks have shifted to 2θ = 8.5°, 12.7° and 20.5° with two broader amorphous peaks at 2θ = 19.2° and 39.5° respectively when the blend is compared with respect to the FG0 XRD spectrum.

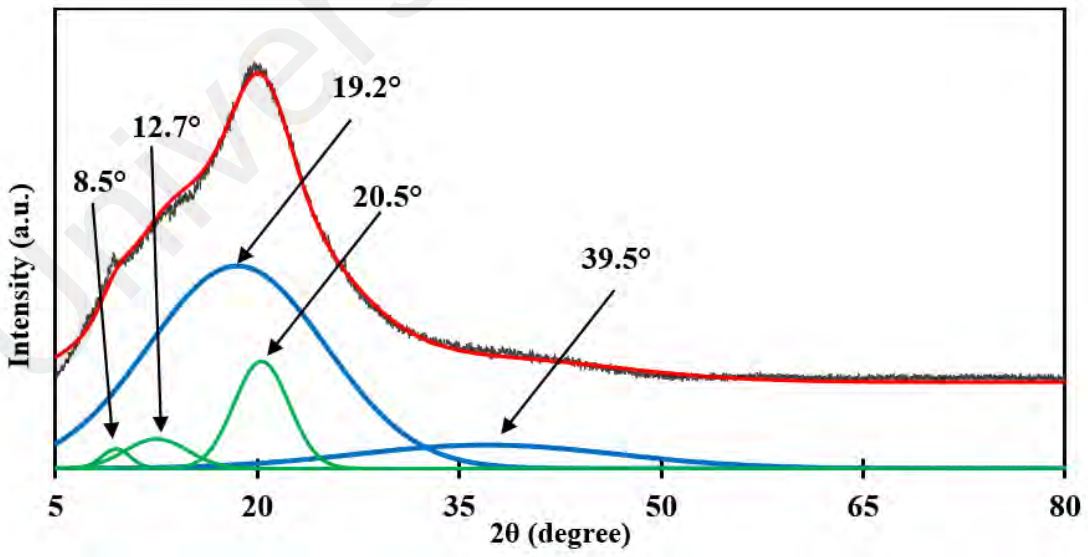

Figure 5.3: Deconvoluted XRD pattern of CF2.

The peak shifts suggest formation of complexation between both polymers (Aziz et al., 2020). Furthermore, it can be assumed that the hydrogen bond between the polymer chains is disturbed and there is a complexation of cations through electrostatic interaction with the polymers functional groups (Abdulwahid et al., 2022). From Figure 5.4, it can be observed crystalline peaks of fish gelatin are observed to continue being suppressed with the addition of 40 wt. % of chitosan. The deconvolution patterns revealed that the electrolytes with 60 wt. % FG:40 wt. % CS (CF4), demonstrated the broadest amorphous region as shown in Figure 5.4. CF4 sample exhibits an additional crystalline peak at 19.8° which it is absence in CF2 sample. This peak could be associated to chitosan crystalline peak as there is a higher chitosan content in CF4 than CF2.

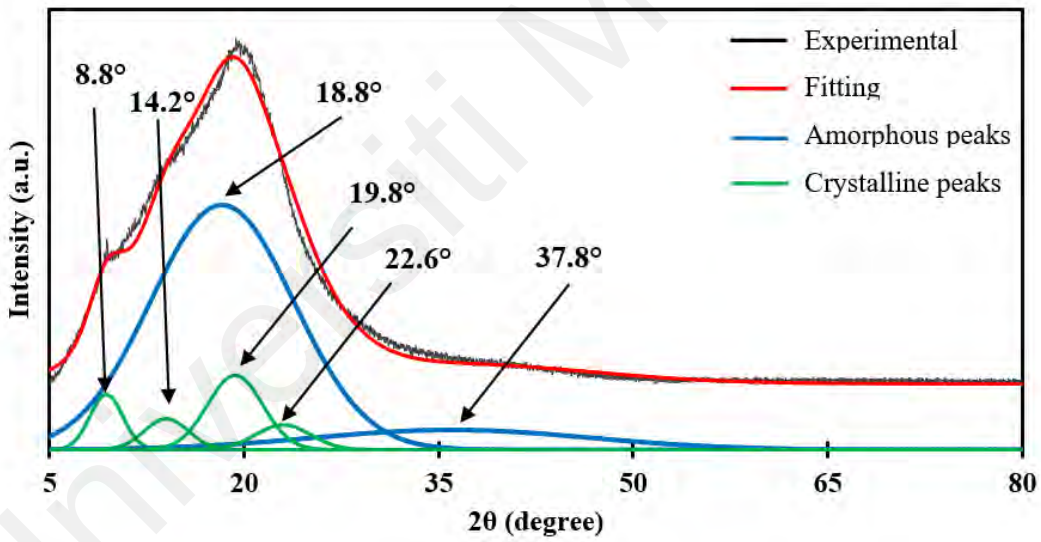

Figure 5.4: Deconvoluted XRD pattern of CF4.

With further addition of chitosan, XRD pattern revealed that the crystalline peaks from chitosan became more prominent and the intensity of amorphous region is reduced. Figure 5.5 shows the deconvoluted XRD pattern for CF6. There are three distintive crystalline peaks at 2θ = 9.2°, 12.7° and 20.0°. As can be seen in the pattern, the crystalline peak at 22.5° has very low intensity which probably due to decreasing amount of fish

gelatin. Thus, based on overall XRD diffractograms, CF4 is expected to host the fastest ionic conduction.

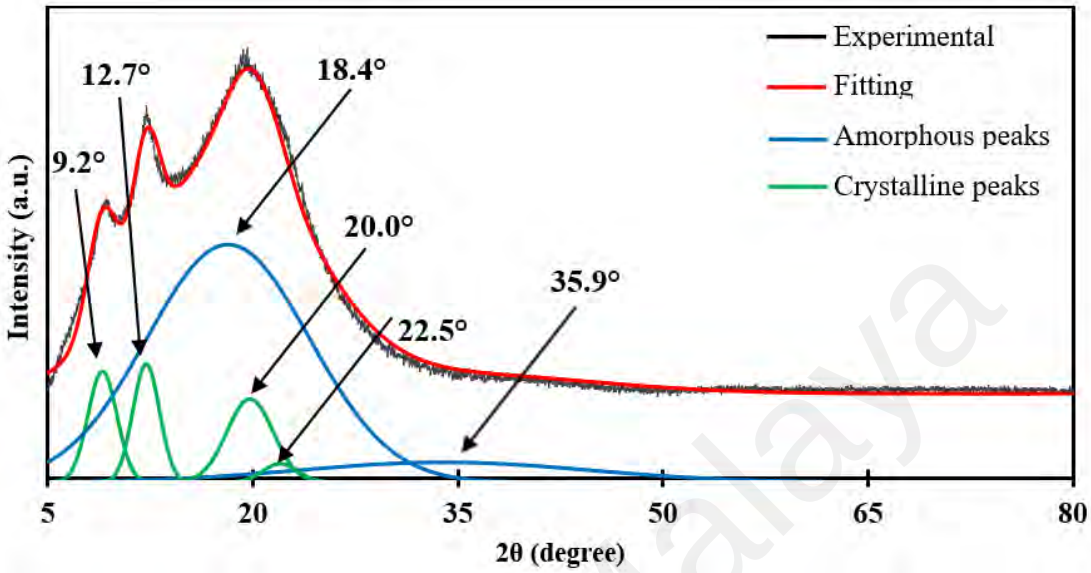

Figure 5.5: Deconvoluted XRD pattern of CF6.

Calculation of degree of crystallinity, X_c is obtained to strengthen the findings and discussions from XRD analysis. The area under the deconvoluted peaks were used to calculate X_c using Equation 4.1. Based on previous calculation, X_c for pure fish gelatin is 21.74 % and that of the X_c for pure chitosan is 23.29 %, respectively. Table 5.1 lists the X_c for different ratio of FG-CS blended system. The X_c has decreased to 19.02 % as 20 wt. % of chitosan is blended and further decreased to 15.38 % with 40 wt. % of chitosan blended into the system. However, with higher amount of chitosan added into the system, the X_c value has increased which in good agreement with the data from XRD diffractograms. From what can be observed, it is confirmed that CF4 is the most amorphous blend film that possesses the lowest value of crystallinity. Thus, CF4 is chosen as the most suitable ratio to be served as polymer blend host. In addition, this result is comparable to the study of gelatin-chitosan blend by Fakhreddin and co-worker (2013). The authors have established the same ratio of 60FG:40CS which they claimed has a

maximum level of interaction between polysaccharides and gelatin and produces a stronger film (Fakhreddin et al., 2013).

Table 5.1: Degree of crystallinity of FG-CS blend polymer.

Electrolytes	X_c (%)
FG0	21.74
CF2	19.02
CF3	16.46
CF4	15.38
CF5	16.82
CF6	19.67
CF7	21.52
CF8	22.30
C10	23.29

5.3 Fourier Transform Infrared (FTIR)

FTIR is carried out to study the interactions between fish gelatin and chitosan in the blend film. FTIR for FG0 has been discussed in Chapter 4. Figure 5.6 depicts the FTIR spectra for chitosan powder and pure chitosan film (C10). From the spectra, hydroxyl band in chitosan is situated at ~3327 cm^{-1} while the carboxamide and amine bands exist at ~1640 cm^{-1} and ~1540 cm^{-1} respectively. Another obvious peak that can be seen in Figure 5.6 is those that is corresponded to saccharide at ~1000 cm^{-1}. All peaks that can be observed in chitosan film spectrum are almost similar to the previous reported value as listed in Table 5.2. The peaks obtained in both chitosan powder and pure chitosan film are within the range of the reported values. Additionally, the intensity of amine peak

increased with the addition of acetic acid into chitosan powder. The interaction between chitosan and acetic acid as a solvent can be seen by the peak's change in intensity (Menazea et al., 2020). Qiao and co-workers (2021) reported that acetic acid interacts with chitosan in amide II region.

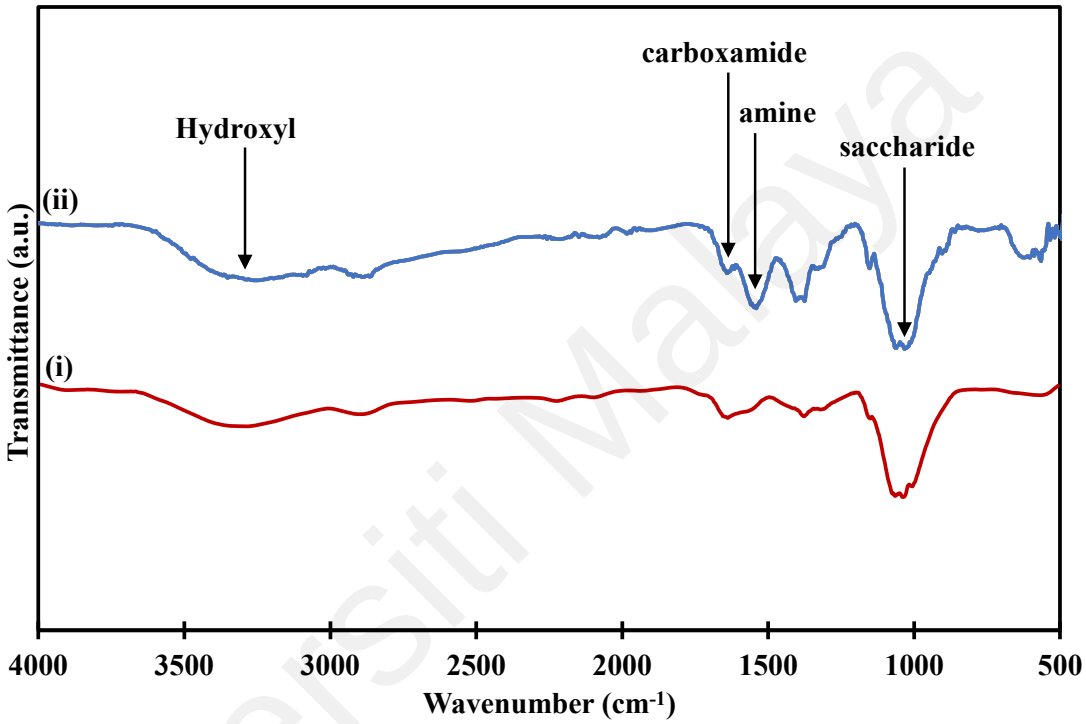

Figure 5.6: FTIR spectra of (i) chitosan powder and (ii) C10.

Based on the XRD analysis, CF4 is found to be the film with the lowest degree of crystallinity. The FTIR spectrum for CF4 is analysed and comparison with FG0 and C10 spectra are made respectively to observe the modifications in molecular structure for the blend polymers. The spectra within hydroxyl range is analysed as shown in Figure 5.7 (a). As discussed in Chapter 4, the hydroxyl peak in fish gelatin is situated at 3288 cm^{-1}. When the polymers are blended, certain modifications have occurred in the spectra which reflects the interactions involving physical and chemical blend. It can be seen that the hydroxyl band of CF4 has shifted to 3279 cm^{-1} and the peak also has broadened indicates

the occurrence of interaction between fish gelatin and chitosan. The gelatin carboxyl groups (COO^-) interacted ionically with the amine group (NH_3^+) from chitosan (Qiao et al., 2017b).

Table 5.2: Characteristic of IR bands for chitosan

Frequency (cm^{-1})	Nature of Bond	Type	References
3400-3200	-OH bonds	hydroxyl	(Dannoun et al., 2021; Koc et al., 2020; Tahir et al., 2022)
3100-2800	C-H stretching vibration		
1650-1600	C=O stretching	Amide I	
1632	O=C-NHR	Carboxamide	
1570-1530	N-H bending	Amide II	
1544	NH2	Amines	
1374	C–N stretching	Amide III	
1025	C-O stretching bond		

Besides hydroxyl band, there are also shifts in carboxamide and saccharide band wavenumber as shown in Figure 5.7 (b) and Figure 5.7 (c), respectively. As soon as chitosan is added into the blend, the carboxamide peaks have shifted to higher wavenumbers of 1635 cm^{-1} and 1534 cm^{-1}, respectively. These values are detected to be in between the wavenumbers of carboxamide for fish gelatin and chitosan. The same situation also occurred for saccharide region. The saccharide peak for CF4 is ~1043 cm^{-1} whilst for fish gelatin and chitosan are ~1075 cm^{-1} and ~1037 cm^{-1}, respectively. The peak intensity also decreased which reflects the occurrence of chemical interactions due to hydrogen bonding when two different polymers are blended.

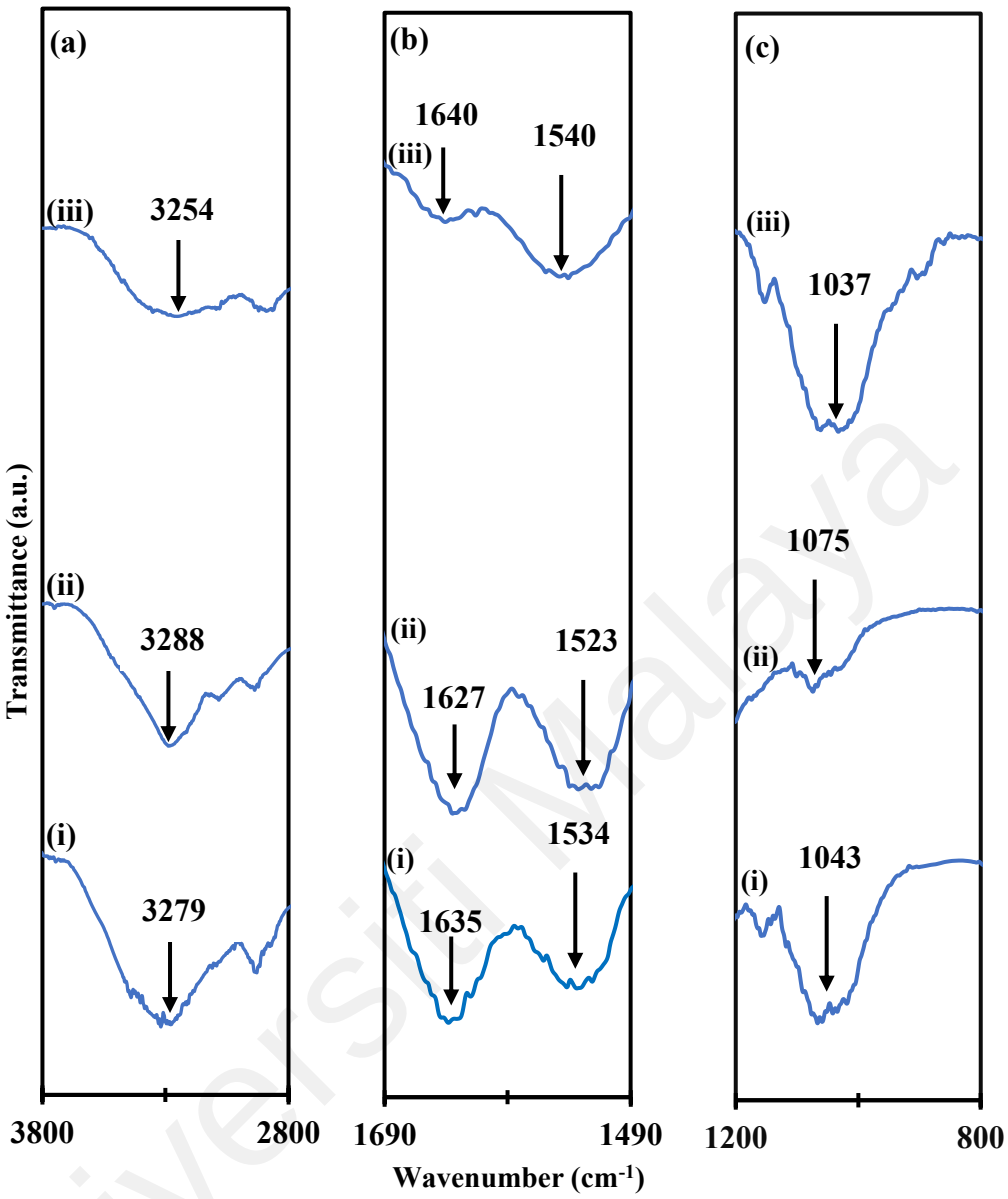

Figure 5.7: FTIR spectra at selected wavenumber (a) hydroxyl band, (b) carboxamide band and (c) saccharide band for (i) CF4, (ii) FG0 and (iii) C10.

Changes within this frequency range in gelatin-containing films are indicative of modifications to collagen or gelatin secondary structure altering the amide-I region (Fakhreddin et al., 2013). The shifted peak positions showed that the existence of single a-helices, random coils, and unstructured complexes reduced as a result of conformational changes induced by chitosan addition (Fakhreddin et al., 2013).

The possible interactions between FG-CS and the interactions between acetic acid (C_2H_3COOH) with chitosan are illustrated in Figure 5.8.

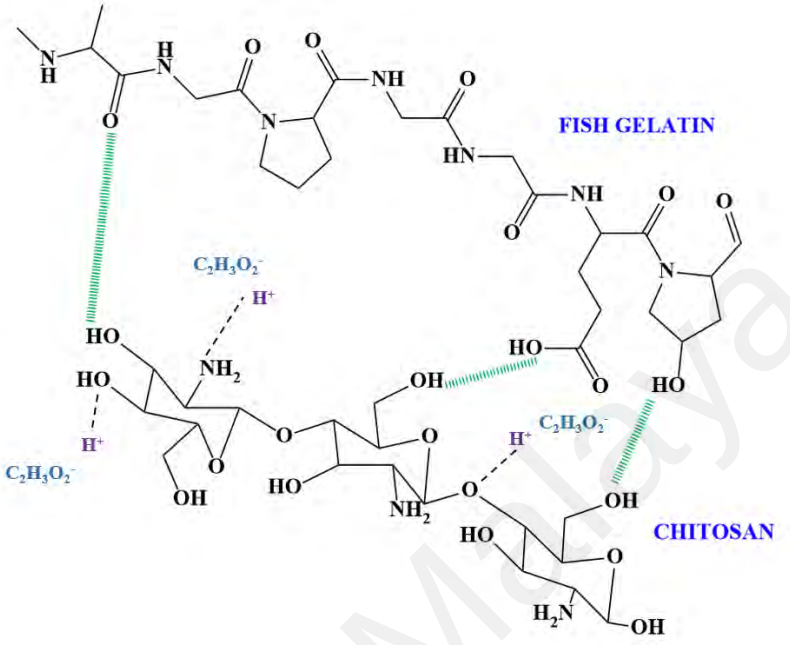

Figure 5.8: Possible interactions between FG-CS

5.4 Field Emission Scanning Electron Microscopy (FESEM)

FESEM is used to study the surface morphology and the cross-section of FG0, C10 and CF4 film to determine the miscibility between these two polymers. Figure 5.9 illustrates the surface and cross-section for (a) FG0, (b) C10 and (c) CF4. The surface morphology of pure fish gelatin film has been discussed in Chapter 4. Based on Figure 5.9 (a) and Figure 5.9 (b), both fish gelatin and chitosan exhibit a homogenous and smooth surface which is comparable with previous studies by Kadir and Hamsan (2018). Figure 5.9 (c) depicts the surface micrographs of CF4 and it can be observed that the surface is smooth and homogenous suggesting that fish gelatin and chitosan are miscible to one another. Additionally, the smooth surface also related to amorphous nature of the samples (Aziz et al., 2019). The ions are able to move easily in the electrolyte with smoother surface resulted in the increment of conductivity (Aziz et al., 2019).

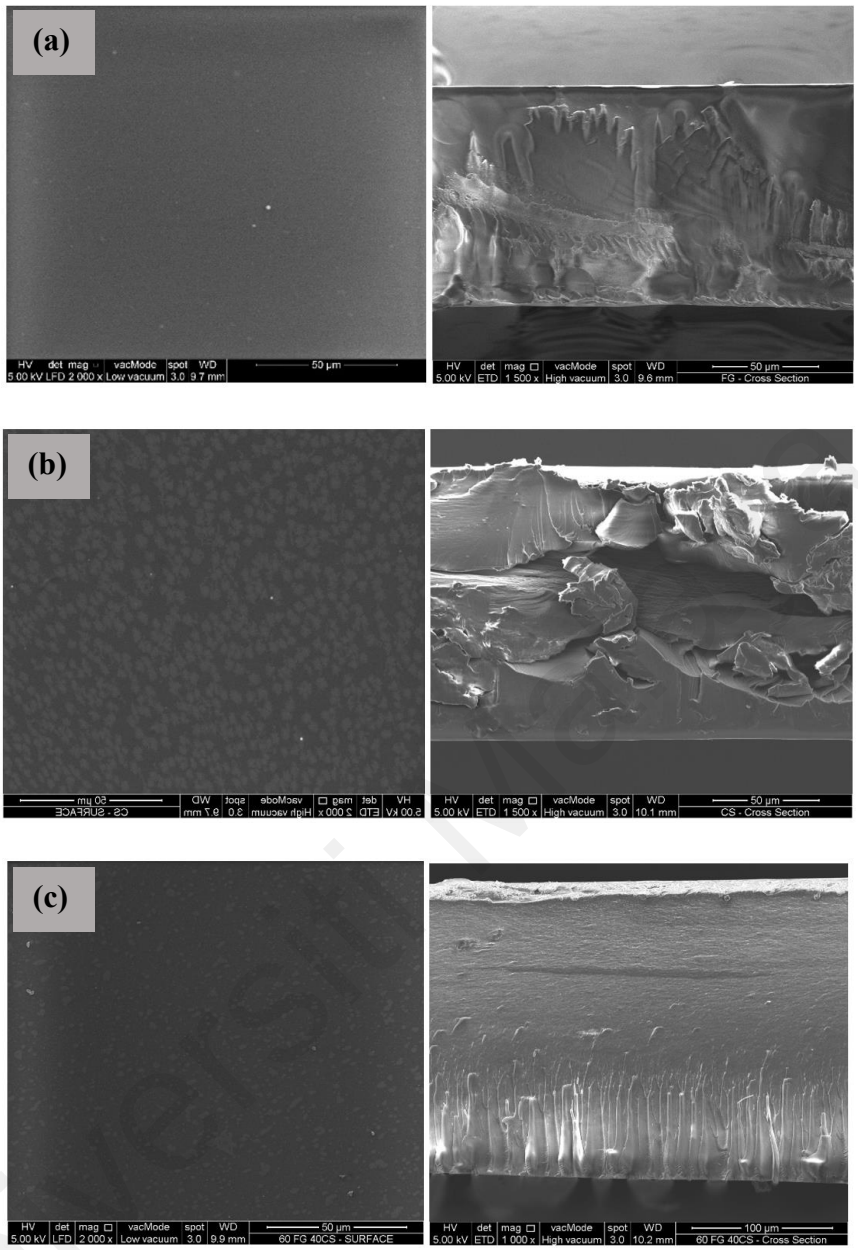

Figure 5.9: FESEM micrographs of (a) FG0, (b) C10 and (c) CF4.

From the cross-sections of these films, FG0 and C10 exhibit a rough structure as can be seen in Figure 5.9 (a) and (b), respectively. However, in Figure 5.9 (c) it can be seen that, after blending these two polymers, a smoother structure is obtained. Furthermore, there are no phase separation in the CF4 cross-section indicates that chitosan is compatible with fish gelatin (Hamsan et al., 2019; Kadir & Hamsan, 2018). The compatibility between gelatin and chitosan was also discussed by other researchers previously (Mousavi et al., 2021; Qiao et al., 2017). It is reported that the interactions

between these two single polymers are produced by electrostatic interactions and hydrogen bonds that facilitate the formation of multiple complexes and hinder the physical gelation of gelatin (Qiao et al., 2017).

5.5 Thermogravimetric Analysis (TGA)

Figure 5.10 shows the TGA curves for weight against temperature for FG0, C10 and CF4 whilst Figure 5.11 illustrates the TGA thermogram with respect to their derivative weight. The derivative weight indicates the point of greatest rate of change on the weight loss curve that also known as inflection point (Chipara et al., 2008). In Figure 5.10, the residual at 800 °C for FG0 is higher upon addition of chitosan. The residue increased from 16 % for FG0 to 33 % as 40 wt. % of chitosan is added into the system. This indicates that the cross-linking density between the dispersed phase and the continues phase of fish gelatin has been improved (Pan et al., 2020). It could also prove that the addition of chitosan influences the thermal stability of FG0 film.

As mentioned in Chapter 4, the 1st degradation is due to the loss of water. Based on Figure 5.10, the weight loss of water in CF4 is ~8 wt. % which is lower than the weight loss of water in FG0. The reduction of the weight loss of water proves that polymer blending is able to overcome the problem related to the moisture sensitiveness in gelatin. 2nd degradation of chitosan film starts at ~200 °C and the major decomposition occur at ~280 °C as depicted in Figure 5.11.

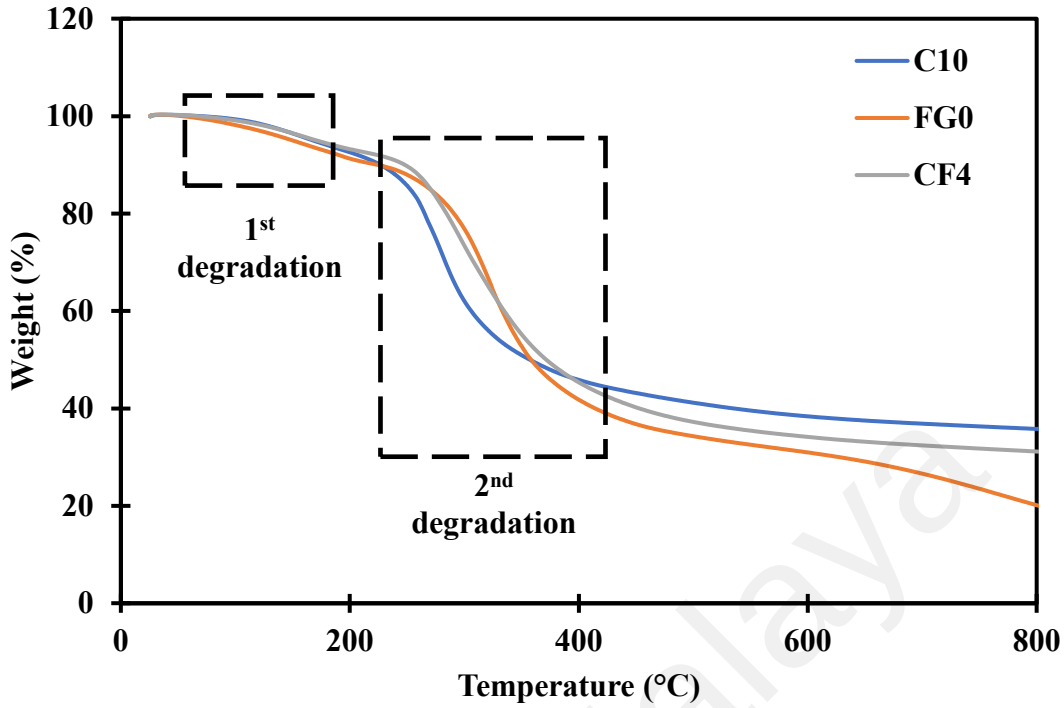

Figure 5.10: TGA curves for the polymer blend.

Table 5.3 shows the comparison between the single polymers and CF4. From the table, it can be concluded that the thermal stability of fish gelatin is improved with addition of chitosan.

Table 5.3: Comparison of single and blended TGA.

Sample	Residue at 800 °C	Major decomposition temperature	Major weight loss
FG0	16 %	335 °C	73 %
C10	36 %	280 °C	56 %
CF4	33 %	298 °C	59 %

These values are similar to a previous study where Alves and his co-worker (2016) reported that chitosan started to be degraded at the 200 °C associated to the thermal and oxidative decomposition. In contrast, fish gelatin can significantly stand a higher temperature as the decomposition starts at ~230 °C and the major decomposition occur at ~335 °C as displayed in Figure 5.11.

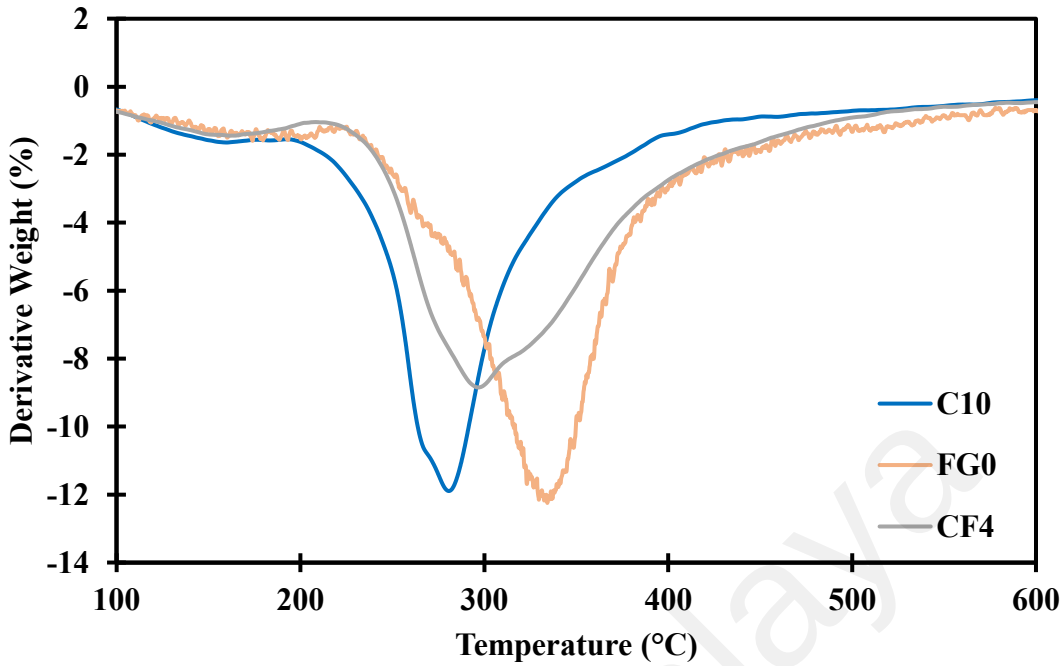

Figure 5.11: TGA thermogram with derivative weight (%).

5.6 Differential Scanning Calorimetry (DSC)

One of the methods to study the miscibility of a polymer blend is by investigating the thermal properties of the films. The glass transition temperature (T_g) is determined from DSC analysis. The values of glass transition temperature are established through the midpoint of the change in heat capacity from a glassy state to rubbery state (Martins et al., 2012). Figure 5.12 shows the DSC curve of C10, FG0 and CF4 film for second heating. The first heating is conducted to the eliminate the absorbed moisture due to hydrophilic group of polymers (Rahman et al., 2021; Vernon-Carter et al., 2017). It can be observed that the T_g for chitosan found in this study equals to 87.35 °C. Kadir and Hamsan (2018) reported that the T_g for chitosan film is at 104 °C whilst Hadidi and his co-workers (2020) found T_g at 85.5 °C. Previous studies reported that the difference in chitosan T_g value was due to the variability in water content, crystallinity and the chemical structure of the chitosan (Qiao et al., 2021; Qiao & Wang, 2019). Figure 5.12 shows the

T_g for CF4 that is detected in between the single polymers indicating that chitosan is compatible to be blended with fish gelatin (Muthuvinayagam & Gopinathan, 2015).

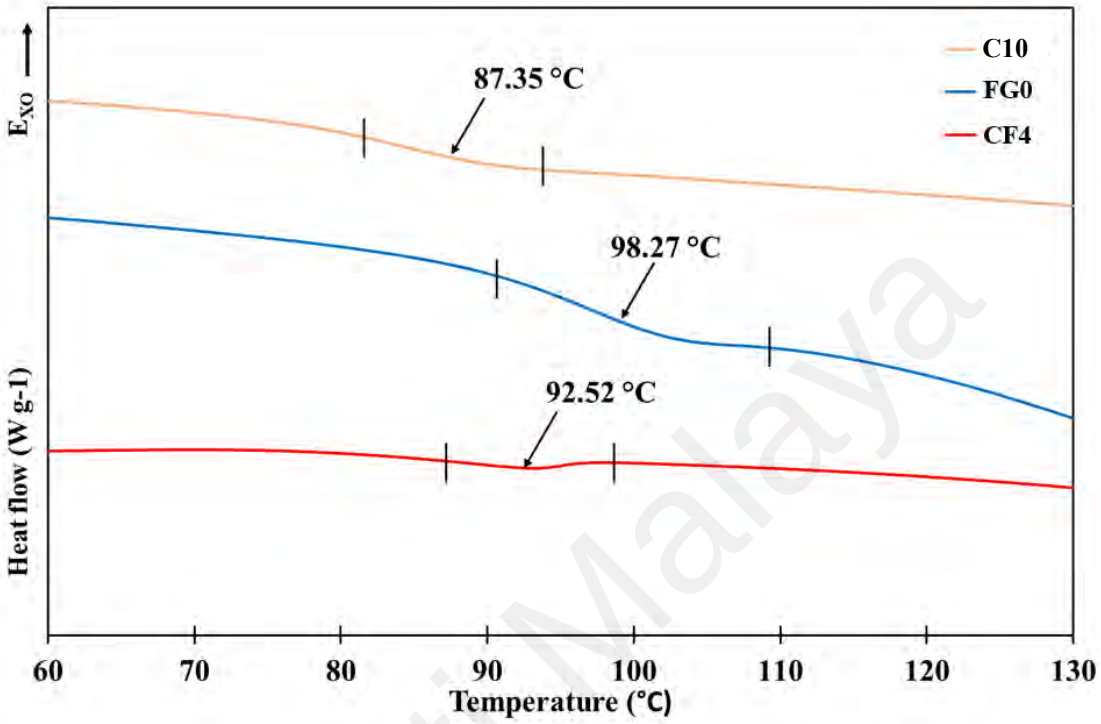

Figure 5.12: DSC thermogram of second heating run, FG-CS.

CHAPTER 6: CHARACTERISATIONS OF FISH GELATIN-CHITOSAN-NH_4NO_3.

6.1 Introduction

From XRD analysis in Chapter 5, the blend of 60 wt. % FG with 40 wt. % of chitosan has the lowest degree of crystallinity. This ratio has been chosen as the polymer host and different amount of salt will be added into the system as charge carriers provider. The system will have a new functional group because of the addition of NH_4NO_3, which could lead to a new chemical interaction. To analyse the interactions between polymer host and salt, FTIR analysis can be used. Several techniques have been used to study the properties of the third system of FG-CS-NH_4NO_3.

6.2 X-Ray Diffraction Analysis (XRD)

XRD analysis has been carried out for selected FG-CS-NH_4NO_3 films to study the amorphousness and the structural changes of polymer electrolytes as different amount of salt were added into the system. Firstly, with addition of 20 wt. % NH_4NO_3. Figure 6.1 illustrates the deconvoluted XRD pattern for CFs20. From the figure, the peaks for crystalline indicated by the green lines appeared almost the same with crystalline peaks for CF4. The four crystalline peaks are situated at 2θ = 8.9°, 15.1°, 19.8° and 23.4°. The amorphous peaks for CFs20 shifted to the right compared to CF4 amorphous peaks. The peaks shifted from 2θ =18.8° to 23.2° and 37.8° to 40.2°, respectively. This result proves that the polymer blend have interacted with the salt and still retained its behaviour (Dannoun et al., 2020). The addition of salt will provide the free ions that will attach to the hydroxyl groups in the polymer host and interrupted the molecular structure (Cyriac et al., 2022).

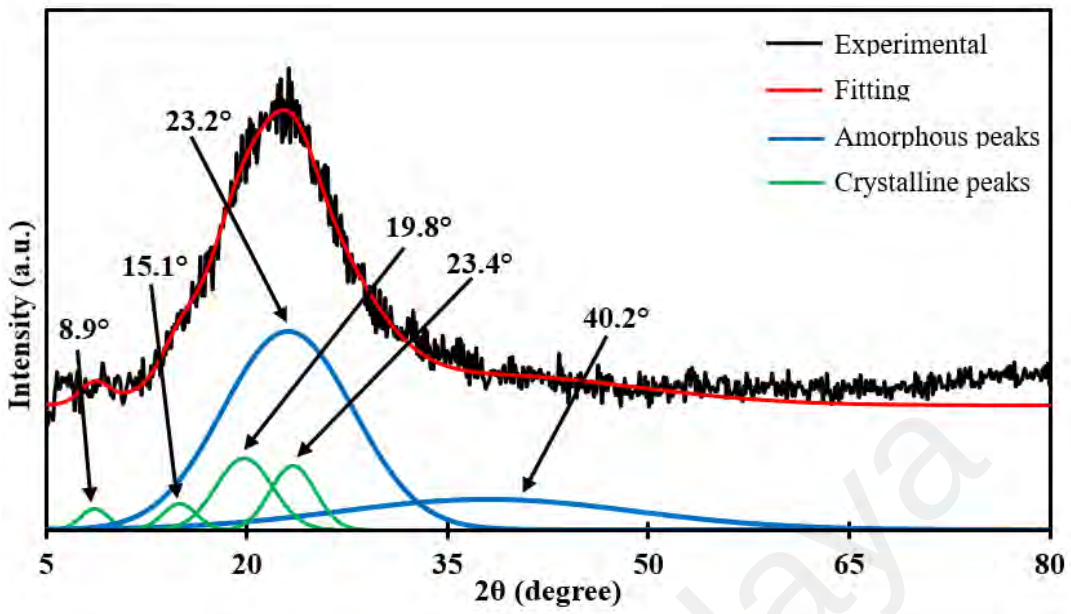

Figure 6.1: Deconvolution XRD pattern of CFs20.

Next, Figure 6.2 represents the deconvoluted XRD pattern for CFs30. With further addition of salt, there are several sharp peaks appeared at about 2θ = 22.4°, 28.9°, 32.9° and 39.9°. These peaks possibly are attributed to the salt that has recrystallised out from the polymer electrolyte.

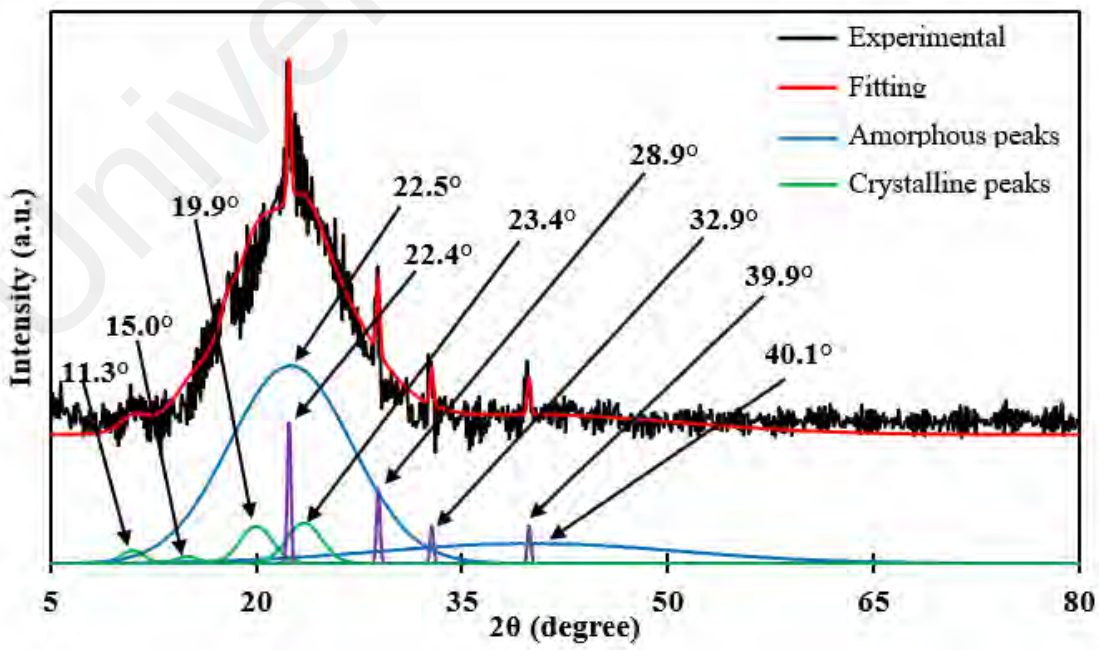

Figure 6.2: Deconvolution XRD pattern of CFs30.

However, the amorphous peaks still become broader compared to CFs20. CFs30 also reveals the existence of two distinct amorphous peaks which originated from CF4. This observation proves that the amorphousness of the polymer host retained in the salted system. Figure 6.3 shows the deconvoluted XRD pattern for CFs40. With more addition of salt, the amorphous peaks at 2θ = 23.0° and 35.3° became broader indicating that it can serve as a good polymer electrolytes (N. M. Ghazali et al., 2022). This is because the backbones of the polymeric chain is more flexible in amorphous region which leads to an increment in charge mobility (M.A. Saadiah, Y. Nagao, 2020).

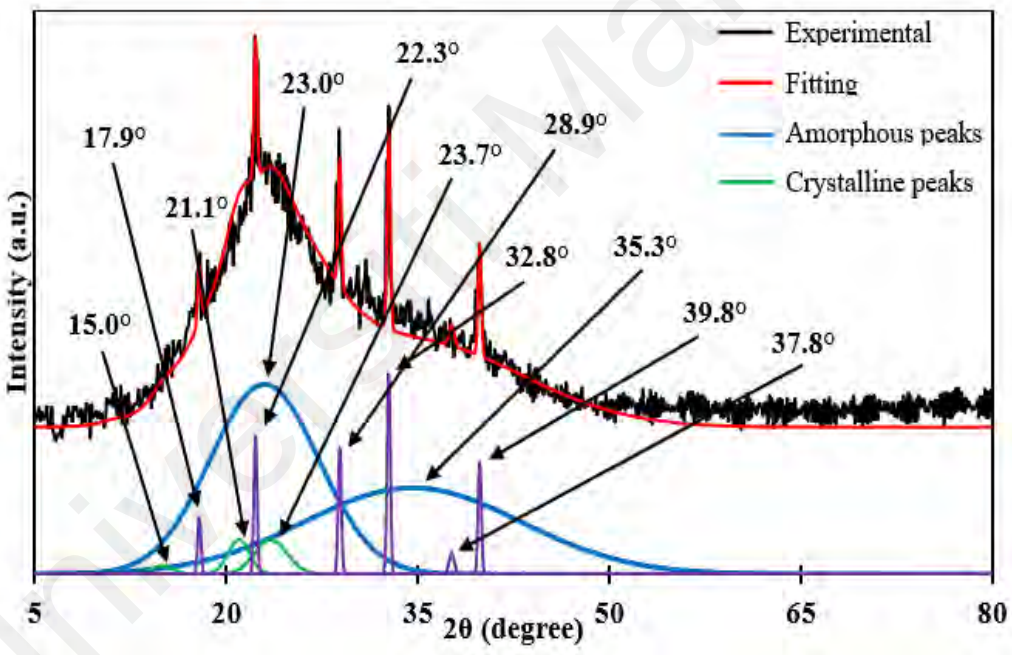

Figure 6.3: Deconvolution XRD pattern of CFs40.

The green peaks at 2θ = 15.0°, 21.1° and 23.7° which referred to crystalline peaks from CF4 are suppressed as more salt added into the system. The four purple crystalline peaks at 2θ = 22.3°, 28.9°, 32.8° and 39.9° became more intense in CFs40 compared to CFs30. In addition, there are additional NH_4NO_3 crystalline peaks that can be observed

in CFs40 at 2θ = 17.9° and 37.8° that are absence in CFs30. These might be due to a higher salt concentration in CFs40 than CFs30.

Figure 6.4 displays the pattern for CFs50. It can be observed that, with further increment of salt, the amorphous intensity of the polymer electrolyte at 2θ = 21.7° and 37.2° have decreased, respectively. More than seven purple sharp peaks appeared, indicating high crystallinity is present in CFs50. The polymer host is no longer able to accommodate the salt which leads to recombination of ions that will led to the decreased in conductivity value.

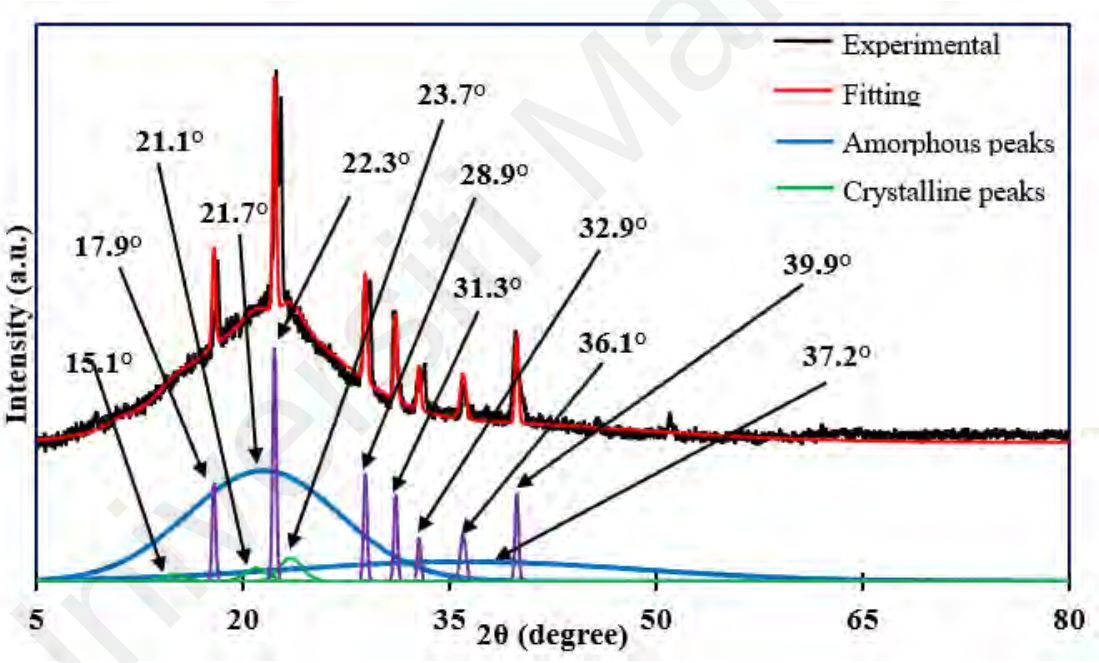

Figure 6.4: Deconvolution XRD pattern of CFs50.

The XRD spectra demonstrate a correlation with the physical appearance of the polymer electrolyte films that have been formed. Figure 6.5 (a) illustrates the physical appearance of CFs20, where the film is very transparent. In the case of CFs30 and CFs40, presented in Figure 6.5 (b) and (c) respectively, the addition of 30 wt. % and 40 wt. % of salt to the system yields less transparent films. Based on the XRD pattern, several

distinctive peaks contributed by NH_4NO_3 can be observed in both CFs30 and CFs40 that could be due to the recrystallization of NH_4NO_3. However, Figure 6.5 (d) exhibits an opaque film of CFs50, indicating that some of NH_4NO_3 particles are undissolved which remain crystals within the mixture. This XRD patterns were supported with the physical appearance of the films.

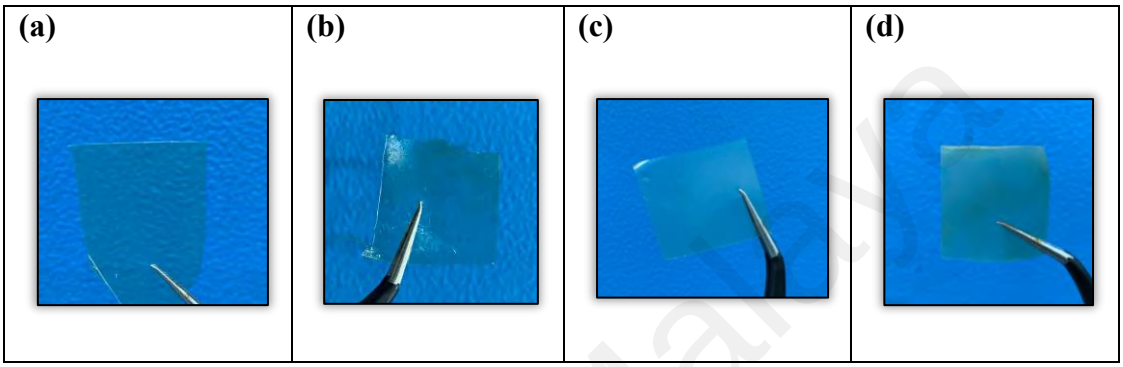

Figure 6.5: The physical appearance of electrolyte film (a) CFs20, (b) CFs30, (c) CFs40 and (d) CFs50.

To strengthen the findings in XRD pattern, the degree of crystallinity, X_c for the selected FG-CS-NH_4NO_3 electrolytes are determined using Equation 4.1 and the values are tabulated in Table 6.2. With addition of 20 wt. % of salt, the X_c decreased from 15.38 % to 13.04 %.

Table 6.2 Degree of crystallinity for selected electrolytes.

Electrolytes	X_c (%)
CF4	15.38
CFs20	13.04
CFs30	12.49
CFs40	10.03
CFs50	12.80

As more salt is added into the system, the value decreased to 10.03 % in CFs40. This indicates that even with additional crystalline peaks emerged from NH_4NO_3, the amorphous region in CFs40 is still vast compared to the crystalline region in CFs40. However, the X_c increased in CFs50 to 12.80 %. As mentioned previously, the polymer host will no longer be able to accommodate the salt at this rate. Thus, from the observation from XRD deconvoluted pattern and X_c calculation, CFs40 has the highest amorphous region with the lowest value of crystallinity in the electrolyte.

6.3 Fourier Transform Infrared Spectroscopy (FTIR)

In order to determine the effect of various amount of NH_4NO_3 salt into CF4, the intensity, position and shape of the peaks from FTIR will be discussed. The interactions and chemical processes between the salt and the blend polymer host can be determined from the band shifts and changes of the peaks wavenumber. The salted FG-CS films (CFs) FTIR spectra were compared with CF4 FTIR spectra as shown in Figure 5.4. Figure 6.6 shows the FTIR spectra for FG-CS-NH_4NO_3 at selected wavenumbers where Figure 6.6 (a) is for hydroxyl band and Figure 6.6 (b) is for carboximide band, respectively.

The first interaction occurred in hydroxyl band (3000 - 3400 cm^{-1}) as shown in Figure 6.6 (a). The adsorption band at this region owing to -OH stretching becomes wider which resulted from the salt incorporation to the system. There is a slight shift towards a lower wavenumber as salt concentration increased which indicates that there is interaction and complexation developed between the polymer blend host and the salt (Abdulkareem, 2021; Mohd Asnawi et al., 2020; Rahman et al., 2021). In Figure 6.6 (a), the peaks shifted from 3278 cm^{-1} to 3248 and 3213 cm^{-1} as 10 wt. % and 20 wt. % of NH_4NO_3 added into the system, respectively. Further addition of salt resulted in the emergence of two

distinguish peaks at 3286 cm^{-1} and 3000 cm^{-1}. These two peaks' range had been identified by Jothi et. al (2022) as O-H stretching and C-H stretching after ammonium salt is added into the system (Jothi et al., 2022). When salt is added to a polymer, the cations are predicted to form interaction within the polymer host, which might alter the polymer's original backbone structure and some infrared active mode of vibrations (Wang & Alexandridis, 2016).

Figure 6.6 (b) shows the carboxamide band for CF4 is located at 1637 cm^{-1}. This value is similar to a study by Chen et al., (2021) where the authors have found a peak at 1630 cm^{-1} refering to amide I: C=O stretching (Chen et al., 2021; Tahir et al., 2022). The peak is down shifted to a lower wavenumber from 1635 cm^{-1} to 1623 cm^{-1} as 10 wt. % to 40 wt. % of salt is added into the system, respectively. The shift denotes that more H^+ and NH_4^+ have interacted with to C=O and the complexation has occurred between CF4 and NH_4NO_3 (Tahir et al., 2022). With further addition of salt, at CFs50, the peak has shifted to a higher wavenumber equals to 1629 cm^{-1} that infers the recombination of salt due to salt saturation as denoted by sample CFs50. Therefore the interaction between the cations if the salt and the polymer host decreases. The peak located at 1533 cm^{-1} in CF4 is assigned to amide I and amide II vibrations (Fundo et al., 2015). In previous study by Rahman and his co-worker, it is reported that the peak at ~1561 cm^{-1} are attributed to the N-H bending in amide II (Rahman et al., 2021). Based on FTIR spectra in Figure 6.7 (b), the peak at 1533 cm^{-1} has down shifted a bit to 1529 cm^{-1} in CFs40. However, the peak has shifted to a higher wavenumber in CFs50. This result is consistent with the other band peak for CFs50.

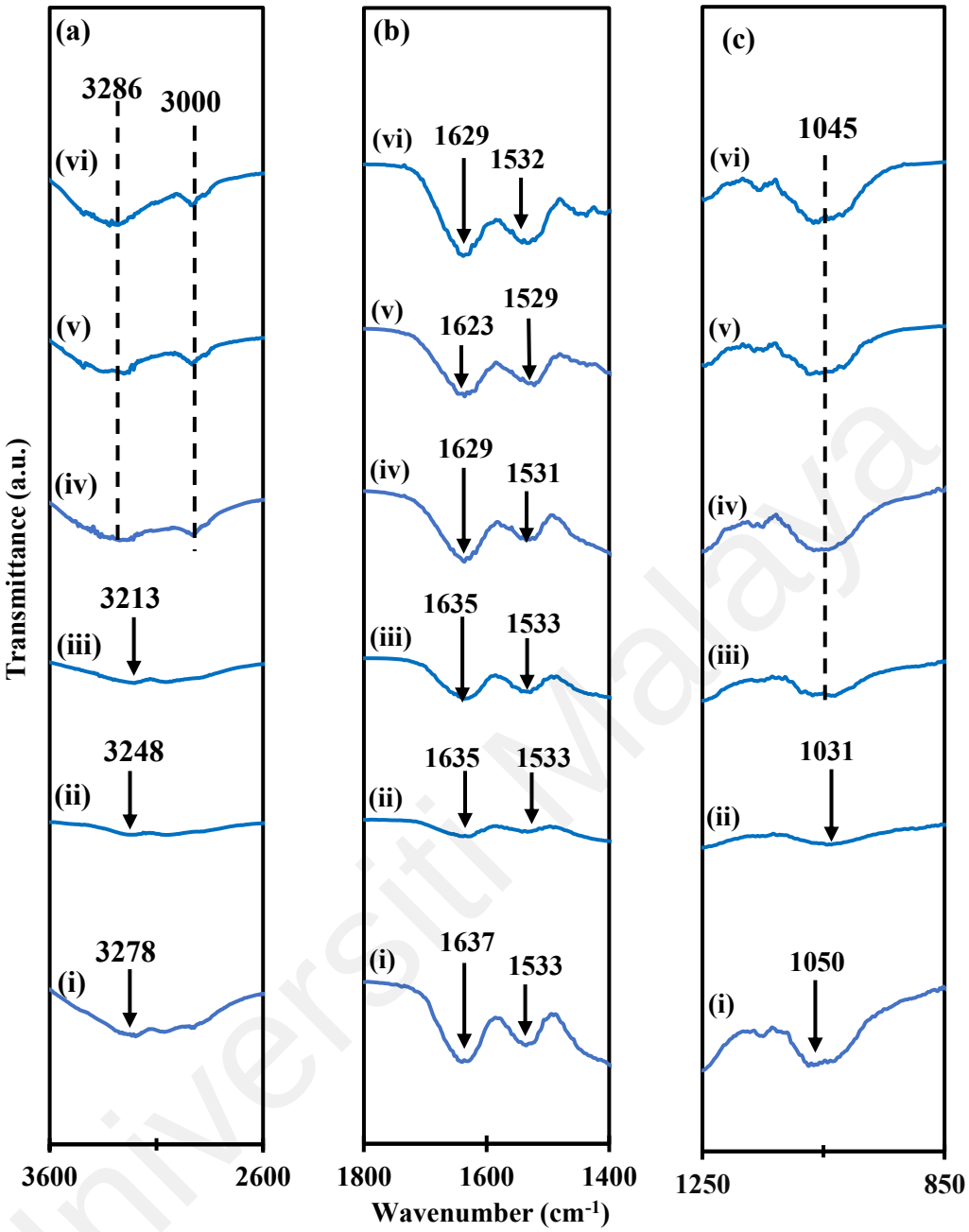

Figure 6.6: FTIR spectra at selected wavenumber (a) hydroxyl band, (b) carboxamide band and (c) saccharide region for (i) CF4, (ii) CFs10, (iii) CFs20, (iv) CFs30, (v) CFs40 and (vi) CFs50.

Figure 6.6 (c) shows the sacharide region between 850 cm^{-1} to 1250 cm^{-1}. These band is assigned to C-O-C asymmetric stretching vibrations of an ester group (Leo Edward et al., 2021). In addition, Rahman and co-worker (2021) reported a similar results for both symmetric and asymmetric stretching vibrations of C–O and C–O–C polysaccharide skeleton within 1151 cm^{-1} to 895 cm^{-1} (Rahman et al., 2021). In this work,

the peak is centred at ~1066 cm^{-1} wavenumber. There was a noticeable shift of the band towards a lower wavenumber as salt is introduced into the system. This change could be attributed to the protonation of the NH_4^+–NO_3^- complex, connecting the H^+ carrier to the oxygen of the C-O-C through weak van der Waals forces (M.A. Saadiah, Y. Nagao, 2020). In the corresponding spectral region, the prominence of a peak at ~1045 cm^{-1} becomes more pronounced with an increasing ratio of NH_4NO_3. This specific peak is recognized as originating from nitrate, which serves as confirmation of the existence of NH_4NO_3 within the polymer electrolytes (Abdulkareem, 2021; M.A. Saadiah, Y. Nagao, 2020; Tahir et al., 2022). Figure 6.7 illustrates the possible interaction between FG-CS-NH_4NO_3.

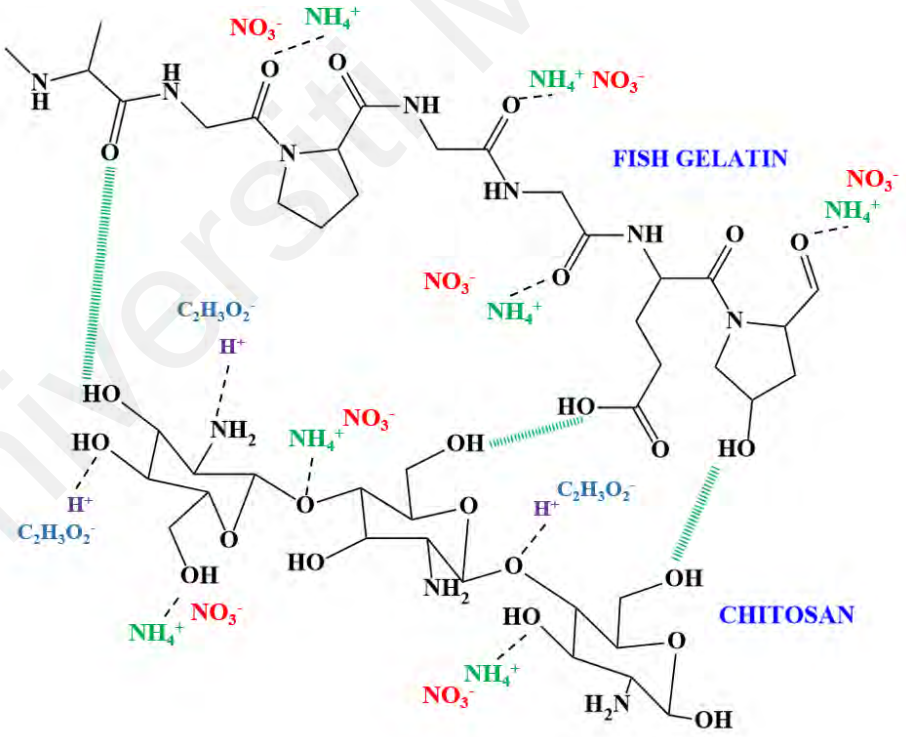

Figure 6.7: Illustration for possible interactions between FG-CS-NH_4NO_3.

6.4 Field Emission Scanning Electron Microscope (FESEM)

Field Emission Scanning Electron Microscopy was used to examine the morphological characteristics of the FG-CS-NH_4NO_3. The FESEM micrographs can provide significant information about the morphology and surface structure of the electrolytes in this work. Figure 6.8 shows the surface micrographs for (a) CFs10 and (b) CFs20, respectively. As salt is added into the system, the smooth surface exhibited by CF4 became rougher as can be observed in Figure 6.8. When salt added into the system, a more porous structure exhibited by the electrolyte surface as shown in the zoom area, served as a proof of successful accumulation of NH_4NO_3 (Qiang et al., 2018). A work by Abdulkadir and co-workers (2021) explained that addition of salt can disrupt the crystalline structure of the polymer hence increases the amorphousness. The porous structure and the voids will also serve as ion migration paths which is a crucial characteristics of good electrolyte (Abdulkadir et al., 2021; Shamsuri et al., 2020).

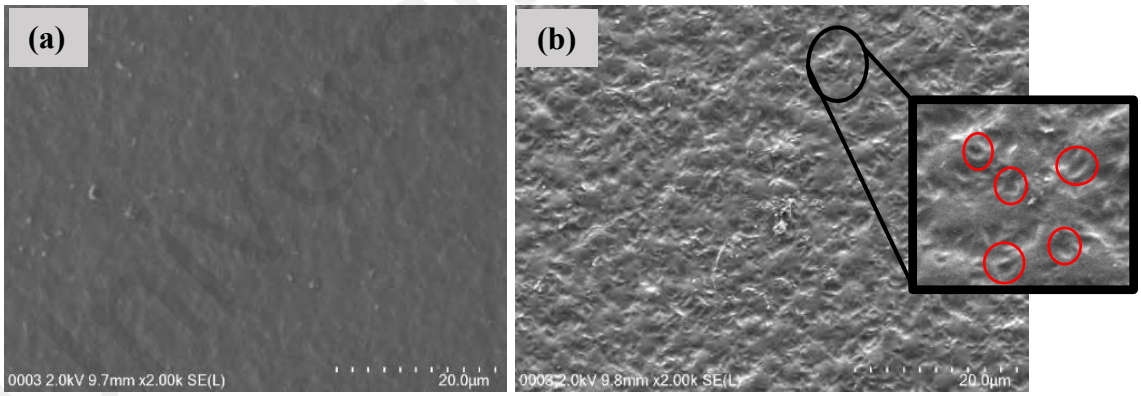

Figure 6.8: Surface micrographs of (a) CFs10, and (b) CFs20.

Figure 6.9 shows the surface morphology of CFs40. From the micrograph, existence of grains at the surface of CFs40 can be clearly seen. These grains are probably attributable by the ion traps as the XRD pattern for this film exhibited peaks that can be assigned to NH_4NO_3. However, based on the calculation of X_c, it can be inferred that CFs40 possesses the lowest value and has the broadest amorphous region as can be seen

in Figure 6.3. Therefore, it can be concluded that in CFs40, the rate of ion dissociation is more than the rate of ion association.

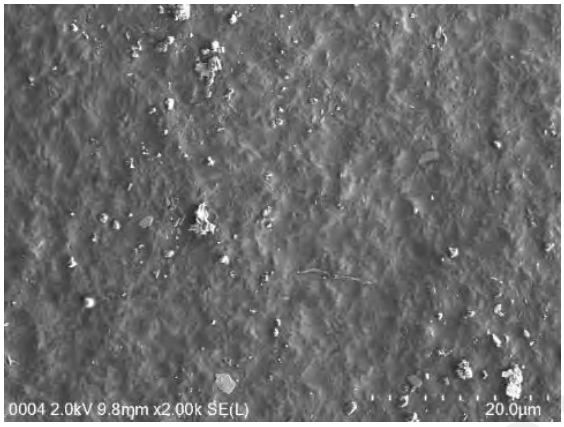

Figure 6.9: Surface micrographs of CFs40

However, with more than 40 wt.% of salt was added, the surface became coarser. Figure 6.10 shows the surface micrographs for CFs50 and CFs60 respectively. The transformation of the surface morphology in both samples could be due to the fact that the polymer host is unable to accommodate large amounts of NH_4NO_3 resulted in salt recrystallization (Abdulkadir et al., 2021).

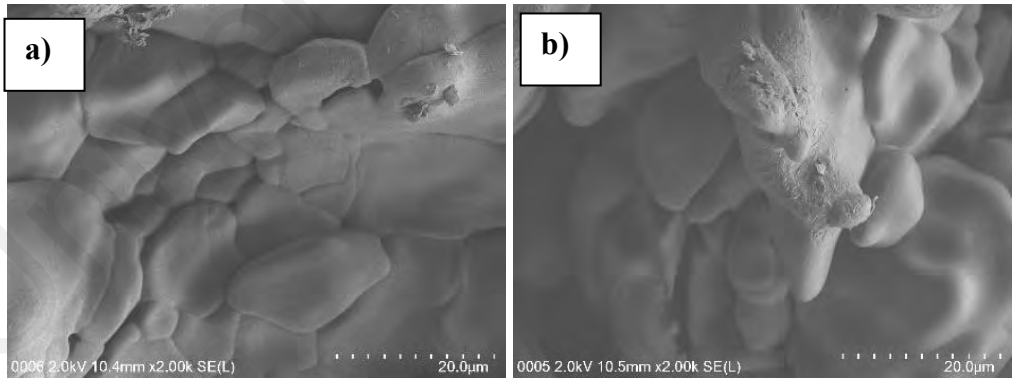

Figure 6.10: Surface micrographs of a) CFs50 and b) CFs60

This phenomenon can be observed from both CFs50 and CFs60 as the solid particles can be clearly seen protruded out from the films surface. The recombination of ions have led to the loss of a significant amount of charge carriers which effected the conductivity badly (Abdulkadir et al., 2021). The XRD pattern for CFs50 also reveals

obvious crystallites peaks contributed by NH_4NO_3. The degree of crystallinity for CFs50 and CFs60 were found to be higher than CFs40. The result from the calculation strengthens the findings in FESEM surface analysis.

6.5 Impedance Studies

Figures 6.11 depicts the Nyquist plots for selected samples in salted polymer blend system at room temperature. Pure FG-CS film as shown in Figure 6.11 (a) exhibits an incomplete semicircle curve. After the addition of 20 wt. % of NH_4NO_3, the plot is adjacent line appeared to the semicircle at low frequency region**.** The bulk resistance can be taken from the interception of the semicircle with real axis. Semicircle represents the bulk conductivity due to parallel combination of bulk resistance and bulk capacitance known as constant phase element (CPE) (Hadi et al., 2020). With combination of spike and semicircle, the spike at low frequency portrays the polarization effect while the semicircle is due to migrations of ions in the bulk of electrolytes (Abdelrazek et al., 2019).

It is reported that when the capacitance is ideal, only the tilted line will appear in the Nyquist plot (Lenz et al., 2020). Due to ions migrating at low frequency, the electrode/electrolyte contact forms a double layer capacitance, which is represented by the inclined spike (Abdelrazek et al., 2019). The tilted straight line should be angled at 90° however the line angle shows in this study is less than 90°. This is due to the roughness of double-layer capacitance in the electrolyte-electrode edge (Azli et al., 2020). Figure 6.12 presents the Nyquist plots for CFs30 and CFs40. With the addition of 30 wt. % and 40 wt. %, the semicircle regions disappeared, left with spike only.

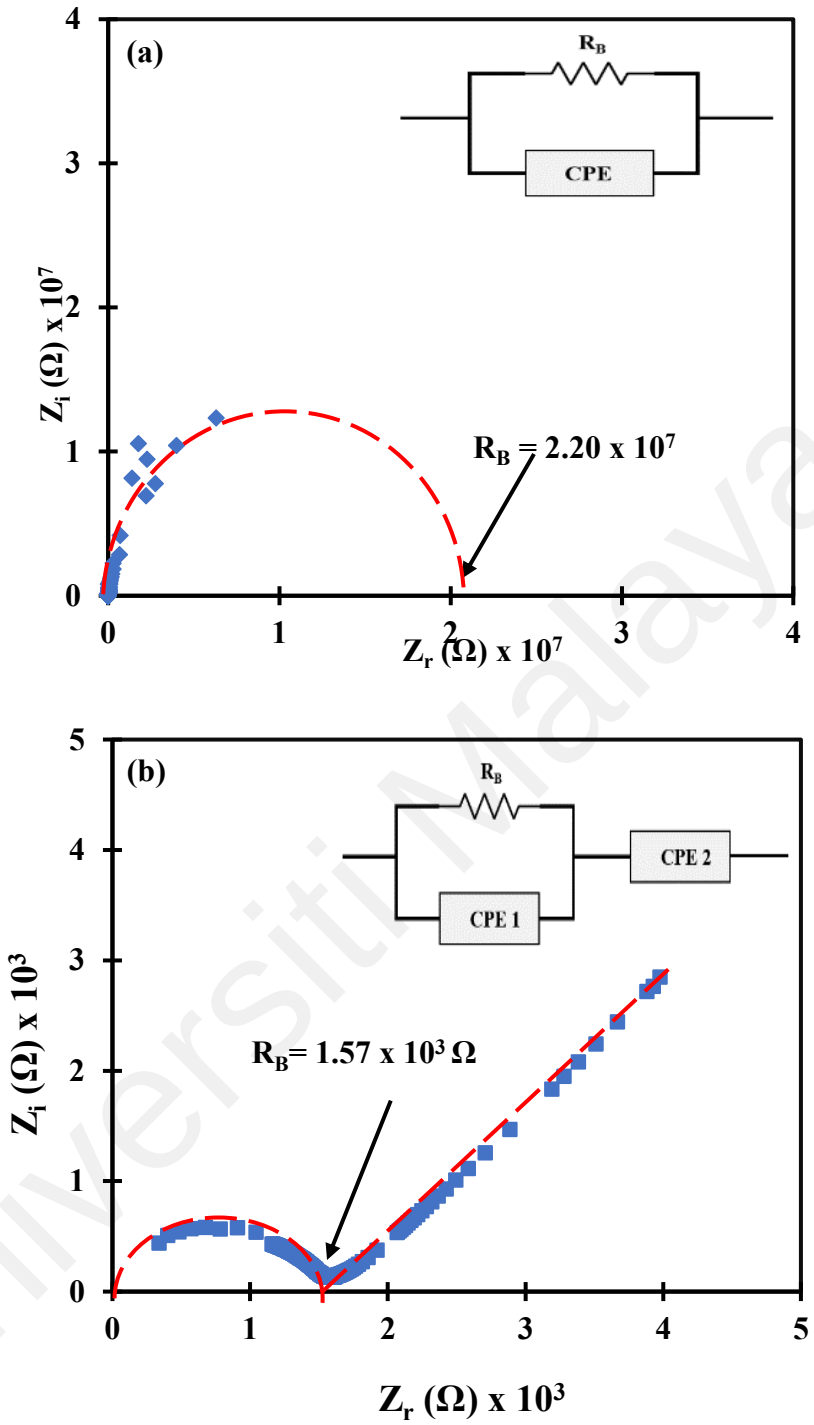

Figure 6.11: Nyquist plots for (a) CF4 and (b) CFs20 at room temperature.

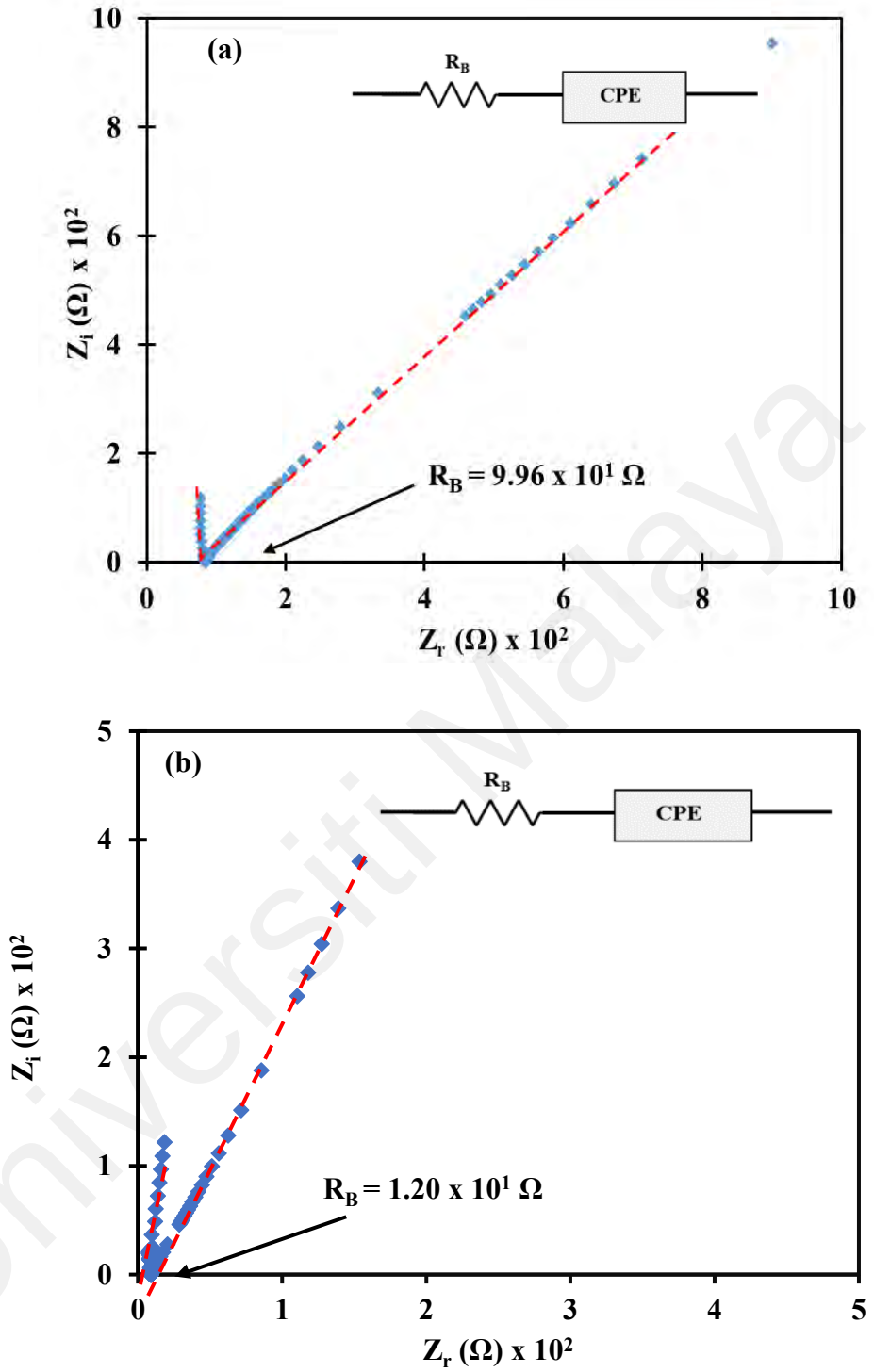

Figure 6.12: Nyquist plots for (a) CFs30 and (b) CFs40at room temperature

When the salt content increases, only the resistive component of composite prevails because of the random orientation of the dipoles in the polymer side chains (Abdelrazek et al., 2019; Mazuki et al., 2020). The R_B value is determined by the interception of the line with the real axis as shown in Figure 6.12. The lowest value of R_B

is found in CFs40 which equals to 1.21×10^1 Ω. The disappearance of semicircle part indicates that resistive parts of the polymer are dominant (Manjakkal et al., 2020). A similar type of impedance plot observed in the polymer matrix consists of NH_4NO_3 in previous study by other authors (Abdulkareem, 2021; S. B. Aziz et al., 2020). Based on the Equation 3.2 in Chapter 3, the lowest R_B possessed by CFs40 will obviously give the highest conductivity value in the system. The impedance of constant phase element (CPE), can be expressed as :

$$Z_{CPE} = \frac{1}{C\omega^p}\left[\cos\left(\frac{\pi p}{2}\right) - i\sin\left(\frac{\pi p}{2}\right)\right] \quad \text{(Equation 6.1)}$$

where C is the capacitance of CPE, ω is angular frequency and p is related to the deviation of the plot from the axis.

With further addition of salt, the interception value increases meaning that salt has been recrystallize . It is also observed in Figure 6.13 that the semicircle at high frequency region reexist. The semicircle in CFs60 is higher than the semicircle in CFs50, indicates a lower conductivity value.

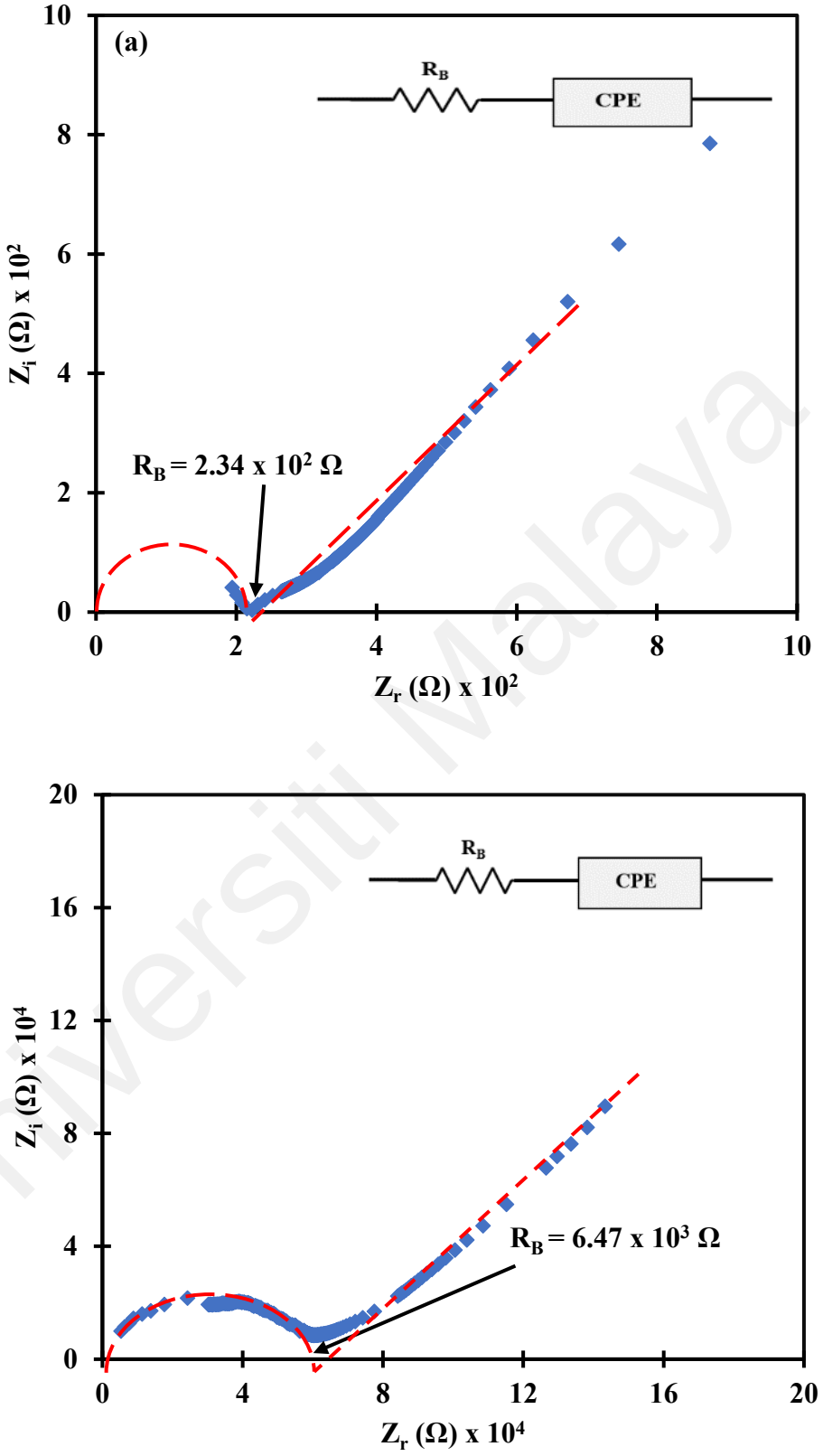

Figure 6.13: Nyquist plots for (a) CFs50 and (b) CFs60 at room temperature

6.6 Conductivity

Variation of room temperature conductivity as a function of NH_4NO_3 concentration for polymer blend FG-CS is presented in Figure 6.14. The conductivity for CF4 was found to be $(5.85 \pm 1.78) \times 10^{-10}$ S cm^{-1}. With the addition of 10 wt. % salt, the electrolyte system has dramatically encountered a transformation where the conductivity value is seen to increase up to $(1.62 \pm 0.15) \times 10^{-6}$ S cm^{-1}. The conductivity kept on increasing to a maximum value of $(1.61 \pm 0.33) \times 10^{-3}$ S cm^{-1} with 40 wt. % of salt addition. This indicates that the conductivity value is able to be improved via polymer blending where the method has created more vacant site effectively for the ions to be transported. Due to more pathways, ions exchange can occur easily and rapidly leading to an increase in conductivity value. With the impregnation of 40 wt. % salt, the conductivity started to decrease as the distance between dissociated ions became too close which enable them to recombine and form neutral ion pairs that do not contribute to conductivity (Aziz et al., 2020). The sample was analysed up to 60 wt. % of salt where the conductivity for CFs60 was further decreased to $(1.40 \pm 1.25) \times 10^{-6}$ S cm^{-1}.

Figure 6.15 depicts the conductivity of CFs40 at elevated temperatures in the range of 303 K to 358 K. The regression values, R^2 for the linearly straight line are all nearly unity which their values are almost ~1 (Yusof et al., 2019). It is well known that temperature will affect the salt dissociation and the segmental motion of the polymer (Arya & Sharma, 2019). In this work, it can be observed that the conductivity increases as the temperature spiking up, that results in the molecular chain becomes more flexible. Furthermore, there are more free ions available, and the segmental mobility increased as temperature increased resulting in an increase in conductivity value. From Figure 6.15, it

can also be seen that all electrolytes did not show any abrupt change in conductivity values with temperature.

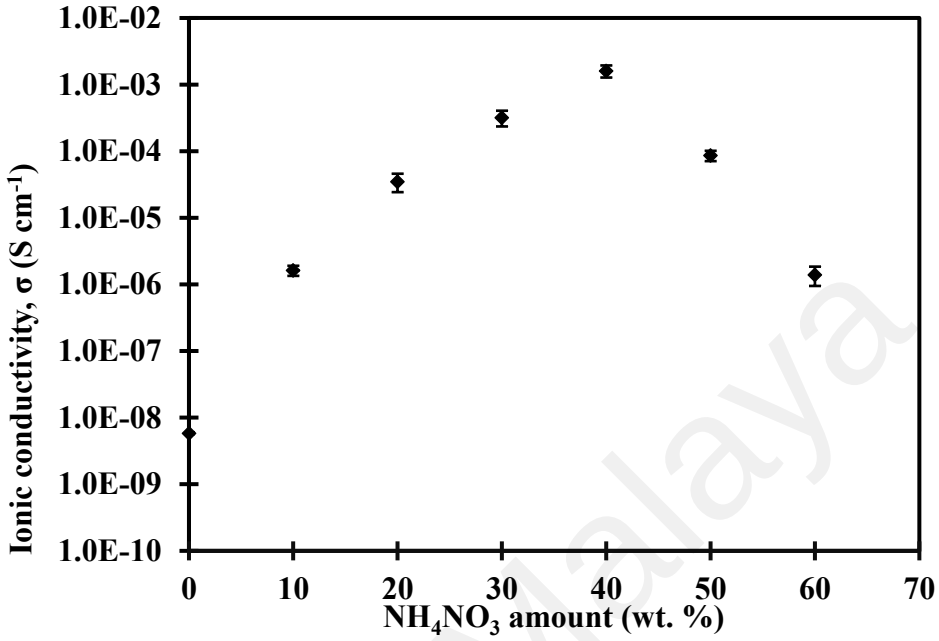

Figure 6.14: Room temperature conductivity of FG-CS-NH_4NO_3

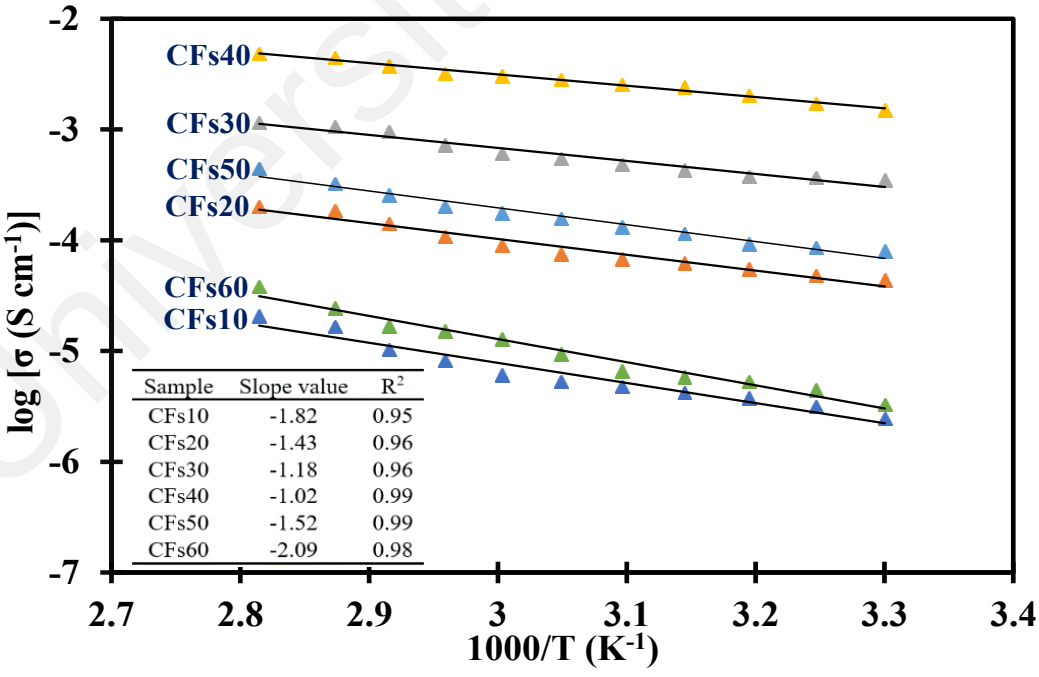

Sample	Slope value	R^2
CFs10	-1.82	0.95
CFs20	-1.43	0.96
CFs30	-1.18	0.96
CFs40	-1.02	0.99
CFs50	-1.52	0.99
CFs60	-2.09	0.98

Figure 6.15: The conductivity of FG-CS-NH_4NO_3 at various temperatures

From the plot of log σ against 1000/T in Figure 6.15, the activation energy for each electrolyte can be obtained. Figure 6.16 shows the activation energy value for different salt concentration in FG-CS films. The study shows that the highest conducting FG-CS-NH_4NO_3 sample possesses the lowest activation energy value. The lowest activation energy of 0.202 eV was established for CFs40 which possesses the maximum conductivity value. This result is comparable with previous study on tragacanth gum-NH_4SCN where the activation energy for the highest conducting polymer, 9.16×10^{-3} S cm^{-1} is 0.2 eV (Jenova et al., 2021).

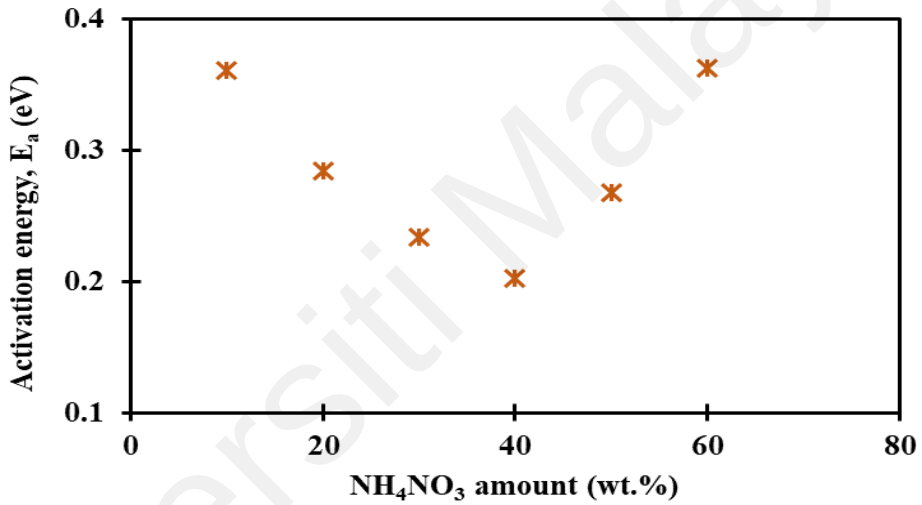

Figure 6.16: The activation energy of FG-CS-NH_4NO_3.

6.7 Ionic Transport Analysis

The conductivity values obtained in FG-CS-NH_4NO_3 system will be further verified and discussed via transport analysis. The τ, η, μ and D were calculated using Equation 4.3, 4.4, 4.5 and 4.6, respectively. All values are tabulated in Table 6.3 and it can be observed that the values of τ, μ *and* D are found increases with increasing amount of salt up to 40 wt. % of NH_4NO_3. The values calculated in this work are comparable with previous study. Aziz and co-worker (2020) have calculated the μ value for carboxymethyl cellulose-chitosan-NH_4Br via Rice and Roth model and they have found that the value

are in the ranged of ~10^{-8} to ~10^{-6} cm^2 V^{-1} s^{-1}. (Aziz et al., 2020). They also claimed that *D* value for glycerolized chitosan-NH_4NO_3 is ~10^{-7} cm^2 s^{-1}. Both studies reported that the values of μ and *D* increases, which causes the value of conductivity to increase as content of salt in the system increased.

With more than 40 wt. % of NH_4NO_3, the values of *τ, μ and D* decrease. This is attributed to the phenomena of overcrowding ions resulted in recombination of ions (Mohamed et al., 2020). The capability of ions to move in the polymer host became restricted, lead to the decreament of *τ, μ and D* values. This is supported by the observed crystallization pattern in XRD analysis as depicted in Figure 6.4. However, for *n,* the value increases even with more than 40 wt.% of NH_4NO_3 is added into the system. Abdulwahid and co-workers (2022) reported similar trend of transport analysis. The values of μ and D decrease with more than 40 wt. % of KSCN doped with CS-PS but value of *n* continues to increase. The authors reported that as more salt added into the system, the number of charge carriers increases and linked to the elevated rate of salt dissociation however there are hindrance of free ion movement caused by the formation of ion clusters lead to the decrement of μ and D values (Abdulwahid et al., 2022).

Table 6.3: Transport parameters of FG-CS-NH_4NO_3 system at room temperature.

Sample	σ (S cm^{-1})	τ (s)	η (cm^{-3})	μ (cm^2 V^{-1} s^{-1})	D (cm^2 s^{-1})
CFs10	$(1.62 \pm 0.28) \times 10^{-6}$	1.20×10^{-13}	1.14×10^{19}	8.89×10^{-7}	2.28×10^{-8}
CFs20	$(3.51 \pm 1.08) \times 10^{-5}$	1.37×10^{-13}	1.24×10^{19}	1.76×10^{-5}	4.52×10^{-7}
CFs30	$(3.20 \pm 0.85) \times 10^{-4}$	1.51×10^{-13}	1.79×10^{19}	1.12×10^{-4}	2.87×10^{-6}
CFs40	$(1.62 \pm 0.33) \times 10^{-3}$	1.62×10^{-13}	3.00×10^{19}	3.35×10^{-4}	8.59×10^{-6}
CFs50	$(8.62 \pm 1.52) \times 10^{-5}$	1.39×10^{-13}	6.42×10^{19}	8.38×10^{-6}	2.15×10^{-7}
CFs60	$(1.40 \pm 0.45) \times 10^{-6}$	1.20×10^{-13}	9.40×10^{19}	9.30×10^{-8}	2.39×10^{-9}

6.8 Dielectric Constant and Dielectric Loss Studies

In this subtopic, the dielectric constant and dielectric studies for FG-CS-NH_4NO_3 were analysed and discussed. The dielectric constant (ε_r) and dielectric loss (ε_i) for the polymer electrolyte system were determined using the Equation 4.7 and 4.8, respectively. The graph demonstrated that at low frequency, the electric permittivity value is large and as frequency increases, the permittivity value decreases. The variation of ε_r and ε_i for FG-CS-NH_4NO_3 are similar to the pattern obtained for FG-NH_4NO_3 system. According to Saeed and Abdullah (2020), both ε_r and ε_i decreases as the frequency increases due to dielectric relaxation processes. Aziz and co-workers reported in some of their studies that dielectric behaviour at low frequencies are normally associated to the build-up of ions at the electrode/electrolyte interfaces whilst at high frequency, the ions accumulations will resulted in polarization decrement (S. B. Aziz et al., 2018; S. B. Aziz, Al-Zangana, Brza, et al., 2019; S. B. Aziz, Dannoun, Abdulwahid, et al., 2022).

From Figure 6.13, it can be observed that the increasing amount of salt added have improved the dielectric constant which indicates a higher amount of H^+ ions available in the electrolytes (Zulkifli et al., 2020). Sample CFs40 exhibits the highest value for both ε_r and ε_i, respectively. The addition of salt has increased the mobile charge carriers which in turn increases the conductivity value (Moniha et al., 2018). The trend in dielectric studies in this work are consistent with the conductivity analysis that had been discussed earlier. After the amount of 40 wt. % salt are added, both ε_r and ε_i values experienced a decrement as depicted in Figure 6.17. Rapid ions re-association occurred at higher salt concentrations, which will hinder ions to move easily (Hamsan et al., 2017b). The variation of ε_r and ε_i with temperature at 303 K to 353 K for CFs40 is depicted in Figure 6.18.

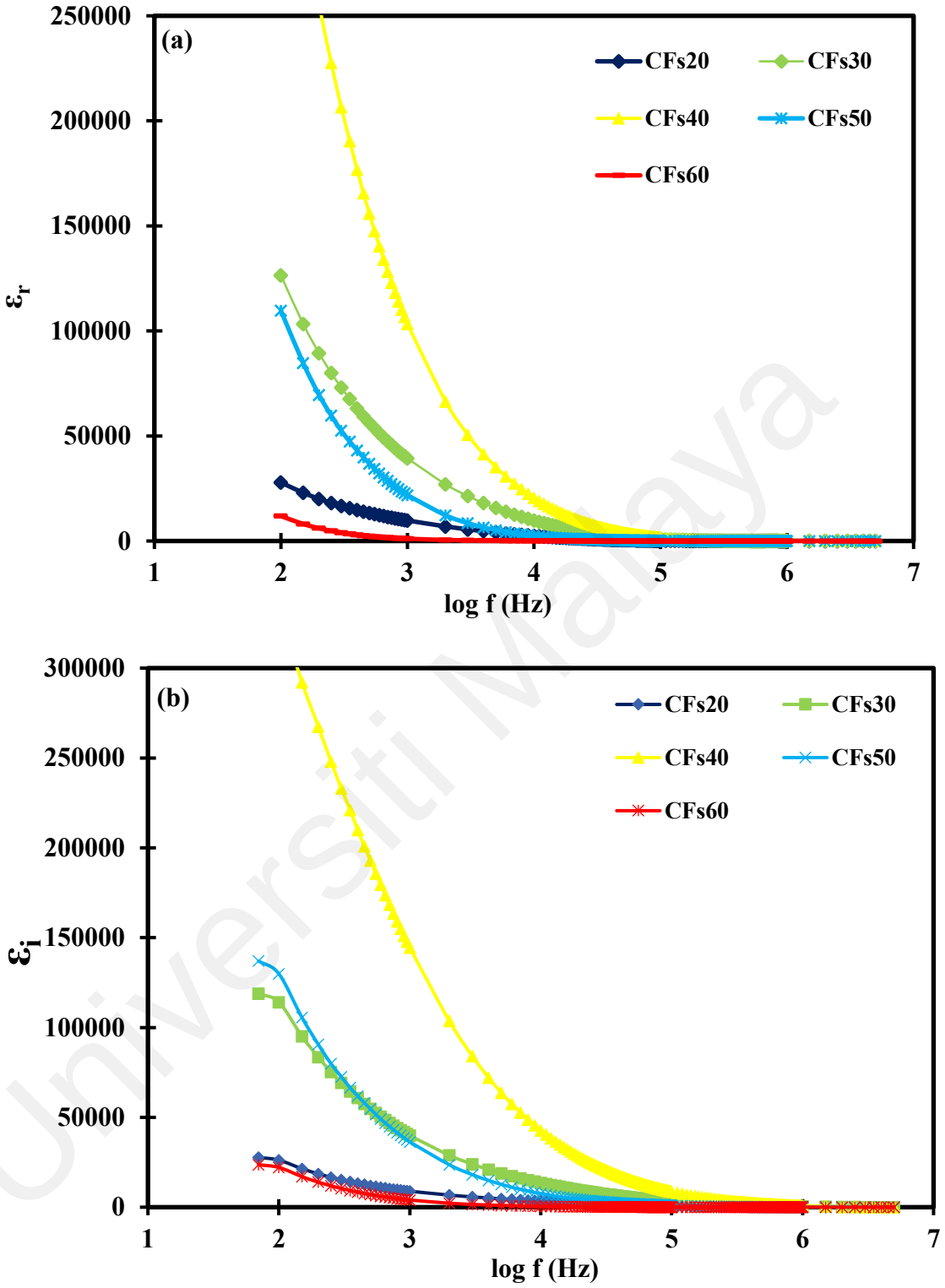

Figure 6.17: (a) The dielectric constant and (b) dielectric loss at room temperature.

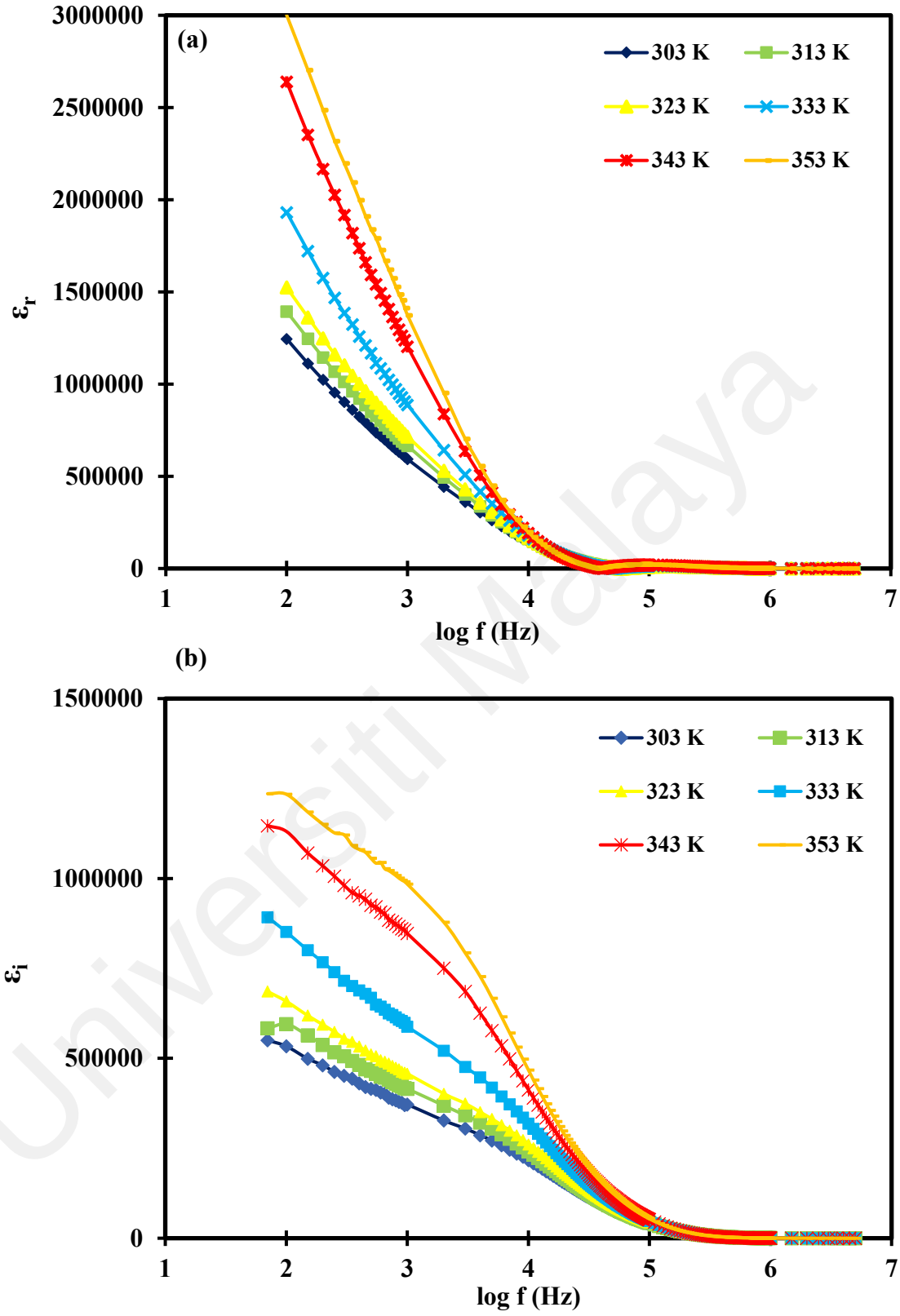

Figure 6.18: (a) The dielectric constant and (b) The dielectric loss at different temperatures.

6.9 Thermogravimetric Analysis (TGA)

Figure 6.19 shows TGA curve for the selected FG-CS-NH_4NO_3 electrolytes from 0 °C to 600 °C. The curves are indicated by blue, orange, and grey lines for CF4, CFs20 and CFs40, respectively. There are 3 stages of thermal degradation as can be seen in the figure. From the Figure 6.18, the first degradation is due to the water weight loss by the removal of moisture attained at temperature between 50 °C to 180 °C. The loss is determined to be ~5.5% for CF4 and about ~4% for both CFs20 and CFs40. The first degradation mainly contributed from water loss that has been absorbed from surrounding moisture and residuals from acetic acid solution (Rahman et al., 2021). Based on the values obtained, the presence of salt has lessened the total weight loss which prove that the polymer blend thermal stability is improved.

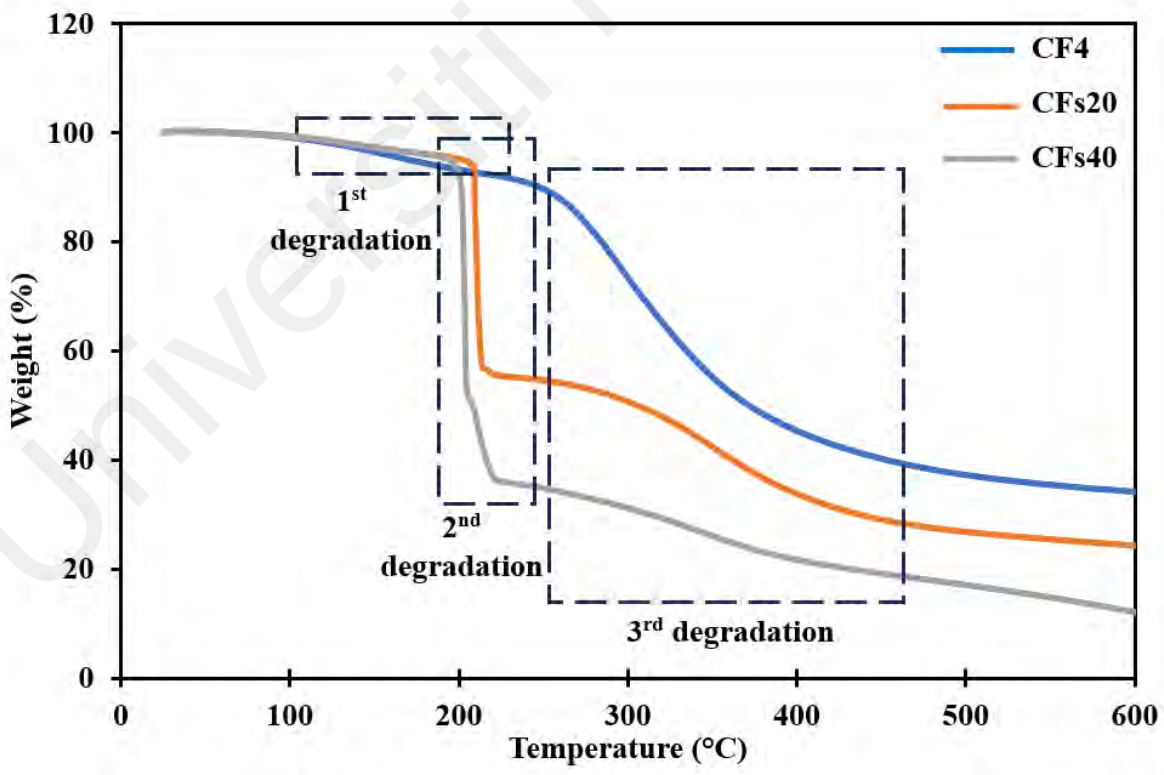

Figure 6.19: TGA thermogram of CF4, CFs20 and CFs40.

Figure 6.20 and Figure 6.21 represent the degradation temperature and the percentage of weight loss for 2nd and 3rd degradation respectively. The 2nd degradation temperature for CFs20 is ~215.13 °C whilst the temperature drops to 205.23 °C for CFs40. From previous study, this temperature range indicates the decomposition of NH_4NO_3 which was absent in CF4 (Hamsan et al., 2017). In addition, this result is comparable with a study from Ghazali and his co-workers. They have found that the decomposition temperature of NH_4NO_3 is within 160 °C to 220 °C (Ghazali et al., 2022).

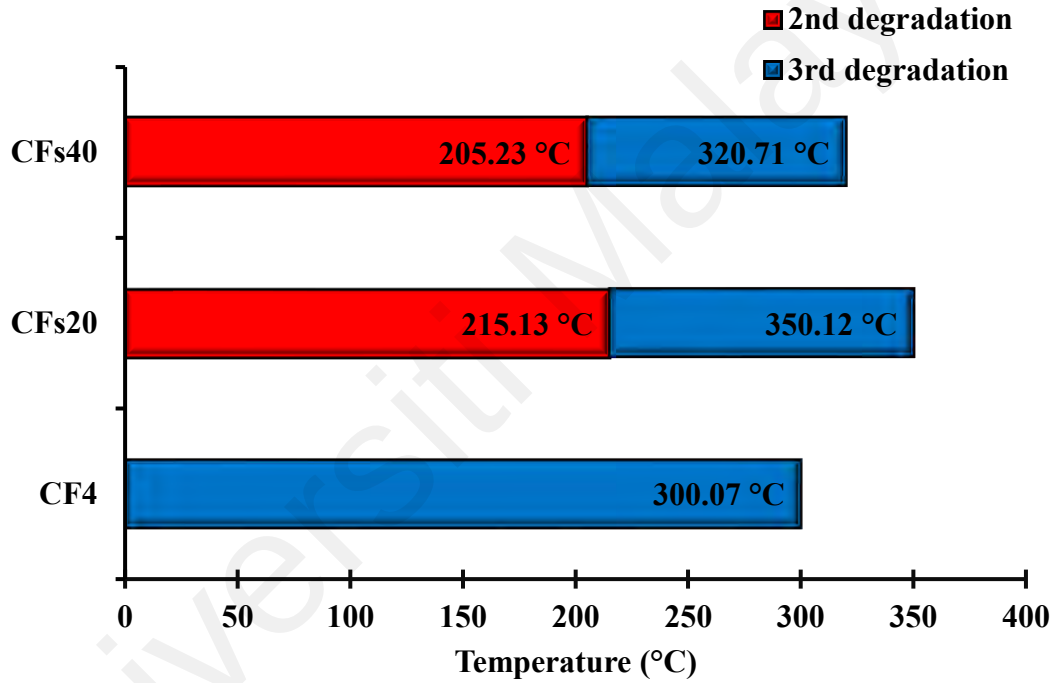

Figure 6.20: Degradation temperature for selected electrolytes in FG-CS-NH_4NO_3.

CFs40 has a higher weight loss percentage in 2nd degradation compared to CFs20 as illustrated in Figure 6.21. The weight loss for CFs20 and CFs40 are determined to be 38.23 % and 58.50 %, respectively. It can be seen that, as more salt is added, there are more weight loss and the decomposition temperature has reduced as a result from the disruption of hydrogen bond between polymer chains by the presence of salt (Kadir, 2021). Thus, higher salt content causes the polymer easier to be degraded. Previous studies found that NH_4NO_3 degraded into NH_3, HNO_3, H_2O, and N_2O when heated around

160 °C to 210 °C (Chaturvedi & Dave, 2013; Izato & Miyake, 2015; Skarlis et al., 2014) . The third degradation in this work could be due to the polymer blend of fish gelatin-chitosan. This degradation occurs between 300 °C to about 350 °C.

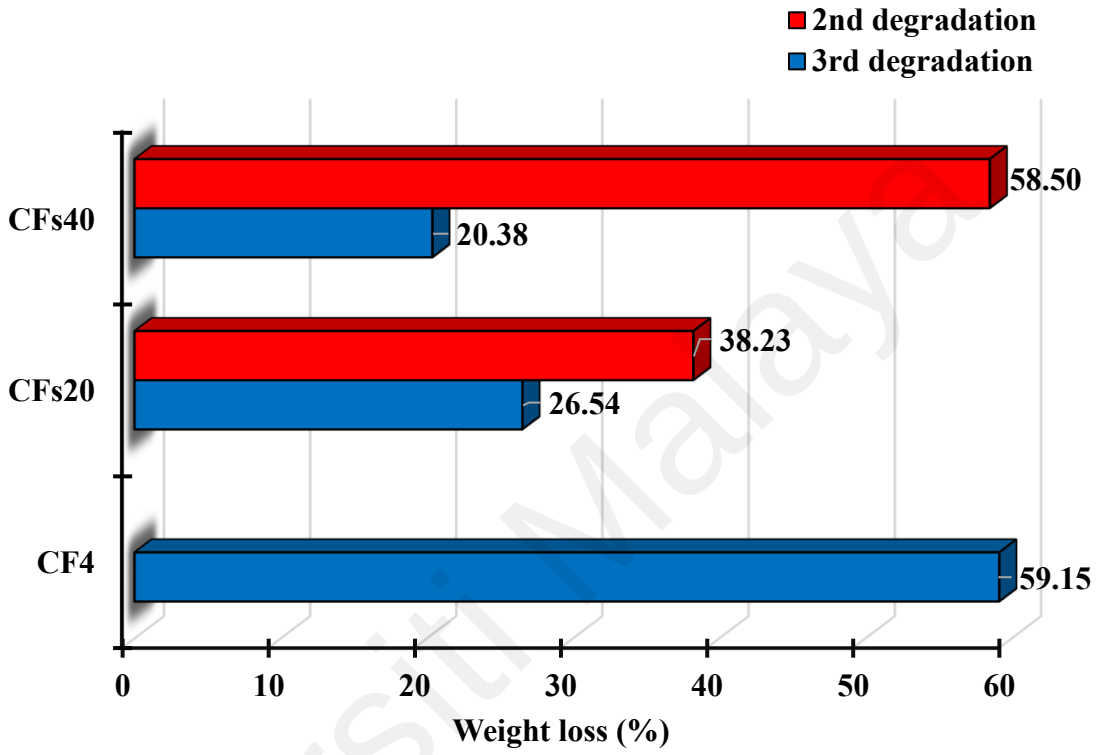

Figure 6.21: Weight loss for selected electrolytes in FG-CS-NH_4NO_3

6.10 Differential Scanning Calorimetry (DSC)

In this section, T_g has been studied in order to confirm the effect of salt on polymer blend electrolytes. Figure 6.22 shows the DSC plot for CF4 in green, CFs20 in blue and CFs40 in red line. Similar to Chapter 4, as salt added into the system, the T_g temperature decreasing from 93.33 °C to 83.33 °C for CF4 and CFs40, respectively. The decreased in the T_g had suggested the occurrence of the disruption of intermolecular hydrogen bond within the polymer host, resulting in cation-anion interaction with the salt (Jridi et al., 2014). As a result, a softer backbone is formed with flexibility enhancement. The H^+ ions

are able to move easily in the polymer host hence, increasing the ionic conductivity (Rasali et al., 2018; Sudhakar & Selvakumar, 2012).

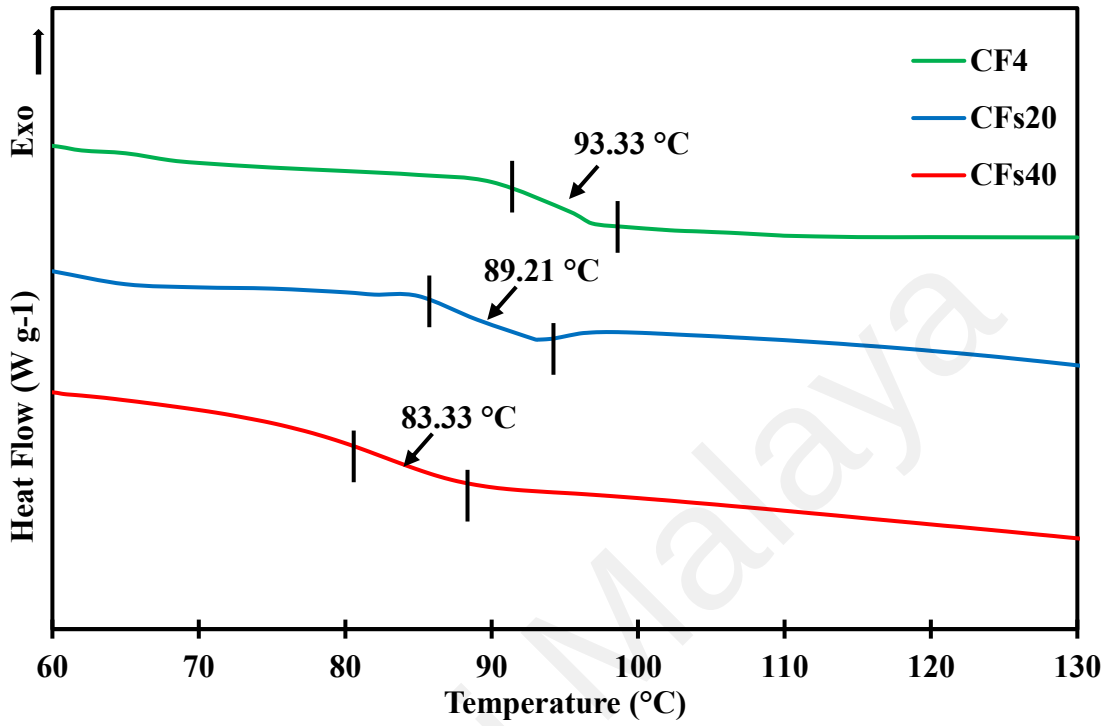

Figure 6.22: DSC thermogram of second heating run for selected FG-CS-NH_4NO_3.

6.11 Transference Number Measurement (TNM)

The conducting species can be evaluated via transference number analysis. The total contribution of total ionic conductivity of the polymer electrolyte is determined by the polarization of the blocking electrode cell configuration of SS|CFs40|SS and monitoring the potentiostatic current as a function of time. The current as a function of time for the highest conducting electrolyte, CFs40 is depicts in Figure 6.23. The transference numbers corresponding to ionic (t_{ion}) and electronic (t_e) can be established respectively using this Equations 4.9 and 4.10.

The current flow within the electrode will show a rapid drop upon time if it is an ionic conductor. The decrement is due to the blocking of ions caused by the characteristics

of the stainless steel electrode which only allows the electron to move (S. B. . Aziz et al., 2021). This can be seen in Figure 6.22 where the current has dropped rapidly at the initial stage before being saturated from 2.4 µA to 0.1 µA.

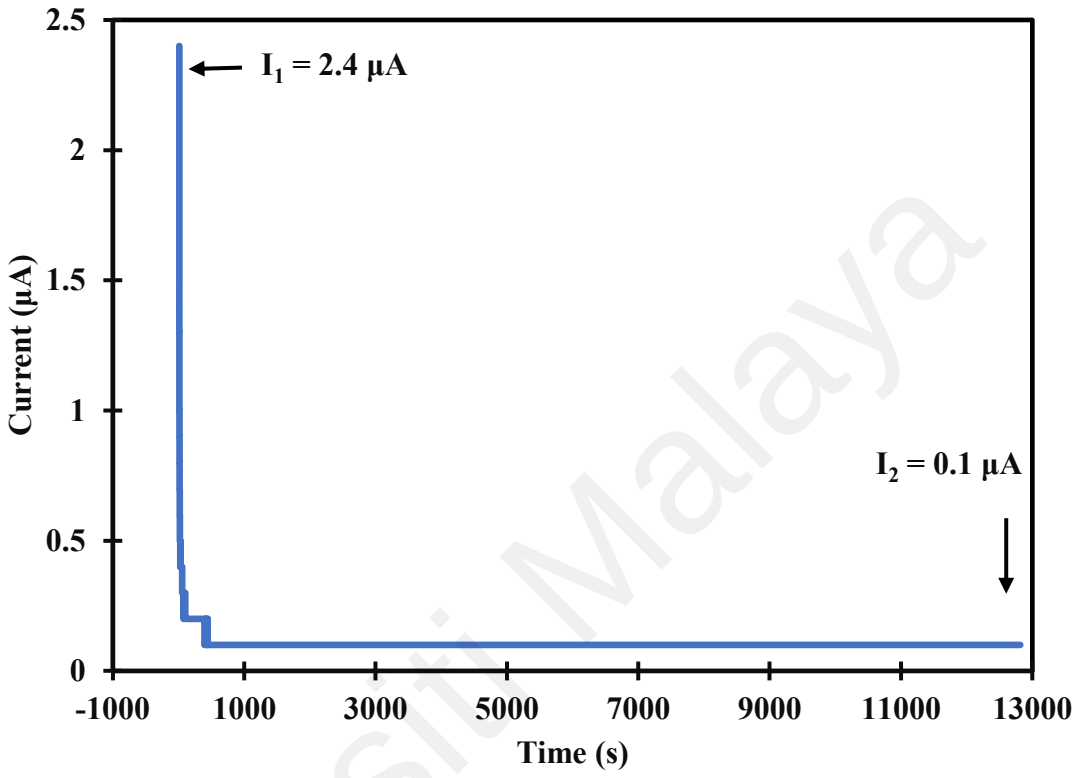

Figure 6.23: Plot for ionic transference number for CFs40

The steady state current has been achieved when the movement is balanced by diffusion process where the current flow is only caused by the electrons without any ions contributions (Aziz et al., 2021). Based on the calculation, the t_{ion} and t_e recorded to be 0.96 and 0.04, respectively. Since CFs40 has achieved high t_{ion} value, it can be inferred that the system was dominantly contributed by the ions to serve as the conducting element (Hamsan et al., 2017). Previous study also found that the dominant charge in chitosan-based polymer electrolyte where the authors reported that the t_{ion} values were ~ 0.95 to 0.96 by Abdulkarem (2021) and Hadi et al (2021).

6.12 Linear Sweep Voltammetry (LSV)

Figure 6.24 shows the LSV plot for the highest conducting electrolyte in this work. For CFs40, the decomposition happens at ~2.6 V. Aziz and co-worker (2022) reported that the electrochemical stability of 2.85 V is achieved with gelatin based electrolyte doped with NH_4NO_3 with conductivity $\times 10^{-4}$ S cm^{-1} (Aziz et al., 2022) whilst Hamsan and co-worker (2020) found that for chitosan based electrolyte, the electrochemical stability is 2.4 V with the same conductivity, $\times 10^{-4}$ S cm^{-1} (Hamsan et al., 2020). The result obtained for FG-CS doped with 40 wt. % of NH_4NO_3 are comparable with these studies. The blended polymer shows an increment of the maximum working voltage which is better than the working voltage of single-salted polymer. This could be due to the improvement in physical properties of the blended polymer.

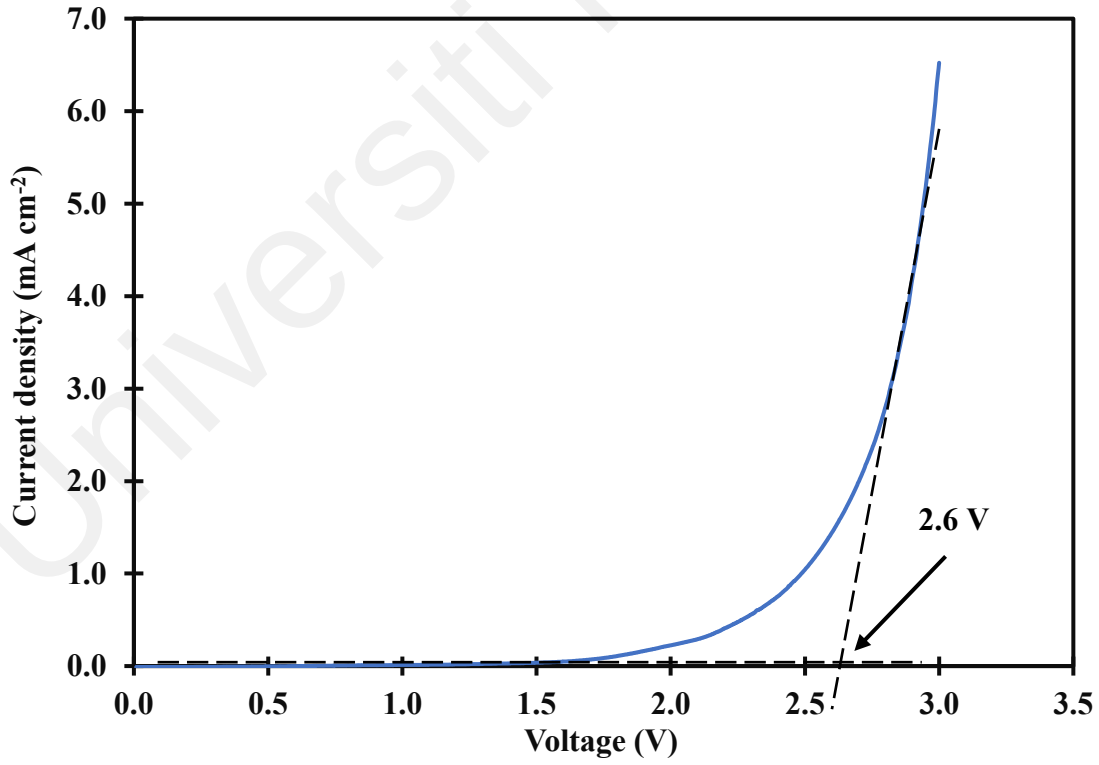

Figure 6.24: LSV plot for CFs40

CHAPTER 7: DISCUSSION

The continual growth in demand for environmentally friendly energy solutions necessitates the investigation of new energy storage materials. Natural inspiration is unquestionably a potential strategy for complying with environmental regulations. Numerous energy conversion and storage technologies, including lithium batteries, fuel cells, supercapacitors, liquid flow batteries, and others, have developed quickly to fulfil the application needs in numerous sectors. Liquid electrolytes have been widely used in commercialization, however there are several safety concerns such as possibility of flammability and explosion (Jian et al., 2022). Concurrently, the long-cycle performance of batteries will be reduced by the formation of dendrites. Thus, it is important to stop the dendrite formation by creating a high-safe solid state electrolytes. SPEs provide superior interfacial compatibility qualities, safety, and flexibility, making them the most desirable candidate electrolytes for the upcoming generation of flexible batteries (Chattopadhyay et al., 2023).

Natural materials are preferable than artificial materials in terms of biocompatibility, accessibility, and modification ease. Furthermore, because native natural materials include reactive groups, it is possible to incorporate other functional groups into them to give the newly created materials amazing functionalities or change their chemical and physical characteristics (Chitra et al., 2020). Numerous studies on polymer electrolyte have revealed that ionic conductivity varied between ~10^{-5} and ~10^{-3} Scm^{-1} and various biopolymers such cellulose, starch, dextran, chitin, gelatin, chitosan and carrageenan had been employed as host polymers (Dannoun et al., 2020). The hydrophilic groups -OH, -COOH, -NH_2, and -$CONH_2$, along with other functional

moieties, provide strong wettability to polar solvents and the capacity to interact preferentially with salt anions, consequently enhancing salinity solubility and cation transport properties on biopolymers (Xu et al., 2022).

By hydrolyzing collagen, it is possible to extract gelatin, a naturally occurring biopolymer, from animal bones and skin. Consequently, the majority of proteins that make up gelatin are composed of a range of amino acids, including glycine, proline, and hydroxyproline, which are covalently bonded by peptide bonds. Fish, cow, and pig bones and skins are a common by-product of the food industry and are sometimes thrown away and seen of as waste, although they have a significant potential to be a useful source of gelatin (Azarian & Wootthikanokkhan, 2020). Chitosan also has been used in a lot of industries due to its advantages such as biodegradable, outstanding mechanical strength and compatible with many solvents. Previous studies have shown that gelatin is compatible with chitosan and able to produce a solid film with good physical properties (Roy & Rhim, 2021).

In this study, three systems were prepared and discussed. The systems are FG-NH_4NO_3, FG-CS and FG-CS-NH_4NO_3. The polymer host was prepared with the amount of 2g to obtain a good peelable film. The first system was prepared using distilled water as the solvent whilst the second and the third systems were dissolved in 1 % acetic acid. Then, the salt was added accordingly to further analyse the electrolytes system. NH_4NO_3 was chosen based on the low lattice energy value (648.9 kJ mol^{-1}) compared to other ammonium salt for example 703.1 kJ mol^{-1} for ammonium acetate and ammonium bromide with 682.0 kJ mol^{-1}. The low lattice energy had offered easier process of

dissociation. All systems in this work were prepared using solution cast method. The loosely bound hydrogen from NH_4^+ served as a good proton donor for ion conduction.

The first system was prepared to study the ability of fish gelatin to serve as polymer host with the aid of ammonium nitrate as dopant. There are numerous previous works on fish gelatin that has been used in other research field however there is very few studies has been carried out employing fish gelatin as polymer host for ionic conduction. In this work, the highest conductivity for the first system maximized at (1.52 $\pm$ 0.30) x 10^{-5} S cm^{-1} with the incorporation of 25 wt. % NH_4NO_3. As more salt added into the system, there are higher number of charges available for ion conduction which increased the conductivity. However, in this system, the conductivity decreased as more than 25 wt. % of salt added into the system due to salt recrystallisation. Beside conductivity in room temperature, the conductivity at different temperatures have been investigated in this study. It has been found that as temperatures increase, the conductivity values also increase due to increment of segmental motion of polymer chain that helps the ions to migrate from one site to another site.

The results from XRD analysis confirmed and strengthen the conductivity trend. In the first system, FG25 is found to be the most amorphous film as shown in Figure 4.3 with the lowest value of X_c. Based on the calculation as tabulated in Table 4.1, X_c has dropped from 26.18 % to 15.77 % for FG0 and FG25, respectively. X_c then increased to 37.98 % in FG30. This value confirmed the conductivity trend that had been calculated. Besides X_c, the conductivity results are consistent with the calculated activation energy value. The lowest activation energy of 0.454 eV is possessed by FG25.

In this work, FTIR spectra for fish gelatin powder was compared with fish skin film's FTIR. The spectra shows that with addition of distilled water, the hydroxyl and amine band of FG becomes more intense due to possible interaction between the distilled water and the functional group of polymer host. FTIR spectra illustrated that with addition of salt to the polymer host, amide III peak has shifted to a lower wavenumber indicating that complexation had occurred between atoms in the amide III functional group and H^+ from the salt. Amide III corresponds to C-N stretching vibrations connected to N-H bending vibrations (Abisharani et al., 2021). In addition, there are also emergence of new peaks within 600 to 1000 cm^{-1} wavenumber corresponds to NH_4NO_3 addition into the system. The FESEM analysis in Figure 4.9 shows that the smooth and homogenous surface of FG0 has transformed into a courser and denser surface as more ions were successfully embedded in the polymer host and became more amorphous. With more than 25 wt. % of salt addition, there is an obvious salt agglomeration as the ion association rate is higher than ion dissociation rate. The decomposition temperature decreases as salt doped into the system which might be caused by the presence of salt that disrupts the bond between the polymer chains in FG.

The thermal stability of the electrolytes has been investigated from TGA analysis. Three stages of degradation were found in FG-NH_4NO_3 electrolyte system. The first stage of degradation is due to the weight loss from water which is at ~130°C to ~180°C. Similar to previous study, second stage of degradation occurred at ~220°C to ~250°C that resulted from NH_4NO_3 degradation, and third degradation is due to the host polymer, fish skin gelatin. In addition, the thermal properties of the polymer electrolyte were also studied from DSC analysis. As shown in Figure 4.19, the T_g values decreased from 98.27 °C to 54.83 °C for FG0 and FG25, respectively. The dipole-dipole connections between the

polymer chains were weakened by the addition of salt, which increased segmental motion that resulted in a lower glass transition temperature (Chitra et al., 2020). In addition to this analysis, only single T_g value has been detected in each selected electrolytes indicating that FG is compatible with NH_4NO_3. The main charge carriers for FG-NH_4NO_3 electrolyte have been successfully determined via TNM analysis where FG25 was placed in between two stainless steel electrodes that only allow electrons to pass through. Based on calculations, it was found that the number of ion 0.92 whilst the number of electrons is 0.08. From the analysis, it can be concluded that there are significantly more ions than electrons thus making both cations and anions the primary charge carriers. Additionally, the electrochemical stability of FG25 was also tested using LSV. The breakdown voltage was determined to be 2.5 V.

To increase the conductivity, fish skin gelatin was blended with chitosan. It has been reported from previous study that gelatin is compatible with chitosan and able to produce a standalone film as discussed in Chapter 2. Previously, edible capsules for drugs and foods have been established from this blend. This study intended to investigate the ability of FG-CS blend to enact as polymer host electrolyte. Thus, a different ratio of chitosan has been blended with fish gelatin. All films were produced using solution cast method. The XRD analysis were carried out to investigate the crystallinity of the various ratios of FG-CS blended system to find the best ratio to serve as the polymer host for blended electrolyte system. From the calculation of X_c, the most amorphous film was established with the ratio of 60:40, FG:CS respectively. The lowest value of X_c was found to be 15.38 %. for CF4 sample.

The interactions between fish gelatin and chitosan were studied from FTIR spectra. The comparison between FTIR spectrum of CF4 and the spectrum of FG0 and C10 has been made respectively. The shifts in hydroxyl, carboxamide and saccharide region indicate that modification existed in the structure of the polymer host as the chitosan was blended to the fish gelatin. Compatibility between fish gelatin and chitosan has been examined via the FESEM cross section image. From the comparison with pure fish gelatin film and pure chitosan film, CF4 was found to possess a smoother cross section area with no distinguish phase separation. This indicated that the two polymers were compatible with each other.

TGA analysis has showed that there was reduction of weight loss as chitosan was blended with fish gelatin. This showed that the addition of chitosan able to reduce the hydroscopic behaviour of fish gelatin. CF4 had a lower major weight loss of ~ 50 %. The glass transition temperature from DSC study also supports the compatibility between chitosan and fish gelatin where it was recorded that the T_g value of CF4 was detected to be in between the T_g value of FG0 and C10 respectively. The results discussed in Chapter 5 proposed that CF4 can be best served as a polymer host and have produced films with better physical and electrical properties when doped with salt.

From all these analyses that has been done and discussed in Chapter 5, different weight percentage of NH_4NO_3 was added into CF4. First, the addition of chitosan into FG-NH_4NO_3 polymer electrolytes has improved the physical properties of the film. Comparing the highest conducting samples in the first system and third system, FG25 and CFs40, respectively. Figure 7.1 shows the difference in physical state of FG25 and CFs40.

After left overnight in room temperature, FG25 film turn to gel-like electrolytes whilst CFs40 film still a stand-alone film and easy to handle.

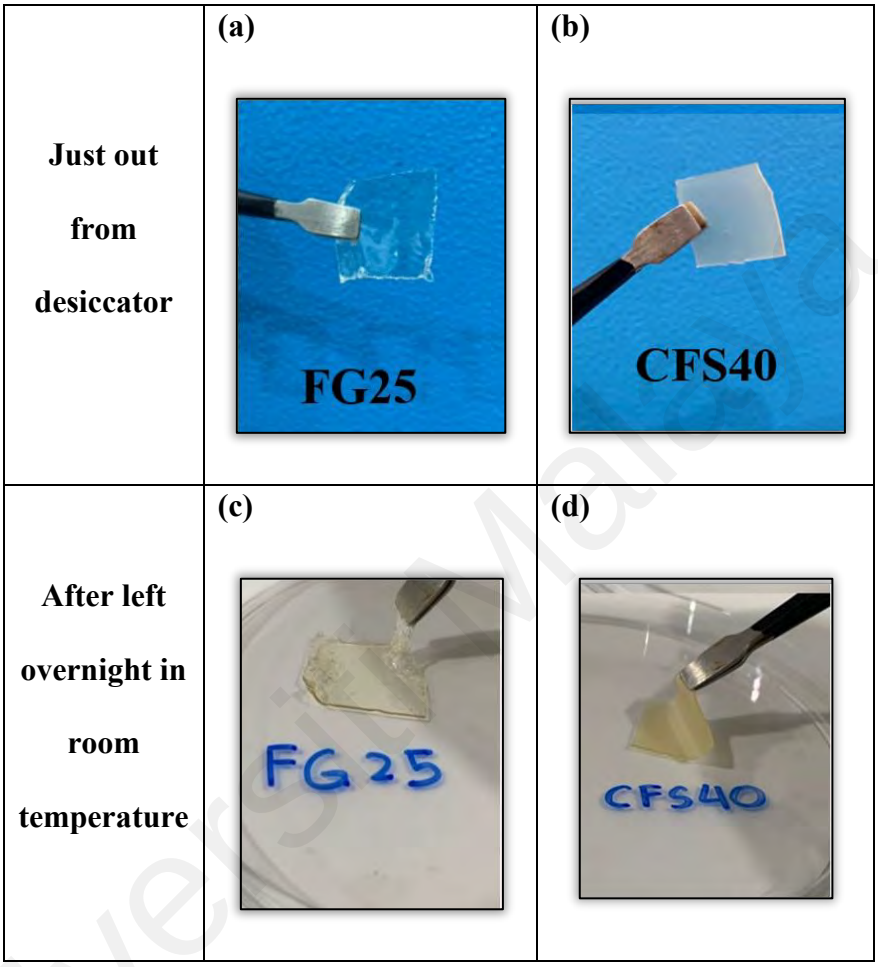

Figure 7.1: Physical appearance of the electrolytes just out from desiccator (a) FG25, (b) CFs40 and after left overnight in room temperature (c) FG25 and (d) CFs40.

From EIS analysis, it was found that the conductivity for blended system has increased up to 2 magnitude order of $(1.61 \pm 0.33) \times 10^{-3}$ S cm^{-1} with 40 wt. % of NH_4NO_3 addition. It can be concluded that polymer blend has aided ion migration better. Polymer blending able to provide more sites for ion to hop through the molecular interaction between polymers and the polymer chain became more flexible thus able to increase the

ionic mobility (Abdulwahid et al., 2022; Zainuddin et al., 2020). The conductivity at elevated temperature were also analysed in the third system. The conductivity increases as temperature increases. As heat was supplied to the system, the ions vibrate faster, the molecular chain becomes more flexible, and the number of free ions also increased. The results found in the conductivity for elevated temperature similar with previous reported works. From temperature dependence conductivity, the graphs showing the variation of conductivity as a function of temperature for all electrolytes exhibit linearity. This indicates that all electrolytes obeyed Arrhenius rule. The lowest activation energy in FG-CS-NH_4NO_3 system was found in CFs40 with energy value of 0.202 eV. This value lower than FG-NH_4NO_3 system with 0.454 eV for FG25. Higher conducting sample has a lower activation energy which are resulting from a better ionic mobility that facilitates the ions to hop to the conducting sites (Jothi et al., 2020).

Transport analysis as tabulated in Table 6.3 for this system shows that the values of τ, μ and D increases as salt was added into the system. The dielectric constant as depicted in Figure 6.16 improves as amount of salt increased up to 40 wt. % of NH_4NO_3. This suggested that a higher amount of H^+ ions are in the electrolyte. However, with more than 40 wt. % of salt, the dielectric constant and dielectric loss decrease, due to the recombination of ions. Comparing the blended with single polymer electrolyte system, the blended polymer has higher dielectric properties value. The maximum values of ε_r and ε_i for electrolyte with highest conductivity in FG-NH_4NO_3 are about 11000 and 30000 respectively. However, after blending fish gelatin with chitosan, the values of ε_r and ε_i are more than 30000 for both properties. This is in line with the conductivity values as after blending the polymer, the conductivity increases from 10^{-5} S cm^{-1} to 10^{-3} S cm^{-1}. The higher dielectric properties indicate higher number density of mobile ions due to the

blending polymer able to dissociate more salt. The electrolytes show a non-Debye behaviour as the dielectric properties decrease when frequency increases (Nofal et al., 2021).

XRD analysis has been carried out for the third electrolyte system. There is a smaller shift in amorphous and crystalline peaks position as salt added into the system. The change in peaks position indicate that there is interaction occurred between the salt and the polymer host. The amorphous region becomes broader as salt added into the system up to 40 wt. %. Table 6.2 shows that the addition of 40 wt. % of NH_4NO_3 to the polymer host, has reduced the degree of crystallinity of the electrolyte from 15.38 % in CF4 to 10.03 % which remarks the lowest degree of crystallinity in FG-CS-NH_4NO_3 system. The increased in conductivity value has been clearly explained by the increased of amorphousness of the electrolyte that aids the mobility of ions as illustrated in Figure 6.3. NH_4NO_3 were no longer fit within the polymer host after the incorporation of more than 40 wt. %, leading to ion recombination and decrement in conductivity value.

From FTIR results in Chapter 6, the addition of NH_4NO_3 up to 40 wt. % has shifted the hydroxyl band, carboxamide band, amide I and amide II to a lower wavenumber. The hydroxyl band is assigned to -OH stretching, carboxamide band assigned to C=O stretching, and saccharide band assigned to C-O-C asymmetric stretching vibrations. The cation interacts with the polymer host when salt is introduced, which change the polymer's original backbone structure, hence resulted in the shift of the peaks. Based on the FTIR result, there are interaction between the salt and the polymer host. In addition, Figure 6.7 shows a surface micrograph from FESEM of a more porous structure as salt is added into the system. This structure is a proved of successful

accumulation of NH_4NO_3 into the system which provides paths for ion migrations. With more than 40 wt.% of salt addition, the surface became coarse as in Figure 6.9 resulted from ion recombination.

From TGA analysis, it was found that CFs20 and CFs40 decomposed at 215.13 °C and 205.23 °C, respectively. It is confirmed that addition of salt has affected the capability of the polymer to sustain its original form when heated, resulted in a lower degradation temperature. From the literature it is known that NH_4NO_3 can be degraded into NH_3, HNO_3, H_2O, and N_2O when heated around 160 °C to 210 °C (Chaturvedi & Dave, 2013; Izato & Miyake, 2015; Skarlis et al., 2014). The salt used in this work able to weaken the backbone of the polymer host resulted in a better flexibility film which can be demonstrated by the decreasing trend of T_g with the increment of NH_4NO_3 content. With the addition of 40 wt. % NH_4NO_3, the T_g value is found lessened from 93.33 °C to 83.33 °C. The reduced in T_g value suggested that the polymer host's intermolecular hydrogen bond has been disrupted, causing the occurrence of cation-anion interaction with the salt (Jridi et al., 2014).

To confirm that the ionic conduction is contributed by ions, TNM has been carried out for both FG-NH_4NO_3 and FG-CS-NH_4NO_3 systems and it was found that the transference number for ions are higher than the transference number for electrons. From the analysis, both t_{ion} and t_e were found be 0.96 and 0.04, respectively. The steady current was established when the movement of ions is balanced by the diffusion process and the current flow is only generated by the electrons with no contributions from ions (Aziz et al., 2021). The transference number of ions in polymer blend was found higher 0.96 compared to 0.92 for FG25. It could be the case that the blend electrolyte has more ions

to be conducted towards stainless steel electrodes and form a double layer compared with single electrolyte.

To evaluate the practicability of the electrolytes and the capability to endure operating voltage, electrochemical stability is tested using LSV. From the study, the electrolyte was stable up to 2.6 V. The value obtained in this system is comparable with previous study by Hamsan and co-worker (2020). This is important to study prior to application of electrochemical devices for future works.

CHAPTER 8: CONCLUSION

8.1 Conclusions

Three polymer electrolytes systems were successfully prepared via solution casting technique; FG-NH_4NO_3, FG-CS and FG-CS-NH_4NO_3.

- The XRD spectra has been analysed to study the amorphousness of the polymer electrolytes at different ratio of salt and chitosan composition.
- The degree of crystallinity was calculated to determine the film with highest amorphousness. In the second system, the most amorphous ratio was found with 60 wt.% of fish gelatin and 40 wt.% of chitosan has been established.
- FTIR results have revealed the interaction between fish gelatin, chitosan and ammonium salt.
- FESEM exhibited a smooth pattern of cross-section micrographs for CF4 film that indicates good compatibility between FG and CS.
- The T_g values of the blend system has been detected at intermediate range of the individual polymers which also confirmed the miscibility of FG and CS. T_g decrease with salt addition referring to that amorphous region of the film has been improved.

The conductivity of the polymer electrolyte based on fish skin gelatin has improved and rise by 2 magnitude order as chitosan was blend into the system. This could be due to several reasons:

- There are more sites for ion migration in blended system.
- The blend polymer electrolyte is more amorphous compared with single polymer electrolyte which was proven by lower degree of crystallinity.

- The number of mobility and number of ion density is greater in blend system compared to single polymer system indicates more ions can be transported within the host that led towards conductivity enhancement.

Transference number analysis for both salted electrolyte systems indicate that ions are the main charge carriers. LSV measurements reveal that the electrolyte was electrochemically stable up to 2.6 V which is sufficient to be employed for further application study.

8.2 Contribution of thesis

The aim of this thesis is to develop good conducting biopolymer electrolytes based on fish skin gelatin and chitosan, which are abundant natural sources. This study able to enhance knowledge on the application of natural polymers and to generate a new idea with certain scientific interpretation. More importantly, this work is an effort towards green and sustainable technology for a better future.

8.3 Future works

Development of electrochemical devices such as battery and EDLC are possible by employing the electrolyte from this work as the conductivity is sufficient at ~10^{-3} S cm^{-1} and the cut off potential value is 2.6 V. Moreover, from the TGA analysis, the FG-CS-NH_4NO_3 system has exhibited a good thermal stability. Plasticizer method can be carried out in the future where a high dielectric constant plasticizer such as glycerol can be added into the electrolyte system to further enhanced the conductivity up to 10^{-2} S cm^{-1}. The results presented here may facilitate improvements in the use of fish skin gelatin

as an alternative source of solid biopolymer electrolyte that holds a lot of potential as a replacement for non-degradable electrolytes in electrochemical power sources.

REFERENCES

Abdelrazek, E. M., Abdelghany, A. M., Tarabiah, A. E., & Zidan, H. M. (2019). AC conductivity and dielectric characteristics of PVA/PVP nanocomposite filled with MWCNTs. *Journal of Materials Science: Materials in Electronics*, *30*(16), 15521–15533.

Abdulkadir, B. A., Dennis, J. O., Al-Hadeethi, Y., Shukur, M. F. B. A., Mkawi, E. M., Al-Harbi, N., Ibnaouf, K. H., Aldaghri, O., Usman, F., & Abbas Adam, A. (2021). Optimization of the electrochemical performance of a composite polymer electrolyte based on pva-k2 co3-sio2 composite. *Polymers*, *13*(1), 1–24.

Abdulkareem, S. S. (2021). Structural, morphological and electrical properties of chitosan/methylcellulose blend polymer doped with different concentrations of NH4NO3. *Materials Research Express*, *8*(8).

Abdullah, S.; Ahmad, A.S; Latif, K.S.A; Sobri, N.A.M; Abdullah, N.; Hashim, N.; Yahya, N.M; Mohamed, R. . (2020). Characterization of Solid Polymer Electrolyte Membrane made of Methylcellulose and Ammonium Nitrate Characterization of Solid Polymer Electrolyte Membrane made of Methylcellulose and Ammonium Nitrate. *Journal of Physics: Conference Series*, *1532*, 012017.

Abdullah, A. M., Aziz, S. B., Brza, M. A., Saeed, S. R., Al-asbahi, B. A., Sadiq, N. M., Ahmed, A., Ahmed, A., & Murad, A. R. (2022). Glycerol as an efficient plasticizer to increase the DC conductivity and improve the ion transport parameters in biopolymer based electrolytes : XRD , FTIR and EIS studies. *Arabian Journal of Chemistry*, *15*(6), 103791.

Abdullah, O. G., Aziz, S. B., & Rasheed, M. A. (2018). Incorporation of NH 4 NO 3 into MC-PVA blend-based polymer to prepare proton-conducting polymer electrolyte films. *Ionics*, *24*(3), 777–785.

Abdulwahid, R. T., Aziz, S. B., & Kadir, M. F. Z. (2022). Insights into ion transport in biodegradable solid polymer blend electrolyte based on FTIR analysis and circuit design. *Journal of Physics and Chemistry of Solids*, *167*(April), 110774.

Abisharani, J. M., Balamurugan, S., Thomas, A., Devikala, S., Arthanareeswari, M., Ganesan, S., & Prakash, M. (2021). Incorporation of organic additives with electron rich donors (N , O , S) in gelatin gel polymer electrolyte for dye sensitized solar cells. *Solar Energy*, *218*(November 2020), 552–562.

Agrawal, R. C., & Pandey, G. P. (2008). Solid polymer electrolytes: Materials designing and all-solid-state battery applications: An overview. *Journal of Physics D: Applied Physics*, *41*(22).

Aguirre-pranzoni, C., García, M. G., & Ochoa, N. A. (2023). Structural and conformational changes on chitosan after green heterogeneous synthesis of phenyl derivatives. *Carbohydrate Polymers*, 120843.

Ahmad, M., & Benjakul, S. (2010). Extraction and characterisation of pepsin-solubilised collagen from the skin of unicorn leatherjacket (Aluterus monocerous). *Food Chemistry*, *120*(3), 817–824.

Ahmad, M., & Benjakul, S. (2011). Characteristics of gelatin from the skin of unicorn leatherjacket (Aluterus monoceros) as in fl uenced by acid pretreatment and extraction time. *Food Hydrocolloids*, *25*(3), 381–388.

Ahmed, H. T., & Abdullah, O. G. (2020). Impedance and ionic transport properties of proton-conducting electrolytes based on polyethylene oxide/methylcellulose blend polymers. *Journal of Science: Advanced Materials and Devices*, *5*(1), 125–133.

Alam, R. B., Ahmad, M. H., & Islam, M. R. (2021). Bio-inspired gelatin/single-walled carbon nanotube nanocomposite for transient electrochemical energy storage: An approach towards eco-friendly and sustainable energy system. *Heliyon*, *7*(7), e07468.

Alves, R., Donoso, J. P., Magon, C. J., Silva, I. D. A., Pawlicka, A., & Silva, M. M. (2016). Solid polymer electrolytes based on chitosan and europium triflate. *Journal of Non-Crystalline Solids*, *432*, 307–312.

Anandha Jothi, M., Vanitha, D., Nallamuthu, N., Manikandan, A., & Asath Bahadur, S. (2020). Investigations of lithium ion conducting polymer blend electrolytes using biodegradable cornstarch and PVP. *Physica B: Condensed Matter*, *580*(December 2019), 411940.

Armand, M. (1994). The history of polymer electrolytes. *Solid State Ionics*, *69*(3–4), 309–319.

Arof, A. K., Kadir, M. F. Z., Yahya, R., & Aspanut, Z. (2011). Chitosan-PEO proton conducting polymer electrolyte membrane doped with NH4NO3. *Materials Research Innovations*, *15*(SUPPL. 2), 3–6.

Arya, A., & Sharma, A. L. (2019). Temperature and Salt-Dependent Dielectric Properties of Blend Solid Polymer Electrolyte Complexed with LiBOB. *Macromolecular Research*, *27*(4), 334–345.

Asnawi, A. S. F. M., Aziz, S. B., Nofal, M. M., Hamsan, M. H., Brza, M. A., Yusof, Y. M., Abdilwahid, R. T., Muzakir, S. K., & Kadir, M. F. Z. (2020). Glycerolized Li+ ion conducting chitosan-based polymer electrolyte for energy storage EDLC device applications with relatively high energy density. *Polymers*, *12*(6), 1–19.

Azarian, M. H., & Wootthikanokkhan, J. (2020). Gelatin-based solid electrolytes for chromogenic windows applications: a review. *Ionics*, *26*(12), 5841–5851.

Aziz, S. B. ., Hadi, J. M. ., Dannoun, E. M. A. ., Abdulwahid, R. T., Saeed, S. R. ., Marf, A. S. ., Karim, W. O. ., & Kadir, M. F. Z. . (2020). The Study of Plasticized Amorphous Biopolymer Blend Electrolytes Based on Polyvinyl Alcohol (PVA): Chitosan with High Ion Conductivity for Energy. *Polymers*, *12*, 1938.

Aziz, S. B. ., Nofal, M. M. ., Kadir, M. F. Z. ., Dannoun, E. M. A. ., Brza, M.A.;, Hadi, J. M. ., & Abdullah, R. M. (2021). Bio-Based Plasticized PVA Based Polymer Blend Electrolytes and Electrochemical Properties. *Materials*, *14*, 1994.

Aziz, S. B., Abdullah, O. G., Saeed, S. R., & Ahmed, H. M. (2018). Electrical and dielectric properties of copper ion conducting solid polymer electrolytes based on chitosan: CBH model for ion transport mechanism. *International Journal of Electrochemical Science*, *13*(4), 3812–3826.

Aziz, S. B., Al-Zangana, S., Brza, M. A., Saeed, S. R., Abdulwahid, R. T., & Kadir, M. F. Z. (2019). Study of dielectric properties and ion transport parameters in Chitosan-Barium Nitrate based solid polymer electrolytes. *International Journal of Electrochemical Science*, *14*(October), 11580–11581.

Aziz, S. B., Asnawi, A. S. F. M., Mohammed, P. A., Abdulwahid, R. T., Yusof, Y. M., Abdullah, R. M., & Kadir, M. F. Z. (2021). Impedance, circuit simulation, transport properties and energy storage behavior of plasticized lithium ion conducting chitosan based polymer electrolytes. *Polymer Testing*, *101*(July), 107286.

Aziz, S. B., Brevik, I., Hamsan, M. H., Brza, M. A., Nofal, M. M., Abdullah, A. M., Rostam, S., Al-Zangana, S., Muzakir, S. K., & Kadir, M. F. Z. (2020). Compatible solid polymer electrolyte based on methyl cellulose for energy storage application: Structural, electrical, and electrochemical properties. *Polymers*, *12*(10), 1–19.

Aziz, S. B., Brza, M. A., Brevik, I., Hamsan, M. H., Abdulwahid, R. T., Majid, S. R., Kadir, M. F. Z., Hussen, S. A., & Abdullah, R. M. (2020). Characteristics of glycerolized chitosan: Nh4 no3-based polymer electrolyte for energy storage devices with extremely high specific capacitance and energy density over 1000 cycles. *Polymers*, *12*(11), 1–23.

Aziz, S. B., Brza, M. A., Saed, S. R., Hamsan, M. H., & Kadir, M. F. Z. (2020). Ion association as a main shortcoming in polymer blend electrolytes based on CS:PS incorporated with various amounts of ammonium tetrafluoroborate. *Journal of Materials Research and Technology*, *9*(3), 5410–5421.

Aziz, S. B., Dannoun, E. M. A., Abdullah, S. N., Ghareeb, H. O., Abdullah, R. M., Abdalrahman, A. A., Nofal, M. M., & Kakroo, S. (2022). The EDLC Energy Storage Device Based on a Natural Gelatin (NG) Biopolymer: Tuning the Capacitance through Plasticizer Variation. *Polymers*, *14*(22).

Aziz, S. B., Dannoun, E. M. A., Abdulwahid, R. T., Kadir, M. F. Z., Nofal, M. M., Al-Saeedi, S. I., & Murad, A. R. (2022). The Study of Ion Transport Parameters in MC-Based Electrolyte Membranes Using EIS and Their Applications for EDLC Devices. *Membranes*, *12*(2).

Aziz, S. B., Hamsan, M. H., Abdullah, R. M., Abdulwahid, R. T., Brza, M. A., Marif, A. S., & Kadir, M. F. Z. (2020). Protonic EDLC cell based on chitosan (CS): methylcellulose (MC) solid polymer blend electrolytes. *Ionics*, *26*(4), 1829–1840.

Aziz, S. B., Hamsan, M. H., Abdullah, R. M., & Kadir, M. F. Z. (2019). A Promising Polymer Blend Electrolytes Based on Chitosan : Methyl Cellulose for EDLC Application with High Specific Capacitance and Energy Density. *Molecules*, *24*(13), 2503.

Aziz, S. B., Hamsan, M. H., Brza, M. A., Kadir, M. F. Z., Abdulwahid, R. T., Ghareeb, H. O., & Woo, H. J. (2019). Fabrication of energy storage EDLC device based on CS:PEO polymer blend electrolytes with high Li+ ion transference number. *Results in Physics*, *15*(July), 102584.

Azli, A. A., Manan, N. S. A., Aziz, S. B., & Kadir, M. F. Z. (2020). Structural , impedance and electrochemical double-layer capacitor characteristics of improved number density of charge carrier electrolytes employing potato starch blend polymers. *Ionics*, *26*(11), 5773–5804.

Azmi, N. S., Basha, R. K., Tajul Arifin, N. N., Othman, S. H., & Mohammed, M. A. P. (2020). Functional properties of tilapia's fish scale gelatin film: Effects of different type of plasticizers. *Sains Malaysiana*, *49*(9), 2221–2229.

Basu, T., & Tarafdar, S. (2016). Influence of gamma irradiation on the electrical properties of LiClO4-gelatin solid polymer electrolytes: Modelling anomalous diffusion through generalized calculus. *Radiation Physics and Chemistry*, *125*, 180–198.

Bommalapura Hanumaiah, A., Al-Gunaid, M. Q. A., & Siddaramaiah. (2021). Performance of nano-K-doped zirconate on modified opto-electrical and electrochemical properties of gelatin biopolymer nanocomposites. *Polymer Bulletin*, *78*(6), 3023–3041.

Boopathi, G., Pugalendhi, S., Selvasekarapandian, S., & Premalatha, M. (2016). Development of proton conducting biopolymer membrane based on agar – agar for fuel cell. *Ionics*, *23*, 2781–2790.

Brza, M A, Aziz, S. B., Anuar, H., Ali, F., Hamsan, M. H., Kadir, M. F. Z., & Abdulwahid, R. T. (2020). Metal framework as a novel approach for the fabrication of electric double layer capacitor device with high energy density using plasticized Poly (vinyl alcohol): Ammonium thiocyanate based polymer electrolyte. *Arabian Journal of Chemistry*, *13*(10), 7247–7263.

Brza, Mohamad A., Aziz, S. B., Nofal, M. M., Saeed, S. R., Al-Zangana, S., Karim, W. O., Hussen, S. A., Abdulwahid, R. T., & Kadir, M. F. Z. (2020). Drawbacks of Low Lattice Energy Ammonium Salts for Ion-Conducting Polymer Electrolyte Preparation : Structural , Morphological and Electrical. *Polymers*, *12*(9), 1885.

Chai, M. N., & Isa, M. I. N. (2013). Electrical Characterization and Ionic Transport Properties of Carboxyl Methylcellulose-Oleic Acid Solid Polymer Electrolytes. *International Journal of Polymer Analysis and Characterization*, *18*(4), 280–286.

Chattopadhyay, J., Pathak, T. S., & Santos, D. M. F. (2023). Applications of Polymer Electrolytes in Lithium-Ion Batteries: A Review. *Polymers*, *15*(19).

Chaturvedi, S., & Dave, P. N. (2013). Review on Thermal Decomposition of Ammonium Nitrate. *Journal of Energetic Materials*, *31*(1), 1–26.

Chen, Y., Duan, Q., Yu, L., & Xie, F. (2021). Thermomechanically processed chitosan:gelatin films being transparent, mechanically robust and less hygroscopic. *Carbohydrate Polymers*, *272*(August), 118522.

Chipara, M., Lozano, K., Hernandez, A., & Chipara, M. (2008). TGA analysis of polypropylene-carbon nanofibers composites. *Polymer Degradation and Stability*, *93*(4), 871–876.

Chitra, R., Sathya, P., Selvasekarapandian, S., & Meyvel, S. (2020). Synthesis and characterization of iota-carrageenan biopolymer electrolyte with lithium perchlorate and succinonitrile (plasticizer). *Polymer Bulletin*, *77*(3), 1555–1579.

Cyriac, V., Ismayil, Noor, I. M., Mishra, K., Chavan, C., Bhajantri, R. F., & Masti, S. P. (2022). Ionic conductivity enhancement of PVA: carboxymethyl cellulose poly-blend electrolyte films through the doping of NaI salt. *Cellulose*, *29*(6), 3271–3291.

Dannoun, E. M. A., Aziz, S. B., Abdullah, S. N., Nofal, M. M., Mahmoud, K. H., Murad, A. R., Abdullah, R. M., & Kadir, M. F. Z. (2021). Characteristics of plasticized lithium ion conducting green polymer blend electrolytes based on CS: Dextran with high energy density and specific capacitance. *Polymers*, *13*(21), 1–19.

Dannoun, E. M. A., Aziz, S. B., Brza, M. A., Al-Saeedi, S. I., Nofal, M. M., Mishra, K., Abdullah, R. M., Karim, W. O., & Hadi, J. M. (2022). Electrochemical and Ion Transport Studies of Li+ Ion-Conducting MC-Based Biopolymer Blend Electrolytes. *International Journal of Molecular Sciences*, *23*(16), 1–16.

Dannoun, E. M. A., Aziz, S. B., Brza, M. A., Nofal, M. M., Asnawi, A. S. F. M., Yusof, Y. M., Al-Zangana, S., Hamsan, M. H., Kadir, M. F. Z., & Woo, H. J. (2020). The study of plasticized solid polymer blend electrolytes based on natural polymers and their application for energy storage EDLC devices. *Polymers*, *12*(11), 1–19.

Dennis, J. O., Adam, A. A., Ali, M. K. M., Soleimani, H., Shukur, M. F. B. A., Ibnaouf, K. H., Aldaghri, O., Eisa, M. H., Ibrahem, M. A., Bashir Abdulkadir, A., & Cyriac, V. (2022). Substantial Proton Ion Conduction in Methylcellulose/Pectin/Ammonium Chloride Based Solid Nanocomposite Polymer Electrolytes: Effect of ZnO Nanofiller. *Membranes*, *12*(7).

Deshmukh, K., Basheer Ahamed, M., Deshmukh, R. R., Khadheer Pasha, S. K., Bhagat, P. R., & Chidambaram, K. (2017). Biopolymer Composites with High Dielectric Performance: Interface Engineering. In *Biopolymer Composites in Electronics*. Elsevier Inc.

Dong, C., Lin, Z., Yin, Y., Qiao, Y., Wang, W., Wu, Q., Yang, C., Rooney, D., Fan, C., & Sun, K. (2021). A robust interface enabled by electrospun membrane with optimal resistance in lithium metal batteries. *Journal of Energy Chemistry*, *55*, 1–9.

Ehrlich, L., Pospiech, D., Uhlmann, P., Tzschöckell, F., Hager, M. D., & Voit, B. (2023). Influencing ionic conductivity and mechanical properties of ionic liquid polymer electrolytes by designing the chemical monomer structure. *Designed Monomers and Polymers*, *26*(1), 198–213.

Fakhreddin Hosseini, S., Rezaei, M., Zandi, M., & Ghavi, F. F. (2013). Preparation and functional properties of fish gelatin-chitosan blend edible films. *Food Chemistry*, *136*(3–4), 1490–1495.

Fox, J. A., & Hanawa Peterson, H. (2004). Risks and implications of bovine spongiform encephalopathy for the United States: Insights from other countries. *Food Policy*, *29*(1), 45–60.

Fundo, J. F., Galvis-Sanchez, A. C., Delgadillo, I., Silva, C. L. M., & Quintas, M. A. C. (2015). The Effect of Polymer/ Plasticiser Ratio in Film Forming Solutions on the Properties of Chitosan Films. *Food Biophysics*, *10*(3), 324–333.

Garidepalli Tejaswi, Parthiban, V., Sunita Sundari, G., & Harikrishna, E. (2022). Ionic Conductivity Studies of Biodegradable Polymer Electrolyte for Mg Ion Batteries. *Asian Journal of Chemistry*, *34*(7), 1742–1748.

Ge, Z., Liu, X., Zou, X., Zhan, Y., & Luo, Y. (2021). Preparation and properties of a novel green solid polymer electrolyte for all-solid-state lithium battery. *Journal of Applied Polymer Science*, *138*(37), 50945.

Ghazali, N. M., Fuzlin, A. F., Saadiah, M. A., Hasan, M. M., Nagao, Y., & Samsudin, A. S. (2022). Studies on H+ ions conducting bio-polymer blend electrolyte based on alginate-PVA doped with NH4NO3. *Journal of Non-Crystalline Solids*, *598*(July).

Ghazali, Nuraziliana Muhd, & Samsudin, A. S. (2022). Progress on biopolymer as an application in electrolytes system: A review study. *Materials Today: Proceedings*, *49*, 3668–3678.

Hadi, J. M., Aziz, S. B., Kadir, M. F. Z., El-Badry, Y. A., Ahamad, T., Hussein, E. E., Asnawi, A. S. F. M., Abdullah, R. M., & Alshehri, S. M. (2021). Design of plasticized proton conducting Chitosan:Dextran based biopolymer blend electrolytes for EDLC application: Structural, impedance and electrochemical studies. *Arabian Journal of Chemistry*, *14*(11), 103394.

Hadi, J. M., Aziz, S. B., Mustafa, M. S., Brza, M. A., Hamsan, M. H., Kadir, M. F. Z., Ghareeb, H. O., & Hussein, S. A. (2020). Electrochemical impedance study of proton conducting polymer electrolytes based on PVC doped with thiocyanate and plasticized with glycerol. *International Journal of Electrochemical Science*, *15*, 4671–4683.

Hadidi, M., Pouramin, S., Adinepour, F., Haghani, S., & Mahdi, S. (2020). Chitosan nanoparticles loaded with clove essential oil : Characterization , antioxidant and antibacterial activities. *Carbohydrate Polymers*, *236*(November 2019), 116075.

Hafiza, M. N., & Isa, M. I. N. (2020). Correlation between structural , ion transport and ionic conductivity of plasticized 2-hydroxyethyl cellulose based solid biopolymer electrolyte. *Journal of Membrane Science*, *597*, 117176.

Hamed, I., Jakobsen, A. N., & Lerfall, J. (2022). Sustainable edible packaging systems based on active compounds from food processing byproducts: A review. *Comprehensive Reviews in Food Science and Food Safety*, *21*(1), 198–226.

Hamsan, M. H., Aziz, S. B., Azha, M. A. S., Azli, A. A., Shukur, M. F., Yusof, Y. M., Muzakir, S. K., Manan, N. S. A., & Kadir, M. F. Z. (2020). Solid-state double layer capacitors and protonic cell fabricated with dextran from Leuconostoc mesenteroides based green polymer electrolyte. *Materials Chemistry and Physics*, *241*, 122290.

Hamsan, M. H., Aziz, S. B., Kadir, M. F. Z., Brza, M. A., & Karim, W. O. (2020). The study of EDLC device fabricated from plasticized magnesium ion conducting chitosan based polymer electrolyte. *Polymer Testing*, *90*(June), 106714.

Hamsan, M. H., Aziz, S. B., Nofal, M. M., Brza, M. A., Abdulwahid, R. T., Hadi, J. M., Karim, W. O., & Kadir, M. F. Z. (2020). Characteristics of EDLC device fabricated from plasticized chitosan:MgCl2 based polymer electrolyte. *Journal of Materials Research and Technology*, *9*(5), 10635–10646.

Hamsan, M. H., Aziz, S. B., Shukur, M. F., & Kadir, M. F. Z. (2019). Protonic cell performance employing electrolytes based on plasticized methylcellulose-potato starch-NH4NO3. *Ionics*, *25*(2), 559–572.

Hamsan, M. H., Shukur, M. F., Aziz, S. B., & Kadir, M. F. Z. (2019). Dextran from Leuconostoc mesenteroides-doped ammonium salt-based green polymer electrolyte. *Bulletin of Materials Science*, *42*(2).

Hamsan, M. H., Shukur, M. F., Aziz, S. B., Yusof, Y. M., & Kadir, M. F. Z. (2020). Influence of NH 4 Br as an ionic source on the structural/electrical properties of dextran-based biopolymer electrolytes and EDLC application. *Bulletin of Materials Science*, *43*(1), 0030.

Hamsan, M. H., Shukur, M. F., & Kadir, M. F. Z. (2017a). NH4NO3 as charge carrier contributor in glycerolized potato starch-methyl cellulose blend-based polymer electrolyte and the application in electrochemical double-layer capacitor. *Ionics*, *23*(12), 3429–3453.

Hamsan, M. H., Shukur, M. F., & Kadir, M. F. Z. (2017b). The effect of NH 4 NO 3 towards the conductivity enhancement and electrical behavior in methyl cellulose-starch blend based ionic conductors. *Ionics*, *23*(3), 1137–1154.

Hassan, M. F., Zainuddin, S. K., Kamaruddin, K. H., Sheng, C. K., & Abdullah, M. A. A. (2018). Ion-conducting polymer electrolyte films based on poly (sodium 4-styrenesulfonate) complexed with ammonium nitrate : studies based on morphology and structural. *Malaysian Journal of Analytical Sciences*, *22*(2), 238–248.

Hemalatha, R., Alagar, M., Selvasekarapandian, S., Sundaresan, B., & Moniha, V. (2019). Studies of proton conducting polymer electrolyte based on PVA, amino acid proline and NH 4 SCN. *Journal of Science: Advanced Materials and Devices*, *4*(1), 101–110.

Hidayati, D., Sabiyla, G. R., Prasetyo, E. N., Sa'adah, N. N., & Kurniawan, F. (2021). The characteristic of gelatin extracted from the skin of adult and sub-adult striped catfish (Pangasius hypophthalmus) using acid-base pretreatment: pH and FTIR. *IOP Conference Series: Earth and Environmental Science*, *755*(1).

Hosseini, S. F., Ghaderi, J., & Gómez-Guillén, M. C. (2022). Tailoring physico-mechanical and antimicrobial/antioxidant properties of biopolymeric films by cinnamaldehyde-loaded chitosan nanoparticles and their application in packaging of fresh rainbow trout fillets. *Food Hydrocolloids*, *124*(May 2021).

Ibnu, M., Ahmad, H., Zainuddin, N. I., Nizam, I., & Isa, M. (2022). Plasticized cmc-ammonium acetate based solid biopolymer electrolyte : ionic conductivity and transport study. *Journal of Sustainability Science and Management*, *17*(5), 139–148.

Izato, Y. I., & Miyake, A. (2015). Thermal decomposition of molten ammonium nitrate (AN): Chemical equilibrium in molten AN. *Journal of Thermal Analysis and Calorimetry*, *122*(2), 595–600.

Jafari, H., Lista, A., Siekapen, M. M., Ghaffari-Bohlouli, P., Nie, L., Alimoradi, H., & Shavandi, A. (2020). Fish collagen: Extraction, characterization, and applications for biomaterials engineering. *Polymers*, *12*(10), 1–37.

Jătariu, A. N., Popa, M., Curteanu, S., & Peptu, C. A. (2011). Covalent and ionic co-cross-linking-An original way to prepare chitosan-gelatin hydrogels for biomedical applications. *Journal of Biomedical Materials Research - Part A*, *98 A*(3), 342–350.

Jenova, L., Venkatesh, K., Karthikeyan, S., Madeswaran, S., Aristatil, G., Prabu, M., & Joice, S. D. (2021). Solid polymer electrolyte based on tragacanth gum-ammonium thiocyanate. *Journal of Solid State Electrochemistry*, *25*, 2371–2383.

Jian, S., Cao, Y., Feng, W., Yin, G., Zhao, Y., Lai, Y., Zhang, T., Ling, X., Wu, H., Bi, H., & Dong, Y. (2022). Recent progress in solid polymer electrolytes with various dimensional fillers: a review. *Materials Today Sustainability*, *20*.

Jothi, M. A., Vanitha, D., Sundaramahalingam, K., & Nallamuthu, N. (2022). Utilisation of corn starch in production of 'eco friendly' polymer electrolytes for proton battery applications. *International Journal of Hydrogen Energy*, *47*(67), 28763–28772.

Jridi, M., Hajji, S., Ayed, H. Ben, Lassoued, I., Mbarek, A., Kammoun, M., Souissi, N., & Nasri, M. (2014). Physical, structural, antioxidant and antimicrobial properties of gelatin-chitosan composite edible films. *International Journal of Biological Macromolecules*, *67*, 373–379.

Kadir, M. F. Z. (2021). Non-Faradaic-based supercapacitor fabricated with fish skin gelatin biopolymer electrolyte. *Ionics*, *27*, 2219–2229.

Kadir, M. F. Z., Aspanut, Z., Majid, S. R., & Arof, A. K. (2011). FTIR studies of plasticized poly (vinyl alcohol)– chitosan blend doped with NH 4 NO 3 polymer electrolyte membrane. *Spectrochimica Acta Part A: Molecular and Biomolecular Spectroscopy*, *78*(3), 1068–1074.

Kadir, M. F. Z., & Hamsan, M. H. (2018). Green electrolytes based on dextran-chitosan blend and the effect of NH4SCN as proton provider on the electrical response studies. *Ionics*, *24*(8), 2379–2398.

Kadir, M. F. Z., Majid, S. R., & Arof, A. K. (2010). Plasticized chitosan-PVA blend polymer electrolyte based proton battery. *Electrochimica Acta*, *55*(4), 1475–1482.

Kchaou, H., Benbettaieb, N., Jridi, M., Nasri, M., & Debeaufort, F. (2019). Influence of Maillard reaction and temperature on functional, structure and bioactive properties of fish gelatin films. *Food Hydrocolloids*, *97*(September 2018), 105196.

Kenawy, E., Omer, A. M., Tamer, T. M., Elmeligy, M. A., & Eldin, M. S. M. (2019). Fabrication of biodegradable gelatin/chitosan/cinnamaldehyde crosslinked membranes for antibacterial wound dressing applications. *International Journal of Biological Macromolecules*, *139*, 440–448.

Koc, B., Akyuz, L., Cakmak, Y. S., Sargin, I., Salaberria, A. M., Labidi, J., Ilk, S., Ozlem, F., Akata, I., & Kaya, M. (2020). Production and characterization of chitosan-fungal extract films. *Food Bioscience*, *35*(May 2018), 100545.

Kumar, L. S., & Selvasekarapandian, P. C. S. S. (2021). Impact of lithium trifate (LiCF3SO3) salt on tamarind seed polysaccharide-based natural solid polymer electrolyte for application in electrochemical device. *Polymer Bulletin*, *78*(7), 1797–1819.

Kumar, M., Tiwari, T., & Srivastava, N. (2012). Electrical transport behaviour of bio-polymer electrolyte system: Potato starch + ammonium iodide. *Carbohydrate Polymers*, *88*(1), 54–60.

Lenz, M., Zabel, J., & Franzreb, M. (2020). New Approach for Investigating Diffusion Kinetics Within Capacitive Deionization Electrodes Using Electrochemical Impedance Spectroscopy. *Frontiers in Materials*, *7*(July), 1–12.

Leo Edward, M., Dharanibalaji, K. C., Kumar, K. T., Chandrabose, A. R. S., Shanmugharaj, A. M., & Jaisankar, V. (2021). Preparation and characterisation of chitosan extracted from shrimp shell (Penaeus monodon) and chitosan-based blended solid polymer electrolyte for lithium-ion batteries. *Polymer Bulletin*, *79*(1), 587–604.

Leones, R., Sabadini, R. C., Esperança, J. M. S. S., Pawlicka, A., & Silva, M. M. (2017). Effect of storage time on the ionic conductivity of chitosan-solid polymer electrolytes incorporating cyano-based ionic liquids. *Electrochimica Acta*, *232*, 22–29.

Leones, R., Sentanin, F., Rodrigues, L. C., Ferreira, R. A. S., Marrucho, I. M., Esperança, J. M. S. S., Pawlicka, A., Carlos, L. D., & Manuela Silva, M. (2012). Novel polymer electrolytes based on gelatin and ionic liquids. *Optical Materials*, *35*(2), 187–195.

Li, Y. J., Fan, C. Y., Zhang, J. P., & Wu, X. L. (2018). A promising PMHS/PEO blend polymer electrolyte for all-solid-state lithium ion batteries. *Dalton Transactions*, *47*(42), 14932–14937.

Liao, W., Guanghua, X., Li, Y., Shen, X. R., & Li, C. (2018). Comparison of characteristics and fibril-forming ability of skin collagen from barramundi (Lates calcarifer) and tilapia (Oreochromis niloticus). *International Journal of Biological Macromolecules*, *107*(PartA), 549–559.

Lim, C.-S., Teoh, K. H., Liew, C. W., & S, R. (2017). Ionic Conductivity Enhancement Studies Of Composite Polymer Electrolyte Based On Poly (Vinyl Alcohol)-Lithium Perchlorate-Titanium Oxide. *Advanced Materials Letters*, *8*(4), 465–471.

Liu, D., Zhang, X., Li, T., Yang, H., Zhang, H., Regenstein, J. M., & Zhou, P. (2015). Extraction and characterization of acid- and pepsin-soluble collagens from the scales, skins and swim-bladders of grass carp (Ctenopharyngodon idella). *Food Bioscience*, *9*, 68–74.

Liu, F., Liu, Y., Sun, Z., Wang, D., Wu, H., Du, L., & Wang, D. (2020). Preparation and antibacterial properties of ε-polylysine-containing gelatin/chitosan nanofiber films. *International Journal of Biological Macromolecules*, *164*, 3376–3387.

Liu, L., Tao, L., Chen, J., Zhang, T., Xu, J., Ding, M., Wang, X., & Zhong, J. (2021). Fish oil-gelatin core-shell electrospun nanofibrous membranes as promising edible films for the encapsulation of hydrophobic and hydrophilic nutrients. *Lwt*, *146*(May), 111500.

Lu, Y., Luo, Q., Chu, Y., Tao, N., Deng, S., Wang, L., & Li, L. (2022). Application of Gelatin in Food Packaging: A Review. *Polymers*, *14*(3).

M.A. Saadiah, Y. Nagao, A. S. S. (2020). Proton (H+) transport properties of CMC–PVA blended polymer solid electrolyte doped with NH4NO3. *International Journal of Hydrogen Energy*, *45*(29), 14880–14896.

Majid, S. R., & Arof, A. K. Ã. (2005). Proton-conducting polymer electrolyte films based on chitosan acetate complexed with NH 4 NO 3 salt. *Physica B*, *355*(3), 78–82.

Manjakkal, L., Pullanchiyodan, A., Yogeswaran, N., Hosseini, E. S., & Dahiya, R. (2020). A Wearable Supercapacitor Based on Conductive PEDOT:PSS-Coated Cloth and a Sweat Electrolyte. *Advanced Materials*, *32*(24).

Martins, J. T., Cerqueira, M. A., & Vicente, A. A. (2012). Influence of α-tocopherol on physicochemical properties of chitosan-based films. *Food Hydrocolloids*, *27*(1), 220–227.

Mazuki, N. F., Abdul Majeed, A. P. P., Nagao, Y., & Samsudin, A. S. (2020). Studies on ionics conduction properties of modification CMC-PVA based polymer blend electrolytes via impedance approach. *Polymer Testing*, *81*(November 2019), 106234.

Mazuki, N. F., Kufian, M. Z., Nagao, Y., & samsudin, A. . (2022). Correlation Studies Between Structural and Ionic Transport Properties of Lithium-Ion Hybrid Gel Polymer Electrolytes Based PMMA-PLA. *Journal of Polymers and the Environment*, *30*, 1864–1879.

Menazea, A. A., Eid, M. M., & Ahmed, M. K. (2020). Synthesis, characterization, and evaluation of antimicrobial activity of novel Chitosan/Tigecycline composite. *International Journal of Biological Macromolecules*, *147*, 194–199.

Mohamed, A. S., Shukur, M. F., Kadir, M. F. Z., & Yusof, Y. M. (2020). Ion conduction in chitosan-starch blend based polymer electrolyte with ammonium thiocyanate as charge provider. *Journal of Polymer Research*, *27*(6).

Mohd Asnawi, A. S. F., Azli, A. A. M., Hamsan, M. H., Abdul Kadir, M. F. Z., & Yusof, Y. M. (2020). Electrical and infrared spectroscopic analysis of solid polymer electrolyte based on polyethylene oxide and graphene oxide blend. *Malaysian Journal of Analytical Sciences*, *24*(5), 682–697.

Moniha, V., Alagar, M., Selvasekarapandian, S., Sundaresan, B., & Boopathi, G. (2018). Conductive bio-polymer electrolyte iota-carrageenan with ammonium nitrate for application in electrochemical devices. *Journal of Non-Crystalline Solids*, *481*(November 2017), 424–434.

Moniha, V., Alagar, M., Selvasekarapandian, S., Sundaresan, B., Hemalatha, R., & Boopathi, G. (2018). Synthesis and characterization of bio-polymer electrolyte based on iota-carrageenan with ammonium thiocyanate and its applications. *Journal of Solid State Electrochemistry*, *22*(10), 3209–3223.

Mousavi, Z., Naseri, M., Babaei, S., Hosseini, S. M. H., & Shekarforoush, S. S. (2021). The effect of cross-linker type on structural, antimicrobial and controlled release properties of fish gelatin-chitosan composite films incorporated with ε-poly-L-lysine. *International Journal of Biological Macromolecules*, *183*, 1743–1752.

Muhamaruesa, N. H. M., & Mohd Isa, M. I. N. (2017). Transport studies of carboxymethyl cellulose/ chitosan-ammonium bromide biopolymer blend electrolytes as an ionic conductor. *Journal of Sustainability Science and Management*, *2017*(Special Issue 2), 58–64.

Muthuvinayagam, M., & Gopinathan, C. (2015). Characterization of proton conducting polymer blend electrolytes based on PVdF-PVA. *Polymer*, *68*, 122–130.

Naachiyar, R. M., Ragam, M., Selvasekarapandian, S., Krishna, M. V., & Buvaneshwari, P. (2021). Development of biopolymer electrolyte membrane using Gellan gum biopolymer incorporated with NH_4SCN for electro-chemical application. *Springer*, *27*, 3415–3429.

Nagahama, H., Maeda, H., Kashiki, T., Jayakumar, R., Furuike, T., & Tamura, H. (2009). Preparation and characterization of novel chitosan/gelatin membranes using chitosan hydrogel. *Carbohydrate Polymers*, *76*(2), 255–260.

Neto, M. J., Leones, R., Sentanin, F., Esperança, J. M. S. S., Medeiros, M. J., Pawlicka, A., & Silva, M. M. (2014). Ionic liquids for solid-state electrolytes and electrosynthesis. *Journal of Electroanalytical Chemistry*, *714*, 63–69.

Nofal, M. M., Hadi, J. M., Aziz, S. B., Brza, M. A., Asnawi, A. S. F. M., Dannoun, E. M. A., Abdullah, A. M., & Kadir, M. F. Z. (2021). A study of methylcellulose based polymer electrolyte impregnated with potassium ion conducting carrier: Impedance, eec modeling, ftir, dielectric, and device characteristics. *Materials*, *14*(17).

Nuvoli, L., Conte, P., Fadda, C., Reglero Ruiz, J. A., García, J. M., Baldino, S., & Mannu, A. (2021). Structural, thermal, and mechanical properties of gelatin-based films integrated with tara gum. *Polymer*, *214*(November), 123244.

Oliveira, A., Rios, A. D. O., Stoll, L., Rahier, H., & Flôres, S. H. (2019). Gelatin capsule residue - based films crosslinked with the natural agent genipin. *Packaging Technology and Science*, *33*(June 2018), 15–26.

Ong, A. C. W., Shamsuri, N. A., Zaine, S. N. A., Panuh, D., & Shukur, M. F. (2020). Nanocomposite polymer electrolytes comprising starch-lithium acetate and titania for all-solid-state supercapacitor. *Ionics*, *27*(2), 853–865.

Osman, Z., Mohd Ghazali, M. I., Othman, L., & Md Isa, K. B. (2012). AC ionic conductivity and DC polarization method of lithium ion transport in PMMA-LiBF 4 gel polymer electrolytes. *Results in Physics*, *2*, 1–4.

Pan, L., Li, P., & Tao, Y. (2020). Preparation and properties of microcrystalline cellulose/fish gelatin composite film. *Materials*, *13*(19), 1–15.

Polu, A. R., Kumar, R., & Rhee, H. W. (2015). Magnesium ion conducting solid polymer blend electrolyte based on biodegradable polymers and application in solid-state batteries. *Ionics*, *21*(1), 125–132.

Premalatha, M., Mathavan, T., Selvasekarapandian, S., Monisha, S., Pandi, D. V., & Selvalakshmi, S. (2016). Investigations on proton conducting biopolymer membranes based on tamarind seed polysaccharide incorporated with ammonium thiocyanate. *Journal of Non-Crystalline Solids*, *453*, 131–140.

Qiang, X., Zhou, S., Zhang, Z., Quan, Q., & Huang, D. (2018). Synergistic Effect of Halloysite Nanotubes and Glycerol on the Physical Properties of Fish. *Polymers*, *10*(11), 1258.

Qiao, C., Ma, X., Wang, X., & Liu, L. (2021). Structure and properties of chitosan films : Effect of the type of solvent acid. *LWT*, *135*(April 2020), 109984.

Qiao, C., Ma, X., Zhang, J., & Yao, J. (2017a). Molecular interactions in gelatin/chitosan composite films. *Food Chemistry*, *235*, 45–50.

Qiao, C., Ma, X., Zhang, J., & Yao, J. (2017b). Molecular interactions in gelatin/chitosan composite films. *Food Chemistry*, *235*(May), 45–50.

Qiao, C., & Wang, X. (2019). *Effect of water on the thermal transition in chitosan films*. *October*, 1–7.

Rahman, N. A., Hanifah, S. A., Mobarak, N. N., Ahmad, A., Ludin, N. A., Bella, F., & Su'ait, M. S. (2021). Chitosan as a paradigm for biopolymer electrolytes in solid-state dye-sensitised solar cells. *Polymer*, *230*(June), 124092.

Ramadan, R., Kamal, H., Hashem, H. M., & Abdel-Hady, K. (2014). Gelatin-based solid electrolyte releasing Li+ for smart window applications. *Solar Energy Materials and Solar Cells*, *127*, 147–156.

Ramos, M., Valdés, A., Beltrán, A., & Garrigós, M. (2016). Gelatin-Based Films and Coatings for Food Packaging Applications. *Coatings*, *6*(4), 41.

Rasali, N. M. J., Nagao, Y., & Samsudin, A. S. (2018). Enhancement on amorphous phase in solid biopolymer electrolyte based alginate doped NH_4NO_3. *Ionics*, *25*, 641-654.

Rasali, N. M. J., & Samsudin, A. S. (2018). Characterization on Ionic Conductivity of Solid Bio- Polymer Electrolytes System Based Alginate Doped Ammonium Nitrate via Impedance Spectroscopy. *AIP Conference Proceedings*, *2030*, 020224.

Rayung, M., Aung, M. M., Azhar, S. C., Abdullah, L. C., Su'ait, M. S., Ahmad, A., & Jamil, S. N. A. M. (2020). Bio-based polymer electrolytes for electrochemical devices: Insight into the ionic conductivity performance. *Materials*, *13*(4), 838.

Riera-Galindo, S., Leonardi, F., Pfattner, R., & Mas-Torrent, M. (2019). Organic Semiconductor/Polymer Blend Films for Organic Field-Effect Transistors. *Advanced Materials Technologies*, *4*(9), 1–20.

Roy, S., & Rhim, J. W. (2021). Fabrication of bioactive binary composite film based on gelatin/chitosan incorporated with cinnamon essential oil and rutin. *Colloids and Surfaces B: Biointerfaces*, *204*(May), 111830.

Saeed, M. A. M., & Abdullah, O. G. H. (2020). Effect of Structural Features on Ionic Conductivity and Dielectric Response of PVA Proton Conductor-Based Solid Polymer Electrolytes. *Journal of Electronic Materials*, *50*(3), 432–442.

Saikia, D., Chen, Y. H., Pan, Y. C., Fang, J., Tsai, L. D., Fey, G. T. K., & Kao, H. M. (2011). A new highly conductive organic-inorganic solid polymer electrolyte based on a di-ureasil matrix doped with lithium perchlorate. *Journal of Materials Chemistry*, *21*(28), 10542–10551.

Salvatore, L., Gallo, N., Natali, M. L., Campa, L., Lunetti, P., Madaghiele, M., Blasi, F. S., Corallo, A., Capobianco, L., & Sannino, A. (2020). Marine collagen and its derivatives: Versatile and sustainable bio-resources for healthcare. *Materials Science and Engineering C*, *113*(December 2019), 110963.

Selvalakshmi, S., Vijaya, N., Selvasekarapandian, S., & Premalatha, M. (2017). Biopolymer agar-agar doped with NH4SCN as solid polymer electrolyte for electrochemical cell application. *Journal of Applied Polymer Science*, *134*(15), 44702.

Sghayyar, H. N. M., Lim, S. S., Ahmed, I., Lai, J. Y., Cheong, X. Y., Chong, Z. W., Lim, A. F. X., & Loh, H. S. (2020). Fish biowaste gelatin coated phosphate-glass fibres for wound-healing application. *European Polymer Journal*, *122*(November), 109386.

Shamsuri, N. A., Zaine, S. N. A., Yusof, Y. M., Yahya, W. Z. N., & Shukur, M. F. (2020). Effect of ammonium thiocyanate on ionic conductivity and thermal properties of polyvinyl alcohol – methylcellulose – based polymer electrolytes. *Ionics*, *26*(3), 6083–6093.

Shenbagavalli, S., Muthuvinayagam, M., & Revathy, M. S. (2022). Preparation and characterization of proton (H+) conducting solid blend polymer electrolytes based on PEO/P(VdF-HFP) incorporated with NH4SCN. *Journal of Non-Crystalline Solids*, *579*(November 2021), 121368.

Shuhaimi, N. E. A., Teo, L. P., Woo, H. J., Majid, S. R., & Arof, A. K. (2012). Electrical double-layer capacitors with plasticized polymer electrolyte based on methyl cellulose. *Polymer Bulletin*, *69*, 807–826.

Shukur, M. F., & Kadir, M. F. Z. (2015). Electrical and transport properties of NH4Br-doped cornstarch-based solid biopolymer electrolyte. *Ionics*, *21*(1), 111–124.

Siburian, W. Z., Rochima, E., Andriani, Y., & Praseptiangga, D. (2020). Fish gelatin (definition, manufacture, analysis of quality characteristics, and application): A review. *International Journal of Fisheries and Aquatic Studies*, *8*(4), 90–95.

Singh, P., Sachdeva, A., & Bhargava, C. (2022). Polymer Electrolyte a Novel Material for Electrochemical Devices: A Review. *Journal of Physics: Conference Series*, *2327*(1).

Singh, T. J., & Bhat, S. V. (2003). Morphology and conductivity studies of a new solid polymer electrolyte: (PEG)xLiClO4. *Bulletin of Materials Science*, *26*(7), 707–714.

Skarlis, S. A., Nicolle, A., Berthout, D., Dujardin, C., & Granger, P. (2014). Combined experimental and kinetic modeling approaches of ammonium nitrate thermal decomposition. *Thermochimica Acta*, *584*, 58–66.

Sohaimy, M. I. H. A., Yusof, Y., & Isa, M. I. N. M. (2022). Improving Ionic Conductivity of Carboxymethyl Cellulose Solid Biopolymer Electrolyte with Assist from Dimethyl Carbonate. *Trends in Sciences*, *19*(19).

Sreekanth, K., Siddaiah, T., Gopal, N. O., Jyothi, N. K., Kumar, K. V., & Ramu, C. (2021). Thermal, Structural, Optical and Electrical Conductivity studies of pure and Mn2+ doped PVP films. *South African Journal of Chemical Engineering*, *36*(August 2020), 8–16.

Sudhakar, Y.; Selvakumar, M.; Bhat, D. . (2018). Biopolymer Electrolytes. In *An introduction of Biopolymer Electrolytes* (pp. 1–34). Elsevier Science Publishing Co Inc.

Sudhakar, Y. N., & Selvakumar, M. (2012). Lithium perchlorate doped plasticized chitosan and starch blend as biodegradable polymer electrolyte for supercapacitors. *Electrochimica Acta*, *78*, 398–405.

Sundaramahalingam, K., Muthuvinayagam, M., Nallamuthu, N., Vanitha, D., & Vahini, M. (2019). Investigations on lithium acetate-doped PVA/PVP solid polymer blend electrolytes. *Polymer Bulletin*, *76*(11), 5577–5602.

Tahir, H. B., Abdullah, R. M., & Aziz, S. B. (2022). The H + ion transport study in polymer blends incorporated with ammonium nitrate : XRD , FTIR , and electrical characteristics. *Results in Physics*, *42*(September), 105960.

Taravel, M. N., & Domard, A. (1995). Collagen and its interaction with chitosan. II. Influence of the physicochemical characteristics of collagen. *Biomaterials*, *16*(11), 865–871.

Teo, L. P., & Buraidah, M. H. (2021). Development on Solid Polymer Electrolytes for Electrochemical Devices. *Molecules, 26*(21), 6499.

Thomas, A., Moinuddin, K., Zhu, H., & Joseph, P. (2021). Passive fire protection of wood using some bio-derived fire retardants. *Fire Safety Journal*, *120*(January 2020), 103074.

Toh, H. W., Toong, D. W. Y., Ng, J. C. K., Ow, V., Lu, S., Tan, L. P., Wong, P. E. H., Venkatraman, S., Huang, Y., & Ang, H. Y. (2021). Polymer blends and polymer composites for cardiovascular implants. *European Polymer Journal*, *146*(September 2020), 110249.

Vernon-Carter, E. J., Alvarez-Ramirez, J., Bello-Perez, L. A., Roldan-Cruz, C., Garcia-Hernandez, A., & Huerta, L. (2017). The order of addition of corn starch/lithium perchlorate/glycerol affects the optical, mechanical, and electrical properties of a solid polymer electrolyte. *Ionics*, *23*(11), 3111–3123.

Voron'ko, N. G., Derkach, S. R., Kuchina, Y. A., & Sokolan, N. I. (2016). The chitosan-gelatin (bio)polyelectrolyte complexes formation in an acidic medium. *Carbohydrate Polymers*, *138*, 265–272.

Wang, H. (2021). A review of the effects of collagen treatment in clinical studies. *Polymers*, *13*(22).

Wang, W., & Alexandridis, P. (2016). Composite polymer electrolytes: Nanoparticles affect structure and properties. *Polymers*, *8*(11).

Wang, Y., Guo, X., Pan, R., Han, D., Chen, T., Geng, Z., Xiong, Y., & Chen, Y. (2015). Electrodeposition of chitosan/gelatin/nanosilver: A new method for constructing biopolymer/nanoparticle composite films with conductivity and antibacterial activity. *Materials Science and Engineering C*, *53*, 222–228.

Wu, J., Sun, X., Guo, X., Ji, M., Wang, J., Cheng, C., Chen, L., Wen, C., & Zhang, Q. (2018). Physicochemical, Antioxidant, In Vitro Release, and Heat Sealing Properties of Fish Gelatin Films Incorporated with β-Cyclodextrin/Curcumin Complexes for Apple Juice Preservation. *Food and Bioprocess Technology*, *11*(2), 447–461.

Xu, T., Liu, K., Sheng, N., Zhang, M., Liu, W., Liu, H., Dai, L., Zhang, X., Si, C., Du, H., & Zhang, K. (2022a). Biopolymer-based hydrogel electrolytes for advanced energy storage/conversion devices: Properties, applications, and perspectives. *Energy Storage Materials*, *48*(January), 244–262.

Xu, T., Liu, K., Sheng, N., Zhang, M., Liu, W., Liu, H., Dai, L., Zhang, X., Si, C., Du, H., & Zhang, K. (2022b). Biopolymer-based hydrogel electrolytes for advanced energy storage/conversion devices: Properties, applications, and perspectives. *Energy Storage Materials*, *48*(March), 244–262.

Xun, Z., Ni, S., Gao, Z., Zhang, Y., Gu, J., & Huo, P. (2019). Construction of polymer electrolyte based on soybean protein isolate and hydroxyethyl cellulose for a flexible solid-state supercapacitor. *Polymers*, *11*(11), 1895.

Yahya, W. Z. N., Meng, W. T., Khatani, M., Samsudin, A. E., & Mohamed, N. M. (2017). Bio-based chitosan/PVdF-HFP polymer-blend for quasi-solid state electrolyte dye-sensitized solar cells. *E-Polymers*, *17*(5), 355–361.

Yeddes, W., Djebali, K., Aidi Wannes, W., Horchani-Naifer, K., Hammami, M., Younes, I., & Saidani Tounsi, M. (2020). Gelatin-chitosan-pectin films incorporated with rosemary essential oil: Optimized formulation using mixture design and response surface methodology. *International Journal of Biological Macromolecules*, *154*, 92–103.

Yin, Y., Li, Z., Sun, Y., & Yao, K. (2005). A preliminary study on chitosan/gelatin polyelectrolyte complex formation. *Journal of Materials Science*, *40*(17), 4649–4652.

Yu, F., Zhao, L., Zhang, H., Sun, Z., Li, Y., Hu, Q., & Chen, Y. (2021). Cathode/gel polymer electrolyte integration design based on continuous composition and preparation technique for high performance lithium ion batteries. *RSC Advances*, *11*(7), 3854–3862.

Yu, S., Schmohl, S., Liu, Z., Hoffmeyer, M., Schön, N., Hausen, F., Tempel, H., Kungl, H., Wiemhöfer, H. D., & Eichel, R. A. (2019). Insights into a layered hybrid solid electrolyte and its application in long lifespan high-voltage all-solid-state lithium batteries. *Journal of Materials Chemistry A*, *7*(8), 3882–3894.

Yusof, Y. M., Shukur, M. F., Hamsan, M. H., Jumbri, K., & Kadir, M. F. Z. (2019). Plasticized solid polymer electrolyte based on natural polymer blend incorporated with lithium perchlorate for electrical double-layer capacitor fabrication. *Ionics, 25*(11), 1-12.

Zainuddin, N. K., Rasali, N. M. J., Mazuki, N. F., Saadiah, M. A., & Samsudin, A. S. (2020). Investigation on favourable ionic conduction based on CMC-K carrageenan proton conducting hybrid solid bio-polymer electrolytes for applications in EDLC. *International Journal of Hydrogen Energy*, *45*(15), 8727–8741.

Zhao, Y., Kang, Y., Fan, M., Li, T., Wozny, J., Zhou, Y., Wang, X., Chueh, Y. L., Liang, Z., Zhou, G., Wang, J., Tavajohi, N., Kang, F., & Li, B. (2022). Precise separation of spent lithium-ion cells in water without discharging for recycling. *Energy Storage Materials*, *45*(September 2021), 1092–1099.